

From Farm to Lab: The Potential of Decellularized Plant Leaves for Sustainable Meat Production



A Dissertation

Submitted to the Faculty of the

WORCESTER POLYTECHNIC INSTITUTE

in partial fulfillment of the requirements for the

Degree of Doctor of Philosophy in

Biomedical Engineering

September 1st, 2023

By

A handwritten signature in black ink, appearing to read "Jordan D. Jones".

Jordan D. Jones

Approved By:

A handwritten signature in black ink, appearing to read "Tanja Dominko".

Dr. Tanja Dominko, DVM, PhD
Professor (Advisor)
Biomedical Engineering Department
Biology and Biotechnology Department
Worcester Polytechnic Institute

A handwritten signature in blue ink, appearing to read "George Pins".

Dr. George D. Pins, PhD
Professor (Committee Chair)
Biomedical Engineering Department
Worcester Polytechnic Institute

A handwritten signature in blue ink, appearing to read "Pamela Weathers".

Dr. Pamela Weathers, PhD
Professor (Committee Member)
Biology and Biotechnology Department
Worcester Polytechnic Institute

A handwritten signature in blue ink, appearing to read "Marsha W. Rolle".

Dr. Marsha W. Rolle, PhD
Professor (Committee Member)
Biomedical Engineering Department
Worcester Polytechnic Institute

A handwritten signature in blue ink, appearing to read "Glenn R. Gaudette".

Dr. Glenn R. Gaudette, PhD
Chair/Professor (Committee Member)
Engineering Department
Boston College

Acknowledgements

I would like to thank Tanja and Glenn for serving as my undergraduate and graduate advisors throughout my academic career. I would also like to thank Pam, Marsha, and George, the remaining members of my thesis committee. I've known most of them for over a decade. Their assistance has been integral to my development as a researcher. I have never enjoyed eating vegetables, and unfortunately this remains true. However, I have learned to appreciate the potential in all of earth's organisms, regardless of their kingdom. They taught me to prioritize value creation and the improvement of others' lives in all that I do, I will undoubtedly carry these teachings into my future endeavors.

I appreciate all my colleagues at WPI, BC, and New Harvest. This includes Rick, my past lab mentors, and all the undergrads that have helped. Their support, like all my friends, has made this journey exciting and fulfilling. Thanks for keeping the dull moments few and far between. I want to thank Lisa and all the supporting staff at WPI and BC for their assistance with my research needs. Brendan should receive special thanks for lending an ear through difficult times. I am grateful to New Harvest and the Koerner Family Foundation for financially supporting my research. Their generosity has made it possible for me to focus on my research and complete this dissertation.

None of this would be possible without my family and close friends. Thank you for your unwavering support, patience, and understanding at every turn. Your love and support form the foundation of my success and personal growth. Thank you for developing my interests and talents and imparting your vision to me. I want to thank my partner and chief editor Yvette for supporting me and my research. I love you all.

I really appreciate everything you all have done. There have been many ups and downs on this journey, but thanks to your support, it was amazing and unforgettable.

Table of Contents

Acknowledgements.....	2
Table of Contents	3
Table of Figures	5
Abbreviations	7
Abstract	11
Chapter 1 – Overview.....	12
1.1 Introduction.....	12
1.2 Aims and Hypothesis.....	14
Chapter 2 - Background and Literature Review	16
2.1 The Societal Significance of Meat.....	16
2.2 Traditional Agriculture and its Global Impact.....	17
2.3 The Prospect of Abolition (Vegetarianism) or Alternative Protein Sources.....	19
2.4 Cells – Skeletal Muscle Physiology and <i>In vitro</i> Culture	22
2.5 Media – Biological Signals and Resources.....	26
2.7 Decellularized Plant Scaffolds and their Potential Application in Cellular Agriculture.....	32
Chapter 3 – Decellularized Spinach Leaves as a Suitable Scaffold	35
Aim 1A: Examine the viability, differentiation capacity, and alignment characteristics of sown satellite cells on the surface of decellularized spinach scaffolds.....	36
3A.1 Introduction	36
3A.2 Materials and Methods	38
3A.3 Results.....	45
3A.4 Discussion.....	51
Aim 1B: Evaluate the significance of decellularization in the long-term culture of satellite cells.	54
3B.1 Introduction	54
3B.2 Materials and Methods	54
3B.3 Results	56
3B.4 Discussion.....	57
Chapter 4 – Decellularization as a Food Processing Step	58
Aim 2: Modify the decellularization procedure to be applied as a food processing step.	58
4.1 Introduction.....	58
4.2 Materials and Methods	61
4.3 Results	66

4.4 Discussion	69
Chapter 5 – Harnessing Plant Topographies for Engineered Muscle	73
Aim 3: Examine how the leaf topographies of dicot and monocot plants affect myoblast alignment and differentiation.....	73
5.1 Introduction.....	73
5.2 Materials and Methods	75
5.3 Results	79
5.4 Discussion.....	87
Chapter 6: Conclusions and Future Work	93
6.1 Conclusions.....	93
6.2 Key Findings and Contribution to the Field.....	93
6.3 Key Limitations and Shortcomings	98
6.4 Defining Success	100
6.5 The Social Challenge	102
6.6 Future Work	103
References	106
Appendix.....	116
ACS Biomaterials Reprint Permission.....	116
Biorender Publication Rights	117
Protocols.....	122
Plant Decellularization	122
Leaf Scaffold Sterilization:	124
Satellite cell Isolation.....	125
Passaging Primary Bovine Satellite cells	126
Gelatin coating	127
Cell Seeding	128
Cyquant DNA Analysis.....	129
Live/Dead Stain	132
Phalloidin and Hoechst Stain	133
Myosin Heavy-chain stain.....	134
Calcofluor White Stain	135
Hematoxylin and Eosin Stain	136

Table of Figures

Figure 1 Diagram of Muscle Contraction	22
Figure 2 Structure of Skeletal Muscle	22
Figure 3 Dicot Vs. Monocot Structure	33
Figure 4 Diagram of cell isolation, expansion and differentiation strategy	35
Figure 5 Directional analysis of phalloidin stained bovine satellite cells cultured on gelatin coated glass. The color of each microfilament represents the orientation relative to the color wheel.	44
Figure 6 Primary bovine satellite cells (PBSC) remain viable after being cultured on decellularized spinach scaffold for 14 days (n=54). (a) PBSCs on decellularized spinach. (b) PBSCs on gelatin. (c) Comparison of PBSC viability	46
Figure 7 Satellite cells show comparable differentiation capacity on decellularized spinach scaffolds after 14 days (n=54). (a) PBSC differentiation on gelatin. (b) PBSC differentiation on decellularized spinach. (c) Comparison of PBSC differentiation capacity	47
Figure 8 Decellularized spinach scaffolds do not appear to direct satellite cell alignment (n=54). (a) Color survey of PBSC cytoskeleton. (b) Histogram of PBSC cytoskeleton orientation. (c) Comparison of PBSC alignment	50
Figure 9 Primary bovine satellite cells have a higher nuclear density when cultured on decellularized spinach compared to non-decellularized spinach after 7 d (n = 6). (a) PBSCs on decellularized spinach. (b) PBSCs on non-decellularized spinach. (c) Comparison on nuclear density	56
Figure 10 PS20 can be used as an effective secondary non-ionic detergent for the decellularization of spinach leaves. (a) DNA content on decellularized spinach leaves by non-ionic detergent. (n=6) (b) DNA content of decellularized spinach leaves by hexanes inclusion. (n=6)	67
Figure 11 Histological analysis shows that both TX100 and PS20 result in significant reduction in intracellular context with minimal impact of cellulose structure	68
Figure 12 Primary bovine satellite cells viability when cultured on GRAS decellularized spinach after 7 days. (a) PBSCs on REG decellularized spinach. (b) PBSC viability on REG decellularized spinach (n=6)	69
Figure 13 Cellular Alignment Cartography (CAC) workflow diagram. Phalloidin images are recolored based on the orientation of each microfilament using OrientationJ. Kappa values are calculated for 1×10^5 regions throughout the image. A heatmap representing the Kappa values is superimposed over the original image displaying relative alignment at specific location on the scaffold.	77
Figure 14 Surface micrographs of decellularized spinach and decellularized corn husk (a) Calcofluor white stain of decellularized spinach. (b) Cross section of spinach leaf surface. (c) Calcofluor white stain of decellularized corn husk. (d) Cross section of corn husk surface	80

Figure 15| Corn husk possess significantly wider feature widths and higher variability in both width and depth. (a) Depth heatmap of decellularized spinach leaf surface. (b) Depth heatmap of decellularized corn husk surface. (c) Topographical comparison of decellularized scaffolds. (n=6)81

Figure 16| QM7 cells exhibit superior alignment characteristics on decellularized spinach compared to decellularized corn husk. (a) Tiled array of micrographs of QM7 cells on decellularized spinach. (b) Tiled array of micrographs of QM7 cells on decellularized corn husk. (c)Global alignment of QM7 cells on decellularized spinach and corn husk. (n=6).....83

Figure 17| Color survey of cell aggregates on decellularized spinach and decellularized corn husk. (a) Decellularized spinach. (b) Decellularized corn husk84

Figure 18| Bimodal distribution of corn husk persists even after isolation of cell populations. (a) Left QM7 population. (b) Right QM7 population. (c) Orientation distribution of left population. (d) Orientation distribution of right population.....84

Figure 19| Kappa heatmaps of QM7 cells cultured on decellularized spinach and decellularized corn husk. (a) Kappa heatmap of decellularized spinach samples. (b) Kappa heatmap of decellularized corn husk samples85

Figure 20| QM7 cells exhibit little differentiation of both scaffolds. Differentiation was slightly higher on decellularized spinach compared to decellularized corn husk. (a) QM7 cells differentiated on decellularized spinach. (b) QM7 cells differentiated on decellularized corn husk. (c) Comparison of QM7 differentiation capacity (n=6).....86

Figure 21| Meat "unit" diagram. The spongy mesophyll is a porous tissue that tissue that could possibly be inhabited by mammalian cell growing on the surface of the leaf103

Abbreviations

2D – Two Dimensional

3D – Three Dimensional

AFM – Atomic Force Microscopy

ANOVA – Analysis of Variance

AQ1 – AlignmentQuant 1

AQ2 – AlignmentQuant 2

C2C12s – Immortalized Mouse Myoblasts Cell Line

Ca – Calcium

CAC – Cellular Alignment Cartography

cm – Centimeter(s)

d – Day(s)

diH₂O – Deionized Water

DMEM – Dulbecco's Modified Eagle Medium

DNA – Deoxyribonucleic Acid

ECM – Extracellular Matrix

EGF – Epidermal Growth Factor

ESC – Embryonic Stem Cell

EtO – Ethylene Oxide

FPS – Frames Per Second

FDA – United States Food and Drug Administration

FGF2 – Fibroblast Growth Factor 2

GAP – Good Agricultural Practices

GMP – Good Manufacturing Practices

H&E – Hematoxylin and Eosin

Hex+ – Includes Hexanes

Hex- – Does not Include Hexanes

hiFBS – Heat-inactivated FBS

hMSC – Human Mesenchymal Stem Cells

hPS-CM – Human Pluripotent Stem Cell Derived Cardiomyocytes

hr – Hour(s)

HUVEC – Human Umbilical Vein Endothelial Cells

HGF1 – Hematopoietic Growth Factor 1

ICM – Inner Cell Mass

ID – Inner Diameter

IPSCs – Induced Pluripotent Stem Cells

IPSC-CM – Induced Pluripotent Stem Cell Derived Cardiomyocytes

IGF1 – Insulin-like Growth Factor 1

K – Potassium

KCl – potassium chloride

Kg – Kilogram(s)

KH₂PO₄ – potassium dihydrogen phosphate

kWh – Kilowatt hour

L6s – Immortalized Rat Myoblasts Cell Line

LC-MS – Liquid Chromatography – Mass Spectrometry

LDCD – lysosomal-dependent cell death

MI – Myocardial Infarction

min – Minute(s)

mm – millimeter(s)

mM – Millimolar

ms – Millisecond(s)

MTT – 3-(4,5-dimethylthiazol-2-yl)-2,5-diphenyltetrazolium bromide

Na – Sodium

Na₂HPO₄ – di-sodium hydrogen phosphate anhydrous

ND – Nuclear Density

OD – Outer Diameter

PBS Phosphate Buffered Saline

Pax7 – Paired Box 7

PDMS – Polydimethylsiloxane

PFA – Paraformaldehyde

PS20 – Polysorbate-20

Qdot – Quantum Dot

QM7s – Immortalized Quail Myoblasts Cell Line

RT – Room Temperature

ROI – Region of Interest

SAA – Sarcomeric α -actinin

SccO₂ – Super Critical Carbon Dioxide

SDS – Sodium Dodecyl Sulfate, Sodium Laurel Sulfate

SEM – Scanning Electron Microscope

TCP – Tissue Culture Plastic

TX100 – Triton X-100

U – Units

VCD – Viable Cell Density

wk – Week(s)

μg – Microgram(s)

μL – Microliter(s)

μm – Micrometer(s), micron(s)

μM – Micromolar

Abstract

The growth of our global population is projected to outgrow the availability of agricultural land by 2050. This looming reality requires major modifications to agricultural methods including crop and livestock production. As one of the new alternative protein technologies, cellular agriculture holds promise for complementing current animal agricultural practices by producing lab-grown meat. One of the challenges that need to be overcome to reach commercial scale production of structured meat products includes identification and characterization of edible tissue scaffold to reduce the number of processing steps and improve the final product. Due to their affordability, familiarity, and accessibility, decellularized plant-derived materials emerge as an appealing option.

Previous research demonstrated that decellularized spinach leaves can support the growth of numerous cell types. In this study, primary bovine satellite cells were grown on decellularized spinach leaves for 7 and 14 days. After 14 days, 99% of cells were alive, 25% expressed myosin heavy-chain, and the average cytoskeletal alignment kappa value was 0.71 ± 0.1 . These findings indicated that decellularized spinach can be used as a scaffold for lab-grown beef. The new decellularization approach utilizing food-safe agents yielded comparable decellularization quality to the previously used detergent-based decellularization method while maintain the integrity of spinach scaffolds. Primary bovine satellite cells grown on such scaffolds for 7 days had 97.4% viability. These findings suggested that the new decellularization method was effective and more closely adhered to food safety regulations that could advance cellular agriculture and cultured meat production. Corn husk, a common food waste product, was also explored for its potential to direct cell alignment and improve the texture of the proposed meat product. Both spinach and cornhusk scaffolds presented challenges in achieving desired cell alignment and fusion indices, suggesting that scaffold topography had little influence. Further research is needed to identify optimal plant species and tissues to serve as scaffolds for sustainable meat production.

Chapter 1 – Overview

1.1 Introduction

In the next few decades, we may witness seismic shifts in agricultural practices that will reduce our reliance on traditional cattle agriculture. Such innovations will have long-lasting effects on the stability of the global food supply and even the longevity of human existence on Earth. Cellular Agriculture describes the use of biotechnology to produce meat, dairy, and other animal-based goods. This technology presents several advantages: it can help reduce livestock populations, reduce the carbon footprint of the agricultural industry, alleviate the pressure for additional agricultural land, and reduce animal suffering.

Despite its promise, cellular agriculture is still a young technology with numerous hurdles to overcome before reaching maturity. There is a growing interest in finding novel techniques for producing and scaling up cell cultures, producing engineered milk and egg products, and developing new methods for producing structured meat products. Among the most noteworthy advancements to date is the generation of unstructured or amorphous animal products.

Traditionally, ground meat is made by grinding meat from animals after slaughter. Cellular agriculture techniques, on the other hand, can be used to grow ground meat in a laboratory setting without the need to sacrifice the animal. The genesis of lab-grown amorphous meats may be traced back to 2013, when Dr. Mark Post unveiled the lab-grown burger patty. Cow satellite cells were used to create the burger patty in a laboratory setting. The resulting burger patty was a breakthrough in the field of cellular agriculture and a proof of concept for the future.

This emerging technology has sparked various startup companies among which are Upside Foods, Mosa Meat, Wildtype Foods, and many more. Price, market acceptance, and government regulation will all play a major role in their success. While amorphous meats have immense potential as a sustainable and ethical

alternative to traditional animal agriculture, they do have several limitations. One of the most challenging obstacles is replicating structured meat products like steak.

In an animal-derived cut of meat, muscle fibers are bundled together and surrounded by connective tissue, and fat thereby giving meat its characteristic texture and chewiness. The production of biomass to generate lab-grown equivalents is prohibitively expensive and still in the early phases of research. This study will explore the use of decellularized plant leaves as a potential scaffold to produce structured meat products. As a cheap, edible, and accessible material, these scaffolds have the potential to meet the design parameters of an ideal scaffold for meat development while also reducing the cost of production.

Some sort of biomaterial scaffold will likely be required to support the growth of muscle tissue to create structured meat products. Apart from the familiar organoleptic properties, lab-grown structured meats may also improve food safety and efficiency. By producing meat in a controlled environment, the risk of foodborne infections such as *Salmonella* and *E. coli* is considerably reduced, as is the requirement for antibiotics that are widely used in traditional animal farming to prevent disease.

1.2 Aims and Hypothesis

By 2050, the growing human population and demand for food will outpace the world's capacity to produce food ¹. The growing popularity of plant-based meat alternatives has done little to suppress the expansion of the meat industry ². Although it has been demonstrated that meat products can be produced *in vitro*, current products are limited to ground meats and are unlikely to have a significant impact on the expansion of the traditionally produced meat ^{3,4}. An *in vitro* alternative to structured meats has a greater potential to reduce the need for traditional meat because it can be used in a wider variety of recipes and directly compete with minimally processed traditional meat products. A vascularized scaffold could facilitate the formation of 3D tissues, paving the way for structured meat products like steak ^{3,5}. However, traditional tissue engineering techniques are too expensive when applied at commercial scale ³. Decellularized spinach leaves have been shown to be a cheap and accessible biomaterial with an innate vascular network that can transport oxygenated media to support the growth of various cell types. By taking full advantage of this vasculature, it may be possible to culture cells in layers thicker than what is achievable with conventional cell culture ^{6,7}. This study aims to investigate the possible use of decellularized plant leaves as a prevascularized scaffold for structured meat products produced *in vitro*.

Aim 1: Investigate the potential use of plant leaves as a scaffold for bovine skeletal muscle cultivation for human consumption. Spinach leaves are vascularized, affordable, palatable, and accessible. They can also be easily grown in greenhouses under controlled conditions. Hypothesis: Decellularized plant scaffolds support viability and differentiation capacity of satellite cells cultured on their surface.

Aim 1A: Measure the viability, differentiation capacity, and alignment characteristics of bovine satellite cells grown on the surface of decellularized spinach scaffolds. The viability, differentiation capacity, and local alignment characteristics of satellite cells sown on decellularized leaf scaffolds will be compared to conventional substrates such as gelatin. These characteristics will be measured with image analysis.

Aim 1B: Measure the necessity of decellularization for the long-term culture of satellite cells. In this aim, we'll examine whether decellularization is required in derivation of leaf-based scaffolds for the support satellite cells. If satellite cells can survive for long periods of time on native spinach leaves, the decellularization procedure can be omitted, saving time and resources while reducing processing steps. Additionally, scaffolds that preserve the nutritional characteristics of the original plant may be produced if the decellularization process is eliminated.

Aim 2: Modify the decellularization procedure to be applied as a food processing step. Current decellularization methods use detergents that are not safe for use in food processing. It may be possible to achieve the same decellularization efficiency by using detergents that are commonly used as food additives, to produce a leaf scaffold that is safe for consumption and that would more closely comply with FDA guidance for food additive compounds. Hypothesis: The use of regulated detergents will not impede the decellularization of spinach leaves or the viability of cells sown on scaffolds that incorporate them in the decellularization process.

Aim 3: Examine how the leaf topographies of dicot and monocot plants affect myoblast alignment and differentiation. Alignment is critical for the structural, mechanical, and functional properties of engineered muscle tissue. Alignment analysis tools will be used to analyze how cell alignment changes over many regions of interest, providing a spatial context to previous alignment studies. Hypothesis: Alignment and differentiation will be greater in regions where linear topography is present on both surfaces. In addition, overall alignment and differentiation will be greater on corn husk compared to spinach due to the higher prevalence of linear topography.

Chapter 2 - Background and Literature Review

2.1 The Societal Significance of Meat

Meat has played a vital role in human survival and development throughout history, as it is a rich source of protein, essential nutrients, and the energy our bodies require to function. The earliest humans were nomadic and subsisted through hunting and gathering. Meat was an integral part of their diet, providing them with the necessary protein and energy to survive. Hunting was a dangerous and difficult endeavor that required teamwork, skill, and patience. However, over time they learned to raise animals for meat, allowing them to settle in one location and develop a more stable food source. This transition from hunting and gathering to animal husbandry was a major step in the evolution of humans.

Domestication of animals began approximately 10,000 years ago in what is now known as the Fertile Crescent, which stretches from the eastern Mediterranean to the Persian Gulf in the Middle East ⁸.

Sheep, goats, and pigs were the first domesticated animals, followed by cattle and horses. Initially, animals were domesticated for food and clothing, but later they were also used for transportation and farming.

The process of domestication started with the capture and captivity of wild animals. Primitive humans understood that captive animals could provide meat, milk, and wool. Over time, humans selected and bred animals that were more docile and manageable to produce more domesticated offspring. This selective breeding resulted in genetic changes that made the animals more suitable for domestication. The discovery by early humans that domesticated animals could be used to plow fields and pull carts facilitated farming and transportation fueling the evolution of agriculture and the cultivation of food and fiber crops. As people settled in one location to tend their crops and animals, the use of animals in agriculture also led to the growth of larger communities ⁸.

As human populations grew, so did the demand for meat and animal products and the domestication of animals. The use of animals for food and clothing also contributed to the development of trade and commerce; people exchanged goods and services to acquire the necessary products. As human communities evolved and fostered agriculture, meat became more accessible and abundant. Domesticated animals such as cows, pigs, and chickens provided a more constant and reliable source of meat, which led to the evolution of diets focused on meat.

Today the U.S. meat industry is a major economic powerhouse, producing more than a 30 billion pounds of meat in 2021⁹. The USDA estimated there were approximately 94 million cattle and calves in the United States in 2021¹⁰. Concerns regarding environmental impact, ethics, and economic feasibility are however bearing heavily on the industry. As a result, many people have turned to alternative diets that do not include meat, such as vegetarianism and veganism. These diets emphasize plant-based foods, which are generally healthier and better for the environment. These diets have grown more popular in recent years, with many people adopting them for health, environmental, or ethical reasons.

2.2 Traditional Agriculture and its Global Impact

Feeding animals with the vital nutrients they need to grow, flourish, and produce meat, dairy, and eggs is a crucial component of animal husbandry. Common types of animals reared for food include cattle, pigs, chickens, turkeys, and sheep, each of which has distinct dietary needs. Animal feed can contain a variety of ingredients including soybeans, alfalfa, corn, and wheat. To facilitate handling and feeding, these ingredients are frequently blended in varied proportions and processed into pellets or other forms. Depending on the unique needs of the animals and the farming methods implemented, animal feed may contain various supplements, such as vitamins, minerals, and antibiotics, in addition to the core nutrients^{11,12}.

In 2021 the US produced approximately 30 billion pounds of meat, and this figure is projected to grow ⁹. To satisfy this demand, farmers and feed producers create millions of tons of feed annually, consuming large quantities of land, water, and energy. Reducing the demand for livestock feed could have major environmental and sustainability benefits. For instance, if people shifted to plant-based diets, the resources currently used for livestock feed production could be reallocated. The land currently used to cultivate animal feed might be repurposed to cultivate crops for human consumption, while the water and energy required for feed production may be reallocated.

In the United States, the demand for land for cattle operations continues to rise. According to projections, by the year 2050, up to 1 billion additional hectares of land may be required to meet the rising demand for food ¹³. Estimates of the quantity of land required to produce one pound of beef vary, but it is generally accepted that beef production requires more land than the production of other animal products. The demand for land in the animal agriculture industry can have severe environmental repercussions, such as deforestation, habitat destruction, soil degeneration, and consequent biodiversity loss ¹³. In addition, deforestation caused by fire contributes to climate change by releasing carbon into the atmosphere and reducing trees' ability to absorb carbon dioxide.

Depending on the type of animal and the stage of production, the amount of water necessary for livestock agriculture can vary. Cattle and dairy cows, for instance, may require up to 4,000 m³ per head of beef, whereas pigs may require 6 m³ per head ¹⁴. In addition, water requirements can increase during times of extreme heat or stress. The sources of water for livestock agriculture in the United States might vary according on geography and farming practices. In certain regions, surface water from rivers, lakes, or reservoirs may be used for livestock, whilst in others, groundwater may be the predominant source. Additionally, some farms may collect and store rainwater for use during drought or water scarcity.

To maintain environmental conditions and feed animals, cattle feedlots demand substantial amounts of energy, but poultry facilities may require less energy. In addition, the transportation and processing of animal products can also be energy intensive. It takes approximately 31.5 kWh of energy to produce 1 pound of beef, whereas chicken only requires 4.4 kWh¹⁴. The energy requirements of animal agriculture can have substantial environmental and sustainability consequences, such as greenhouse gas emissions. The production and consumption of fossil fuels for energy generation constitute a substantial contributor to global warming. In addition, animal agriculture can contribute to greenhouse gas emissions via the production and management of animal waste, deforestation for feed production, transportation and processing of animal products, and methane released from cattle belching. Agriculture accounts for about 12% of global greenhouse gas emissions, with livestock being the most prominent source^{15,16}. Reducing the energy demand and pollution from animal agriculture and switching to renewable energy sources may have major environmental benefits, including the reduction of greenhouse gas emissions and the promotion of more sustainable energy practices.

2.3 The Prospect of Abolition (Vegetarianism) or Alternative Protein Sources

In recent years, vegetarianism has grown in popularity as a dietary practice. It refers to a lifestyle that excludes the ingestion of beef, pork, poultry, and fish. Vegetarians prefer plant-based foods such as fruits, vegetables, legumes, grains, and nuts. Approximately 680 million people worldwide are vegetarian¹⁷. This amount varies by location, with India having the highest proportion of vegetarians, comprising approximately forty percent of the country's population^{17,18}. Comparatively, just roughly 6% of the population in North America identified as a vegetarian as of 2021¹⁸. There are numerous reasons why individuals select a vegetarian diet. Economic factors and concerns for animal welfare are among the most frequent cited reasons¹⁸. Many vegetarians consider the killing of animals for sustenance to be immoral and inhumane. Additionally, vegetarians frequently cite health concerns as a rationale for their diet. A plant-based diet provides various health benefits, including a lower risk of heart disease, certain malities,

and type 2 diabetes, according to research. In addition, vegetarianism is frequently associated with environmental consciousness and sustainability. Since the livestock industry is a major contributor to greenhouse gas emissions, deforestation, and water pollution, a plant-based diet is a more sustainable option.

The introduction of alternative protein sources and plant-based meat substitutes such as those produced by Impossible Foods and Beyond Meat have potential to alter this trend. These products strive to provide consumers with the flavor and texture of meat without the ethical and environmental concerns connected with conventional meat production. Plant-based meat analogs have gained popularity lately, and the market for these products is growing at a rate of approximately 8% per year ^{19,20}. Even some fast-food restaurants, including Burger King and Dunkin Doughnuts, have begun to provide plant-based options.

Algae are one of the most promising alternative sources of protein. Algae have been used in Asian cuisine for ages and are quite nutritious. Algae contain up to 60% protein (w/w) and are an excellent source of vitamins and minerals ²¹⁻²³. Algae may be grown in either saltwater or freshwater, and their production requires less land and water than traditional protein sources such as meat. In addition, algae have a high photosynthetic efficiency, indicating that they convert sunlight into energy more efficiently than other plants. There is an increasing interest in the development of algal-based foods, with some companies currently employing algae to manufacture protein-rich supplements and snacks.

Insects also are a potential alternate source of protein. Insects are a staple food in many civilizations around the globe, but they are just beginning to appeal to western cultures ^{24,25}. Protein-rich insects can be produced with minimum environmental impact, requiring less area, water, and feed per pound than conventional cattle. There are numerous ways to prepare insects, from entire roasted crickets to cricket flour for baking. However, large-scale insect farming may be complicated with a need to maintain sanitary conditions to meet regulatory pressure ²². Some of these sources, including algae and insects, are either

unpalatable or inedible and need to undergo additional processing stages to be used as a source of protein^{22-24,26}. Even with all of the money, energy, and technological advancement that these procedures will need, there will still likely be protein loss²²⁻²⁵.

Soy, beans, and pulses are all forms of plant-based protein that have been consumed for ages in a variety of cultures.² Numerous foods contain soy, including tofu, tempeh, and soy milk. Beans and pulses, such as lentils and chickpeas, are similarly high in protein and can be used in a wide range of recipes, from salads to stews. They are also rich in fiber and other essential minerals. As they require less land and water to produce, plant-based protein sources like soy, beans, and pulses are more sustainable than traditional livestock.

To lessen reliance on traditional meat products and change consumer behavior, plant-based substitutes will need to mimic the inherent organoleptic characteristics of traditional structured meat. For instance, crosslinking plant proteins through heat extrusion can give products a chewy texture and fibrous structure more akin to structured meat². Leghemoglobin, a heme protein present in the roots of soy plants, and red beet extract can be used as coloring agents to give plant-based meat substitutes a blood-like coloring that resembles traditional meat^{2,27}. Despite these improvements, it is still difficult to replicate the myofibrillar structure, texture, and juicy nature of structured meat. The organoleptic discrepancy between traditional meat and plant-based analogs is further exacerbated by the fact that many plant-based products have a distinctive aftertaste and frequently have an odor resembling that of beans²⁸. Even when plant-based alternatives advance, it might not be advisable to completely exclude animal protein from diets. The advantages of eliminating large herds of cattle may be diminished if humanity simply relies on the cultivation of food plants¹³. Cattle can convert inedible plant matter into edible protein¹³. Despite the rise of vegetarianism and alternative protein products, it appears that the meat industry is here to stay for the foreseeable future. Therefore, there is still a need for more effective ways to compete with traditional agriculture.

2.4 Cells – Skeletal Muscle Physiology and *In vitro* Culture

Meat is the term applied to animal skeletal muscle tissue that has been designated for consumption as food for humans and domestic animals. Skeletal muscle is a vital tissue for many organisms, as it is responsible for movement and support. There are 3 types of muscle in the body: skeletal, cardiac, and smooth muscle. Skeletal muscle is the most prevalent form of muscle in the body, accounting for around 40% of body mass. It is dispersed throughout the body, connected to bones via tendons, and is responsible for voluntary actions, such as walking and lifting objects^{29,30}. When a muscle contracts, it pulls on the bone to which it is anchored, actuating the joint. For example, when the biceps muscle contracts, it pulls the forearm towards the upper arm, resulting in the movement of the elbow joint.

Skeletal muscle is also vital for maintaining posture and body position.

Skeletal muscle works by contracting and relaxing in response to signals from motor neurons as shown in Figure 1^{29,30}. Each muscle fiber is formed of myofibrils, which are made up of repeating units called sarcomeres^{29,30}. A sarcomere consists of two types of protein filaments: thick filaments made of myosin and thin filaments made of actin, tropomyosin, and troponin^{29,30}. An action potential, which is an electrical signal that goes along a neuron, initiates contractions. When the action potential reaches the terminal end of a motor neuron, it initiates the release of acetylcholine, a neurotransmitter. The binding of

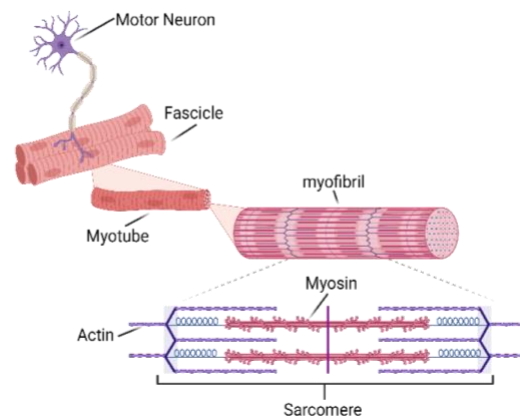


Figure 1 | Structure of skeletal muscle

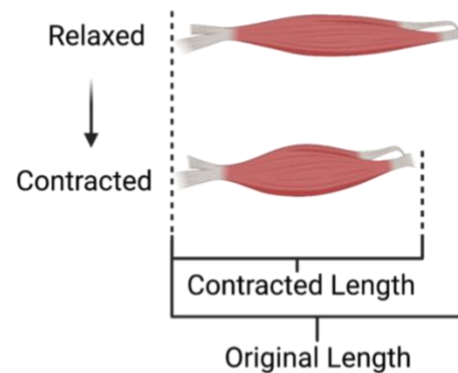


Figure 2 | Diagram of muscle contraction

acetylcholine to receptors on the surface of the muscle fiber alters the membrane's electrical charge. This change in turn triggers the release of calcium ions from the muscle fiber's sarcoplasmic reticulum. Calcium ions bind to troponin, creating a conformational change in the protein complex that displaces tropomyosin from its binding location on the actin filament, allowing the myosin heads to bind to α -actin^{29,30}. The myosin heads subsequently undergo a conformational change, shortening the sarcomere and causing the muscle fiber to contract, as seen in Figure 2³¹. Hydrolysis of ATP provides the energy necessary to reset the myosin head. Any disturbance of this mechanism can result in dysfunctional muscle.

There are two paradigms of *in vitro* skeletal muscle culture: prenatal and postnatal. Prenatal involves embryonic stem cells (ESCs) and targeted differentiation stimuli to drive ESCs towards myogenic cell types³². A hallmark of ESCs is that they can only be found and collected from the inner cell mass (ICM) of embryos in the blastocyst phase of development, which has presented an ethical challenge in terms of social acceptance of the technology. With a postnatal approach there are more options for cell sources: whole muscle fibers, satellite cells, and induced pluripotent stem cells (iPSCs)^{33,34}. Postnatal approaches are often favored over prenatal approaches. This is because of the ethical questions associated with embryonic stem cell research and the complex differentiation pathways that must be navigated to direct the differentiation of the embryonic stem cells³². iPSCs are formed from the dedifferentiation of somatic cells such as fibroblasts³⁴. Like the use of ESCs, this method of postnatal muscle culture is not ideal due to the complex differentiation pathways that must be navigated for dedifferentiation and differentiation into the myogenic lineage^{32,34}.

In vivo, satellite cells are muscle specific stem cells that reside between the basement membrane (basal lamina) of the sarcolemma^{16,35-42}. These cells differentiate and subsequently fuse to form multinucleate myotubes^{35,36}. To replicate this process *in vitro* satellite cells must be differentiated while they are on the desired substrate, as fused myotubes will not adhere to a surface once removed from their original surface. Whole muscle fiber culture relies on this same process but eliminates the need to isolate the

satellite cells from the basal lamina³⁸. Though seemingly simpler, whole muscle fiber culture is less ideal when compared to using isolated satellite cells because it requires more muscle tissue to start the culture³⁸. Satellite cells can be isolated and expanded under traditional tissue culture conditions while requiring very little muscle tissue to start³⁸. Alternatively, skeletal muscle tissue can be cultured using immortalized cells.

The current state-of-the-art: Several cell lines are commonly used for skeletal muscle research, including quail muscle clone 7 (QM7s), mouse myoblasts (C2C12s), and rat myoblasts (L6). Though these cell lines may not be suitable for food applications, immortalized cell lines can be created from more suitable primary cell types⁴³. Hayflick's Limit describes the number of times that a somatic cell can divide due to the shortening of telomeres⁴⁴. Immortalized cell lines differ from primary cell lines in that they are not subject to Hayflick's Limit, and as such proliferate much longer than primary cells while maintaining predictable proliferation and differentiation characteristics^{44,45}. This characteristic makes immortalized cell lines ideal for commercial meat production as it would greatly reduce the amount of tissue that the meat industry would consume once an immortalized cell line is established. In the case of bovine satellite cells, such a cell line can be created through upregulation of bovine telomerase reverse transcriptase (TERT) and Cyclin-dependent kinase 4 (CDK4)⁴³. However, repeated expansion may increase the potential of significant mutations and emergent properties over time. Sufficiently mature skeletal muscle tissue is characterized by the fusion of myoblast cells resulting in multinucleated myofibers. Additionally, such mature muscle tissue will also possess fully developed sarcomeres. Sarcomere development can be assessed visually using light microscopy and by the presence of contraction associated proteins like myosin heavy-chain (MyHC), sarcomeric α -actin (SAA), and desmin. Mature skeletal muscle fibers also possess many more mitochondria than other cell types. Lastly mature skeletal muscle is both electrically and mechanically active. Mechanical contractions can be induced by exposing the cells to an electrical current. This mechanical contraction can be observed and quantified by recording the contraction using

light microscopy. The electrical activity of the muscle fibers can be observed using fluo-4, which fluoresces in the presence of intracellular calcium allowing the reaction to be observed using fluorescence microscopy.

At the laboratory scale, cells are typically expanded in tissue culture flasks. However, the scale required for commercial meat production would render the use of tissue culture flasks prohibitively expensive, space-intensive, and ultimately impractical. Producing biomass on a large scale is essential for meeting the demand for structured meat products and reducing production costs. Anchorage-dependent cell types, which require a substrate for adhesion and growth, pose challenges in generating sufficient biomass. To address this, many bioreactors utilize suspension culture, where microcarriers act as a substrate for anchorage-dependent cells. These microcarriers can be tailored to match specific cell requirements by adjusting properties like size, shape, porosity, stiffness, and surface functionalization^{46,47}. Microcarriers can be constructed from different materials, some of which are non-edible (e.g., glass, polystyrene) and require cell removal post-expansion, while others are biodegradable or edible (e.g., cellulose, alginate, chitosan), eliminating the need for cell separation^{46,47}. For example, edible microcarriers, like decellularized broccoli florets, have been used to culture satellite cells, which can potentially be consumed along with the cells when producing lab-grown meat products like chicken nuggets and ground beef⁴⁸.

Stirred-tank bioreactors are widely employed for cultivating various microorganisms and anchorage-dependent cells adhered to microcarriers. They use impellers to agitate the culture, ensuring uniform temperature, oxygen levels, and nutrient distribution⁴⁹⁻⁵¹. However, impeller-induced shear forces may damage or dislodge cells from their microcarriers⁵². Airlift bioreactors, another microcarrier-based cell culture system, rely on sparging gases to induce agitation. While gentler on cells and reducing shear stresses, they can pose challenges in maintaining consistent flow when scaled up⁵³. Rotating wall bioreactors create a low-shear environment by continuously rotating a cylindrical vessel filled with cells

and culture medium, simulating microgravity. This prevents cell settling, reduces aggregate formation, and promotes uniform nutrient and gas distribution ⁵⁴. In contrast, other designs involve fixed cells with medium perfused through a cell-laden substrate. Examples include hollow fiber bioreactors, consisting of thin, semi-permeable fibers for cell growth, and fixed-bed bioreactors, which immobilize cells in a porous substrate, making them compact but challenging for cell harvesting ⁵⁴⁻⁵⁶.

So far, bioreactor designs covered in this section have been discussed within the context of cell proliferation and biomass generation. However, once enough biomass is achieved, the role of bioreactors extends to differentiation. Creating a bioreactor specifically tailored to produce structured skeletal muscle tissue poses significant challenges due to the unique requirements for skeletal muscle maturation. Ideal conditions for skeletal muscle differentiation include not only fundamental elements like specialized differentiation media but also nuanced factors like precise mechanical tension ^{41,57-59}. While bioreactors for skeletal muscle differentiation exist at the laboratory scale, there is a lack of widely adopted bioreactors specifically designed for large-scale skeletal muscle differentiation ^{60,61}.

2.5 Media – Biological Signals and Resources

The term medium refers to the cocktail of substances that supports the growth of cells in several ways. A combination of salts allow media to serve most basic functions of media which is to maintain osmotic balance. Media are also responsible for providing essential amino acids, which support essential cellular processes and allow the cells to produce the proteins to form their cell type specific structures and functions. One of the most essential functions of culture media is to provide an energy source, typically in the form of glucose. Mammalian cells undergo glycolysis to convert glucose into pyruvate followed by aerobic respiration to generate ATP ⁶². To facilitate aerobic respiration, the cell incubator's atmosphere is adjusted to maintain 5% CO₂ and 21% O₂ ⁶³. In dense cell populations oxygen may become depleted and lactic acid may begin to accumulate as a byproduct of anaerobic respiration in long-term cultures ^{63,64}. The dissociation of lactic acid into lactate and hydrogen ions lowers the pH of the culture medium. As pH

decreases, the medium becomes increasingly toxic to the cells ⁶³. To counteract this acidification of the culture medium, a buffering agent such as bicarbonate is added. Bicarbonate reacts with excess hydrogen ions in the medium to form carbonic acid, which slows the pH decrease ⁶⁴. Carbonic acid dissociates into water and carbon dioxide. Some media formulations use zwitterions like HEPES as a chemical buffering agent. HEPES is capable of both accepting and donating H⁺ ions, accepting H⁺ ions when the medium becomes acidic and donating H⁺ ion when the medium becomes more basic ⁶³. Phenol red is frequently added to cell culture media as a pH indicator, where its color change indicates when the medium needs to be replaced. Experiments involving the use of light-based assays of estrogen-responsive cells may warrant the exclusion of phenol red from culture media. The phenol red color may interfere with light-based measurements such as flow cytometry and the estrogen-like structure of phenol red may stimulate proliferation and suppress the response of estrogen-responsive cells to estrogenous estrogen ^{63,65}.

Media also contain serum sources from the blood of animals, typically fetal bovine serum (FBS). The serum serves several functions, and the specific mechanisms of its functions are not well understood. It provides a cocktail of proteins that absorb to the substrate and aid in cellular attachment. Some of the proteins in FBS have a mitogenic effect and stimulate cells to proliferate. Modulating serum concentration is a common strategy used to trigger many myoblast cell lines to differentiate and form myotubes. Finally, the cell culture medium is also supplemented with additional cytokines and growth factors that are specific to the cell type that it is designed to support. Fibroblast Growth Factor 2 (FGF2), one of the most well understood growth factors, is a protein produced in many different tissues in the body known to stimulate satellite cell proliferation and inhibit differentiation. The proliferation promoting qualities of HGF are shared with other growth factors including Hepatocyte Growth Factor (HGF), which is also expressed in a wide range of tissues, Epidermal Growth Factor (EGF), and Platelet-derived Growth Factor (PDGF) ^{40,58,66,67}. Most notably known for its metabolic role in the body, insulin can also promote cell proliferation. Transferrin's role is to aid DNA and protein synthesis by transporting Fe³⁺ ions into the cell. Albeit not a

protein, selenium is a mineral that helps protect cells from free-radical induced damage. Insulin, transferrin, and selenium are often used together in a supplement aptly named insulin-transferrin-selenium (ITS).

There are many different types of cell culture media, each tailored to support a specific cell type. However, designing a medium to support more than one cell type in the same culture is more complicated. Such a scenario is called co-culture. A medium designed to support a coculture must satisfy all the needs of each of the cell types in the co-culture. This is no trivial task considering that often the needs of one cell type may conflict with the needs of another cell type. A situation relevant to the context of this research is the co-culture of muscle and fat cells. Muscle tissue contains skeletal muscle cells, but it also contains intramuscular fat. In meat, this intramuscular fat forms the marbling in more premium cuts of meat. However, it has been suggested that the cells themselves may release cytokines that influence one another. For example, it has been suggested that the differentiation of satellite cells into myoblasts may inhibit the differentiation of preadipocytes ⁶⁸. More accurate *in vivo* models would incorporate more supportive cell types. Fibroblasts form connective tissues, which then form ECM, that helps to support the structure of skeletal muscle tissues ⁶⁹. Connective tissues, for example, aid in the arrangement of muscle fibers into fascicles and offer paths for nerves and blood vessels ⁶⁹. Replicating these tissues would necessitate the inclusion of neurons, smooth muscle, and epithelial cells, complicating the media composition even further. However, such accurate models that include nervous and vascular tissues are unlikely to be required for meat as it may not be necessary to replicate the contractile performance of *in vivo* skeletal muscle. In addition to the biological challenges of media formulation, media also pose challenges to biomass production at large scale.

Media are one of the most expensive elements in cell culture. Most of this cost comes from the serum and supplemented proteins. This extensive cost is exacerbated by the fact that the media needs to be frequently replaced, typically every 48 hours, to replace proteins that have been exhausted or denatured.

Several strategies have been used to use media more efficiently. Some of these strategies include finding alternative substances to serve the same function as the serum. In pursuit of a serum-free medium, other organisms such as bacteria, algae, or barley are used to produce growth factors and other proteins. For example, B8 is a serum-free media that has been demonstrated to support the growth of mesenchymal stem cells. However, to support the growth of satellite cells, B8 media must be supplemented with proteins such as recombinant albumin ⁷⁰.

2.6 Scaffolds – Substrates and Applicable Fabrication Methods

There are several materials that can be used to create 3D scaffolds for skeletal muscle tissue engineering, however the process is more difficult than the creation of 2D cultures. In 3D culture systems, the biopolymer scaffold must support cell growth in all 3 dimensions, necessitating a more intricate structure and mechanical properties. In addition, the scaffold must provide adequate nutrient and oxygen supply to the cells in the scaffold's core, which may be limited by diffusion constraints. Most cells must be within 200 μm of an oxygen source else they quickly begin to die. Nature has overcome this challenge by developing complex plumbing systems, vasculature, to transport oxygen and other essential compounds to every cell within large multicellular organisms. To avoid the formation of necrotic regions in engineered skeletal muscle tissues, similar vasculature networks are required.

There are 3 paradigms of vasculature solutions for tissue engineering applications: neoangiogenesis, neovascularization, and prevascularization ⁵. Neoangiogenesis exploits endothelial cells and their ability to form new vasculature when exposed to stimuli like Vascular Endothelial Growth Factor (VEGF) ⁷¹. Neovascularization involves using existing vascular tissue and stimuli to encourage new vessel formation ^{5,71}. Though promising for regenerative medicine applications, neoangiogenesis and neovascularization strategies are too expensive to be feasible at the scale of commercial meat production ³. Prevascularization involves using biopolymers, such as collagen and gelatin, or manufactured synthetic

polymers, such as polycaprolactone (PCL) and polyurethane (PU) to create conduits that facilitate the transport of oxygen and nutrients to cells growing on the scaffold ⁷².

Hydrogels are versatile materials and are suitable for numerous applications due to their tunable porosity, topography, and mechanical properties ^{73,74}. There are many different polymers and biopolymers that can be used to make hydrogels by crosslinking in a water-based solution. They are also moldable and can take on almost any desirable shape. Electrospinning is a fabrication method that employs electrostatic force to drag material onto a collection drum ⁷³. Like hydrogels, electrospinning can be used with many different substances and the resulting material can be customized further because the fiber diameter may be precisely controlled ⁷¹. Due to evidence suggesting that scaffold fiber diameter affects the efficiency with which skeletal muscle differentiates ⁷⁵, Controlling fiber diameter makes electrospinning particularly useful for skeletal muscle culture. Using 3D printing, it is possible to precisely distribute several cell types on a substrate ^{76,77}. Cells are suspended in "bioinks," which serve as the cells' 3D media. They contain all of the necessary substances that would normally be found in the culture medium. Though there are many proprietary bioinks, many of the same hydrogels used in traditional biomaterial manufacturing methods can also be utilized to create these bioinks, and they can be mixed with other materials to alter the mechanical, chemical, and bioactive properties of the entire structure ^{78,79}. In combination with other manufacturing methods, 3D printing allows for more exact control over the spatial distribution of cell populations on a surface and allows for the modification of topographies.

Each of these fabrication methods has shown promise for growing skeletal muscle in one manner or another ^{73,75,78,80-82}. They share, however, some similar limitations in terms of progress toward *in vitro* meat production. The availability of a suitable biomaterial to produce meat for human consumption is currently limited. Collagen, fibronectin, laminin, and gelatin are biopolymers that are commonly used in skeletal muscle cell culture. These biopolymers can be coated on the surface of culture dishes, plates, and other surfaces to promote cell adhesion and proliferation. Biopolymers can influence cell behavior and

differentiation by providing biochemical cues that mimic the extracellular matrix (ECM) of natural tissue. The choice of biopolymer for 2D culture is influenced by factors such as the type of cells used, the desired mechanical properties of the substrate, and the biochemical signals required to promote cell growth and differentiation. However, these substrates are typically obtained from animal tissues, so their use is counterproductive. If we continue to rely on animal derived materials, we will just be contributing to the problems caused by industrialized meat production.

Alternatively, these same biopolymers can be synthesized or produced using genetically modified organisms. This would reduce the reliance on animal derived materials, However, using synthetic or recombinant biopolymers as the primary mass component is both expensive and unfeasible on a commercial scale. Synthetic polymer like polycaprolactone (PLC) and polyurethane (PU) would need to be removed during tissue development to clear the lumen of the manufactured conduits and to remove the inedible components of the scaffold ^{3,5}. Thoroughly removing the synthetic materials from microscopic conduits would become cumbersome. Even bioresorbable materials like polylactic acid (PLA) and polylactic-glycolic acid (PLGA) would require significant tuning of the degradation rate to ensure that the material is completely removed ⁸³. Failure to remove the material will result in insufficient perfusion of the scaffold and user consumption of inedible materials remaining in the finished product.

Rather than developing complex conduits artificially, many studies have used natural vasculature through the process of decellularization ^{6,7,84}. Decellularization, is the process of removing all cellular material from a tissue or organ leaving only the extracellular matrix and the vasculature remains intact ^{6,7,84}. Decellularization of mammalian tissues, like recombinant biopolymer scaffolds, is unproductive because it requires sacrificial mammalian tissue to create the scaffold. Decellularization can also be used, however, on plant and fungal tissue to produce scaffolds with properties that are unique to the specific species and tissue type used.

When grown under certain conditions, skeletal muscle tissue can self-delaminate from 2D substrates to form cylindrical muscle contracts without the use of scaffolding to facilitate the 3D structure ⁶⁰. This method is not ideal because recombinant biopolymers are used for the 2D substrate, and the delamination process is not optimal for commercial scale.

Recently, studies have used a heterogeneity of satellite cells and fibroblasts to produce self-assembling skeletal muscle tissues *in vitro* when the usage of biopolymers is not suitable. The fibroblasts are responsible for producing the necessary ECM, which the satellite cells inhabit. Micropatterned substrates can also be used to direct cell alignment within a tissue. The tissue self-delaminates as the satellite cells differentiate and fuse into myotubes within the ECM ⁸⁵.

2.7 Decellularized Plant Scaffolds and their Potential Application in Cellular Agriculture

Plant leaves are composed of various layers, the outermost layer is the epidermis, which provides protection and produces the cuticle, a waxy coating ^{86,87}. Beneath the epidermis is the mesophyll, differentiated into palisade and spongy tissues ⁸⁶. The palisade tissue contains cells that are closely packed to capture sunlight for photosynthesis, while the spongy tissue facilitates gas exchange ⁸⁶. Scattered throughout the leaf's surfaces are stomata, small openings that regulate gas and water vapor exchange ⁸⁶. There are two types of vascular tissue in plants: xylem and phloem ^{72,88,89}. Their vascular configuration is one characteristic that distinguishes the two. The parallel, uniformly sized vascular bundles of monocots diverge at the base of the leaf, run parallel throughout the length of the leaf, and converge at the distal tip as shown in Figure 3 ⁹⁰. Dicots have vascular bundles that branch out in fractal patterns from a single,

large bundle. With each generation of daughter bundles, the vascular bundles' diameter gets smaller. Dicot plants have a large, centralized bundle that is useful for the active perfusion of the vascular system inside the leaf. The vascular network eventually terminates within the porous intervascular tissue (spongy mesophyll) of the leaf.

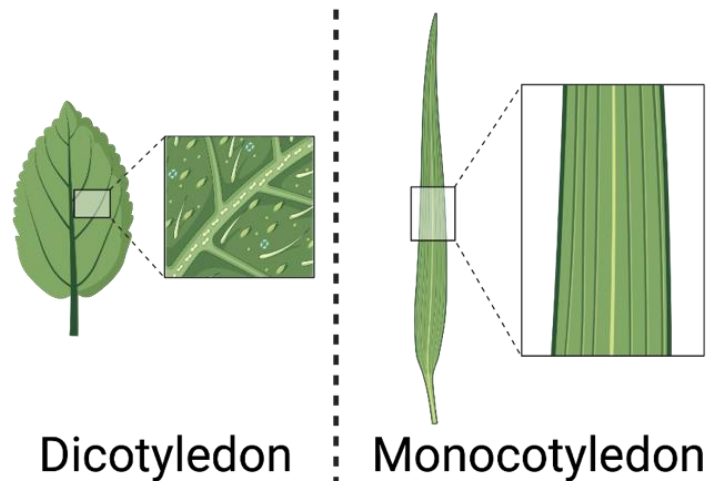


Figure 3 | Dicot vs. monocot structure

CO₂ enters the leaf through the stomata on the surface of the leaf and the CO₂ diffuses throughout the pores of the spongy mesophyll⁹¹. In respect to the leaf's function as a scaffold, the mesophyll, acts as a spongy medium that facilitates the movement of perfused fluids to the pores in the leaf's surface where the fluid can exit⁹². The palisade mesophyll is the tissue layer directly adjacent to the spongy mesophyll and contains most of the chloroplasts in the leaf. As such, the palisade mesophyll is responsible for light collection for photosynthesis⁹¹.

The leaf's extracellular matrix is composed of cellulose. Two major components of this matrix in plant cells are lignin and pectin^{86,88}. Lignin, a phenolic polymer, is primarily found in the secondary cell wall and is crucial for providing rigidity⁸⁸. whereas, pectin, a polysaccharide, is primarily located in the primary cell wall and middle lamella, playing a vital role in plant cell adhesion. Lignin and pectin greatly influence the stiffness and rigidity of plant tissues. Lignin provides rigidity, making plants stand upright and resist mechanical stresses. Pectin offers flexibility. The amount and distribution of these components in the cell walls determine the stiffness. A leaf with a higher lignin content will generally be stiffer and less pliable, whereas one with more pectin will be more flexible. The surface stiffness of the leaf could have a significant influence on the ability of the PBSCs to fuse and differentiate⁹³.

Our laboratory has previously demonstrated that decellularized plant tissue can be used as a prevascularized scaffold to support functional stem cell derived cardiomyocytes^{6,48,94}

3D tissue culture may be achieved with plant scaffolds by growing 200 µm thick tissue layers on the surface of the leaf scaffolds and stacking multiple cell laden scaffolds on top of one another to form even thicker tissues. The vascular network of the leaf can then be perfused to deliver oxygen and nutrients to cells located between scaffolds that are isolated from the cell growth medium. Additionally, many plant species such as spinach and leek are edible and can be consumed whole as a finished product without complications. This feature eliminates the need to remove material from the finished product as required with synthetic polymer scaffolds. The edibility of plants like spinach and leek may also render the decellularization process unnecessary, further reducing processing steps and streamlining the manufacturing process. In addition to the beneficial features of edible plants, different plant vascular topologies may offer unique advantages when attempting to produce structured meat products.

Chapter 3 – Decellularized Spinach Leaves as a Suitable Scaffold

Some of the content in this chapter is contained in the publications:

1. Jones, J. D., Rebello, A. S. & Gaudette, G. R. Decellularized spinach: An edible scaffold for laboratory-grown meat. *Food Biosci* **41**, (2021).
2. Jones, J. D. *et al.* Decellularization : Leveraging a Tissue Engineering Technique for Food Production. (2023) doi:10.1021/acsbmaterials.2c01421.

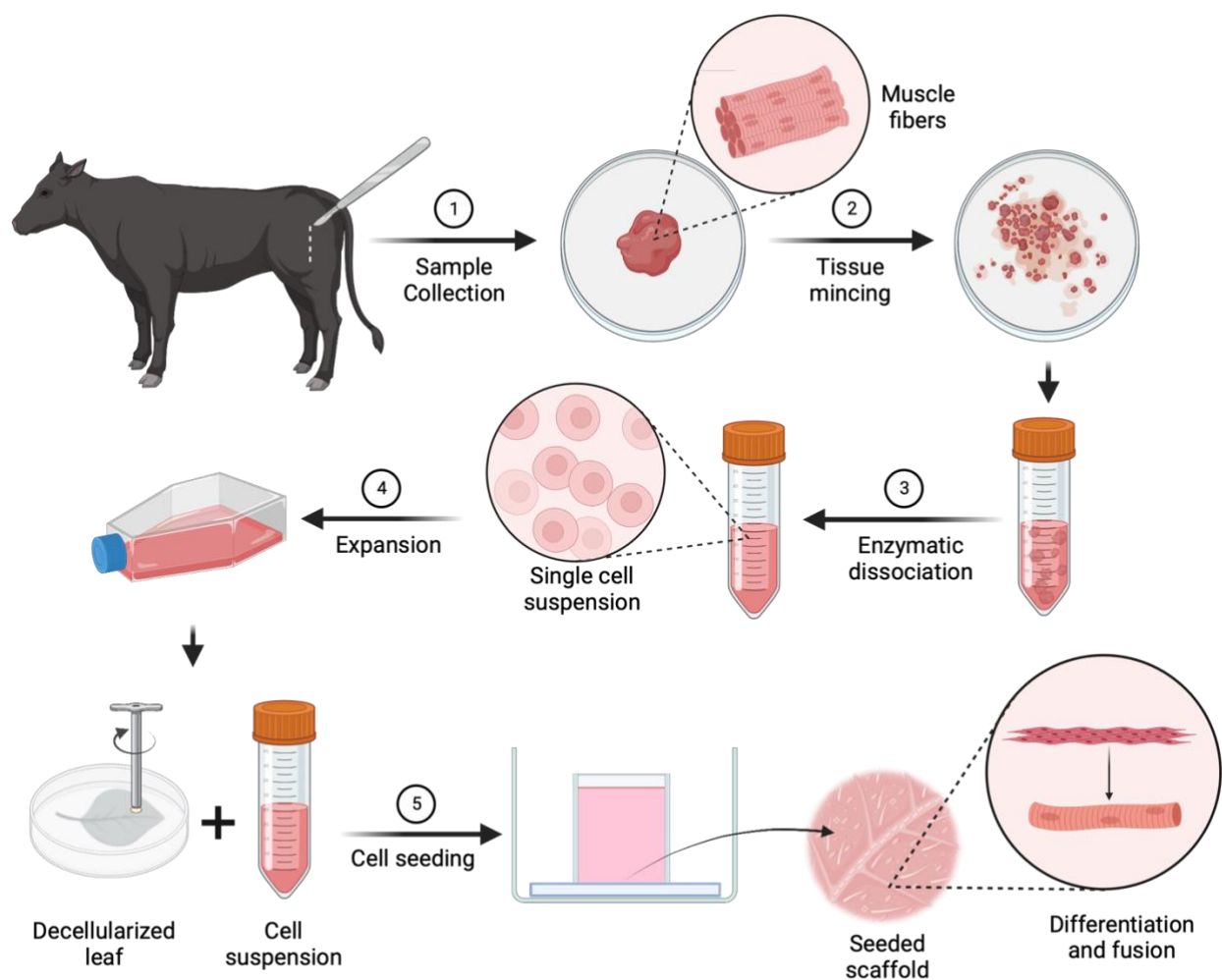


Figure 4| Diagram of cell isolation, expansion and differentiation strategy

This aim will assess the feasibility of decellularized plant leaves as a scaffold for satellite cell culture and differentiation. Hypothesis: There will be no statistically significant difference in satellite cell viability and fusion index between the group grown on decellularized leaves and the group cultured on gelatin covered glass. There will be a statistically significant reduction in satellite cell viability when cultured on the surface of non-decellularized leaves compared to those cultured on the surface of decellularized leaves.

Aim 1A: Examine the viability, differentiation capacity, and alignment characteristics of satellite cells grown on the surface of decellularized spinach scaffolds.

3A.1 Introduction

Several cell lines are used in skeletal muscle research, with C2C12s being among the most common. While they serve as a valuable model, they are not only unpalatable but also unrepresentative of cells from species that are frequently consumed as food. In the US, the primary animals consumed for food are cows, pigs, chickens, and fish, which are processed into beef, pork, poultry, and seafood respectively. For cows, bovine satellite cells tend to have slower proliferation rates ¹⁶. In contrast, avian satellite cells from chickens exhibit faster growth rates but tend to differentiate into myotubes more rapidly, which can limit their expansion potential. Porcine satellite cells fall between the bovine and avian satellite cells in terms of proliferation rates, but they have their own unique culturing requirements, needing distinct growth factors and signaling molecules ¹⁶. Fish satellite cells, particularly from species like salmon, show adaptability to various culturing conditions. However, they require colder culture temperatures to simulate their natural cold aquatic habitats ¹⁶.

Poultry is rapidly becoming the most widely consumed meat. In 2019, around the world, an average of 14.7 kg of chicken was consumed per capita, compared to 6.4 kg of beef ⁹⁵. However, the environmental footprint of each species can vary greatly. It is generally accepted that beef production requires more land

than the production of other animal products. Cattle require up to 4,000 m³ per head of beef, whereas pigs may require 6 m³ per head¹⁴. It takes approximately 31.5 kWh of energy to produce 1 pound of beef, whereas chicken only requires 4.4 kWh¹⁴. Given these figures, research related to bovine cells might yield the most significant insights due to its larger footprint.

Meat is comprised of several cell types including satellite cells (muscle), preadipocytes (fat), and fibroblasts (connective tissue). A parallel study on preadipocytes would offer insights into their viability and differentiation capacity on decellularized spinach scaffolds. These precursor cells are an integral part of adipose tissue, which is primarily responsible for lipid storage. Unlike mature adipocytes, which are characterized by large lipid droplets, preadipocytes lack droplets and express different genes such as *pref-1*⁹⁶. The transition from a preadipocyte to a mature adipocyte is a process called adipogenesis, which is driven by a complex cascade of gene expression changes influenced by transcription factors like PPAR γ and C/EBP α . Differentiation is induced by exposing the cells to a cocktail of agents, including insulin, dexamethasone, and isobutylmethylxanthine (IBMX)⁹⁷. Upon successful differentiation, cells begin to accumulate lipid droplets. This data is valuable because any meat substitute using this scaffold will require fat integration to mimic the taste and texture of traditional meat. Large adipocyte regions could emulate the marbling seen in conventional meat cuts. Additionally, bovine fibroblasts represent the fascia surrounding other tissues and contribute extensively to the texture of meat, making them invaluable for comprehensive studies. Given that the primary component of meat is skeletal muscle tissue, satellite cells appear to be ideal for this study.

3D scaffolds for skeletal muscle tissue engineering pose significant challenges compared to 2D cultures, primarily due to the need to provide adequate nutrient and oxygen supply to cells in the interior of the tissue. Cells located more than 200 μ m from an oxygen source will begin to die, forming a necrotic region in the tissue. This challenge has led to convergent evolution, resulting in several variations of vascular networks that transport vital nutrients across different species. Traditional tissue engineering methods,

which use growth factors and cells to stimulate vasculature formation in vitro, are too expensive for large-scale meat production. Both natural and synthetic polymers can be employed to create scaffold materials through various methods. Electrospinning provides control over scaffold features, such as porosity. In contrast, 3D printing facilitates the placement of different cell types within the scaffold. Despite the potential of these techniques, there is still a lack of a comprehensive material and fabrication solution for 3D skeletal muscle culture. Relying on animal-derived substrates is not sustainable for meat production and using recombinant biopolymers prohibitively expensive. While natural vasculature from decellularized tissue can serve as conduits, depending on animal tissues is counterproductive. Spinach leaves lack the animal-derived components found in other commonly used scaffolds like gelatin and are inexpensive, familiar, and widely accessible. By assessing the viability, differentiation, and alignment of bovine primary satellite cells on a leaf scaffold, this study expands on past work by investigating the efficiency of decellularized spinach in meat production.

3A.2 Materials and Methods

3A.2.1 Experiment Design Overview

Three biological replicates from 3 different 2-year-old male Holstein bulls grown for meat without the use of growth hormones were used in these trials. The animals came from Adams Farm in Athol, Massachusetts, and were electrocuted before being killed. Each animal's front legs' shank area was used to obtain tissue samples, yielding a total of 9 samples (3 technical replicates for each biological replicate). Isolated satellite cells cultured on glass slides coated with gelatin as a control group were compared to cells grown on decellularized spinach. Gelatin, a derivative of collagen, has the potential for culinary applications that support the growth of cells, making it a useful material to compare with decellularized leaf scaffolds³

3A.2.2 Spinach Leaf Decellularization and Scaffold Preparation

The immersion method of leaf decellularization was used ^{6,7}

Triple washed packaged baby spinach leaves (Olivia's Organics, Chelsea, MA, USA) were acquired from a local food store. Cuticles were removed from spinach leaves by agitating them in 98% hexane (VWR, Radnor, PA, USA) for 3 min, followed by 1x phosphate buffered saline (PBS) (137 mM sodium chloride (NaCl), 112.7 mM potassium chloride (KCl), 10 mM di-sodium hydrogen phosphate anhydrous (Na₂HPO₄), 1.8 mM potassium dihydrogen phosphate (KH₂PO₄) in deionized water (diH₂O)) for 3 minutes (min). All solutions used deionized water produced by the Ultrapure Direct-Q water system (MilliporeSigma, Burlington, MA, USA). Three cycles of hexanes and PBS were sufficient to remove the cuticle. After complete removal of the cuticle, spinach leaves were placed in 50 mL conical tubes and submerged for 5 days (d) in 1% SDS (Sigma-Aldrich, St. Louis, MO, USA) in diH₂O, with the solution being refreshed every 24 hours (hr). After 5 d, the SDS solution was replaced with 0.1% Triton X-100 (Sigma-Aldrich) and 10% concentrated bleach (The Clorox Co., Oakland, CA, USA) in diH₂O for 48 hr, with the solution being refreshed every 24 hr. The spinach leaves were then washed for 24 hr in diH₂O. After rinsing, the leaves were incubated for 24 hr in 10 mM tris buffer (Sigma-Aldrich). The leaves were stored overnight at 20 °C. Lyophilization (Labconco Corp., Kansas City, MO, USA, FreeZone Triad 74000 series) was performed at 25 °C and 0.21 Torr for 24 hr. Decellularized spinach scaffolds were stored at room temperature (RT), approximately 21 - 23 °C, for up to two weeks (wk) until required. The room's ambient temperature was not monitored.

A 12 mm diameter biopsy punch with a 12 mm diameter was used to create scaffolds of uniform size. The scaffolds were then rehydrated for 15 min at RT using a 10 mM tris buffer with a pH of 9.0. The scaffolds were sterilized by incubating them for 30 min in a sterile dish containing 70% ethanol inside a laminar flow hood. Following sterilization, the scaffolds were rinsed 3 times with sterile PBS, with a 5 min interval between each rinse. The cell seeding process was completed in a polystyrene 12-well plate (Thermo Fisher

Scientific) coated with polydimethylsiloxane (PDMS) (Dow Chemical, Midland, MI, USA). The PDMS was crosslinked by combining the base PDMS elastomer and the proprietary platinum-based curing agent at a ratio of 10:1 and degassing it for 1 hr in a Bel-Art benchtop polycarbonate vacuum desiccator (Bel-Art Products, South Wayne, NJ, USA) to eliminate air bubbles. Each well of the 12-well plate received approximately 1.5 mL of PDMS. The plate was then placed on a level surface overnight to allow the PDMS to cure. The hydrophobic nature of PDMS is used to prevent the cell suspension from overflowing the well's surface. Additionally, this prevented cells from adhering to the plate's surface. During the initial seeding period, the hydrophobicity ensured that most of the cell suspension adhered to the scaffold and that non-adherent cells could be washed away (Figure 4). Using sterile forceps, each leaf scaffold was transferred to a well on the PDMS-coated plate. Cloning cylinders with a 10 mm o.d. and 8 mm i.d. (Corning Life Sciences, Tewksbury, Massachusetts, United States) were placed over the scaffolds to further confine the cell suspension to a specific area. The cloning wells remained in place for the duration of cell seeding.

3A.2.3 DNA Analysis of Decellularized Leaf Scaffolds

DNA content was quantified to confirm sufficient decellularization. The samples were chopped to approximately 1 x 1 mm and placed in a 1.5 mL microcentrifuge tube (Eppendorf, Hamburg, Germany). The samples were flash-frozen in liquid nitrogen and pulverized immediately using a mortar and pestle to further reduce their size. The DNA content of the samples was determined using a fluorescence-based DNA quantification method, the CYQUANT® DNA assay kit (Thermo Fisher Scientific, Waltham, MA, USA). To release the DNA present in the sample, 100 µL of the lysis buffer included in the CYQUANT® DNA assay kit was added to each pulverized sample. The DNA was subsequently fluorescently labeled by adding 100 µL of CYQUANT® GR dye. Non-decellularized leaf samples served as the control to create a standard curve against which decellularized leaf samples were compared. Using a PerkinElmer Victor3 spectrophotometer (PerkinElmer, Waltham, MA, USA) with an excitation wavelength of 480 nm and an

emission wavelength of 530 nm, the fluorescence intensity was measured. Using a linear regression of the standard curve values, the fluorescence intensity value was then converted to DNA content.

3A.2.4 Primary Satellite Cell Isolation

The muscle samples were transported from the slaughterhouse to the laboratory in separate containers on ice for 30 min. Isolation of satellite cells began immediately upon arrival, (Figure 4). The isolation was completed within a laminar flow hood. Prior to isolation, all instruments and dishes were sterilized using a Tuttnauer EZ9-PLUS Steam Sterilizer (Tuttnauer NY, Huappaugue, NY, USA). The muscle tissue was placed on a sterile dish and incubated for 10 minutes in rinse medium (Ham's Dulbecco's modified Eagle's medium (DMEM/F12) (Thermo Fisher Scientific), with 1% penicillin/streptomycin (P/S) (Thermo Fisher Scientific).

The inner tissue was exposed by making a shallow horizontal cut through the muscle's center. The muscle tissue on either side of this incision was removed with sterile instruments to expose the interior tissue. The exposed interior muscle was collected and then dissected into 1 mm³ pieces. The samples were then placed in a sterile dish containing digestion medium (Ham's DMEM/F12, 1% P/S, and 10% recombinant collagenase derived from *Clostridium histolyticum* (Worthington, Lakewood, NJ, USA)) and incubated at 37 °C for 1 hr, while the dish was periodically stirred every 15 min. The contents of the dish were transferred to a conical 50 mL tube and allowed to settle. The supernatant was removed, filtered through a 100 µm sterile cell strainer (VWR), and centrifuged at 300 G for 5 min at room temperature. The tissue pellet was resuspended in 25 mL of sterile rinse medium (Ham's DMEM/F12, 1% P/S. The pellet was resuspended after each filtration using 70 µm and 40 µm cell strainers three times (Thermo Fisher Scientific) and centrifuged as already described. Following the final filtration, the pellet was resuspended in 12 mL of growth medium (Ham's DMEM/F12, plus 10% heat-inactivated fetal bovine serum (hiFBS) (Thermo Fisher Scientific), 1% P/S, 4 ng/mL recombinant human fibroblast growth factor 2 (FGF2), 2.5 ng/mL recombinant human hepatocyte growth factor (HGF), 10 ng/mL recombinant human epidermal

growth factor (EGF), and 5 ng/mL recombinant human insulin-like growth factor 1 (IGF)). To allow cell attachment, the isolated cells were incubated overnight at 37 °C and 5% CO₂ in a HERAcCell 150i CO₂ incubator (Thermo Fisher Scientific). Due to the inherent heterogeneity of the isolated population, the satellite cell population had to be enriched. Previous research has demonstrated that the satellite cell population can be enriched by pre-plating with differential adhesion⁹⁸. To remove unwanted cells from the population prior to subculturing, the cell suspension was plated on non-tissue culture polystyrene Petri dishes (Thermo Fisher Scientific) and incubated at 37 °C and 5% CO₂ for 30 min.

3A.2.5 Seeding Cells on Decellularized Leaf Scaffolds

A 20 µL sample was taken from the cell suspension. A hemocytometer (Hausser Scientific, Horsham, PA, USA) was used to estimate the number of cells present in the sample and the total cell population. Approximately 2x10⁵ cells were deposited directly onto the scaffold within the cloning well. After 24 hr of cell seeding, non-adherent cells were removed by gently rinsing the leaf surface with sterile PBS. The growth medium within the cloning well was replaced, and an additional 1 mL of cell growth medium was gently added to submerge the decellularized leaf completely.

3A.2.6 Viability Assessment of Satellite Cells

Cells were cultured in growth media after being sown. Every 48 hr, the growth medium was replaced. At 7 and 14 d, cells were examined. At the conclusion of each time point, the samples were stained with a LIVE/DEAD[®] staining kit (Thermo Fisher Scientific), a fluorescence-based viability stain consisting of calcein AM and ethidium homodimer-1, and fixed in 4% paraformaldehyde (PFA) for 10 min. Calcein AM is a fluorescent dye used to label the cytoplasm of living cells with an excitation wavelength of 494 nm and an emission wavelength of 514 nm. Used to label the nucleus of dead cells, ethidium homodimer-1 is a fluorescent dye with an excitation wavelength of 517 nm and an emission wavelength of 617 nm. Cells incubated in 70% ethanol for 30 min were used as a negative control. Hoechst 33342 (Thermo Fisher Scientific) was used to confirm the presence of a cell nucleus by staining samples with DNA. The viability

percentage was calculated using the image processing software FIJI-ImageJ 1.8.0 172 (National Institutes of Health (NIH), Rockville, MD, USA), downloaded from <https://imagej.net/Fiji>, to count the number of dead and living cells in each image ^{99,100}. Dead cells were indicated by the coincidence of the positive ethidium homodimer-1 signal and with the nucleus as indicated by the Hoechst signal. Cells lacking the dead marker were viable. Images were averaged to represent the overall viability.

3A.2.7 Assessment of differentiation potential

For 2 d, cells were maintained in growth medium. The specimens were then transferred to differentiation media containing 2% hiFBS, with the remaining media components remaining unchanged. At 5 and 12 d after differentiation media exposure, differentiation was examined (corresponding to 7 and 14 d after seeding). Specimens were fixed in 4% PFA and stained for myosin heavy chain (MyHC) with MF20 primary antibody (Developmental Studies Hybridoma Bank, Iowa City, IA, United States) and Alexa fluor 488 secondary antibody (Thermo Fisher Scientific). The specimen was stained with Hoechst 33342 and using the software FIJI-ImageJ 1.8.0 172 nuclei in each image were counted, and the percentage of differentiation was calculated. If the nucleus coincided with the fluorescent signal of the secondary antibody of the MyHC antibody, it was determined that the cell had differentiated. The remainder of the nuclei were identified as non-differentiated cells. The average of these images was used to represent the overall percentage of differentiation for the sample.

3A.2.8 Assessment of Cell Alignment

After exposure to the differentiation media for 5 and 12 d, alignment was measured. At the conclusion of each time point, the specimens were fixed in 4% PFA and stained with Phalloidin 488 (Life Technologies, Carlsbad, CA, USA) and Hoechst 33342 to detect F-actin.

At 20x magnification, samples were imaged with a Leica SP5 point scanning confocal microscope (Leica Microsystems). Measuring the orientation of the cell nuclei and cytoskeleton allowed the relative alignment of the cells to be determined.

OrientationJ, a Fiji plugin downloaded from <http://bigwww.epfl.ch/demo/orientation/>, was also used to generate a color survey of each image in order to better visualize the orientation of each microfilament as seen in Figure 5. The angle distribution of both the nuclei and the cytoskeleton was derived from these data. Each distribution's kurtosis, an index of the variability of the distribution of the measured variable, can be compared to another distribution's kurtosis to determine the degree of their relative alignment. As directional data were being collected, directional statistics were employed to examine the distributions. The most relevant metric is kappa, the angular analog to kurtosis¹⁰¹. Kappa represents the concentration of angle values in the distribution, with a value between 0 and 1^{101,102}. A value of 0 denotes a distribution with no discernible alignment, while a value of 1 denotes perfect and obvious alignment. The cell nuclei and cytoskeletons were measured independently for their alignment.

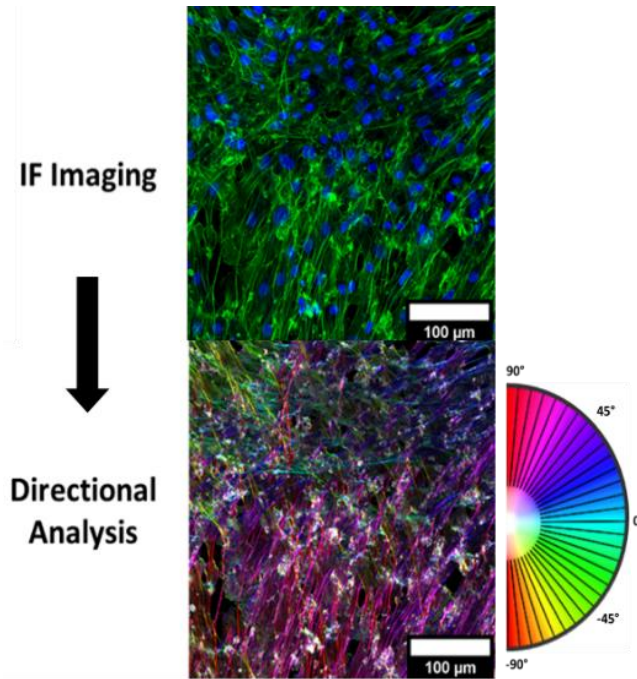


Figure 5 | Directional analysis of phalloidin stained bovine satellite cells cultured on gelatin coated glass. The color of each microfilament represents the orientation relative to the color wheel.

The directional data from these images were imported into MATLAB (MathWorks, Natick, Massachusetts, United States) and analyzed using the CircStat toolbox ¹⁰³. The mean vector length, angular standard deviation, and kappa value of the distribution were calculated using the circstat toolbox. The average kappa value for each image was used to represent the overall percentage of alignment for each sample.

3A.2.9 Imaging and Analysis

Unless specified otherwise, samples were imaged using a Leica SP5 point scanning confocal microscope (Leica Microsystems, Wetzlar, Germany) at 20X. Five images were taken per replicate in total. One image was taken from the center of the scaffold and from 4 locations around the edges of the seeded area. A total of 18 scaffolds were analyzed.

3A.2.10 Statistical Analysis

Statistical analysis was done using GraphPad Prism 9.0.0_121 (GraphPad, San Diego, CA, USA). Preliminary data demonstrated that the FI and kappa values for satellite cells cultured on gelatin coated glass were 0.14 ± 0.09 and 0.39 ± 0.13 respectively. When cultured on spinach leaf scaffolds the differentiation and alignment values were 0.27 ± 0.1 and 0.4 ± 0.3 respectively ³⁶

FI and kappa were expressed as mean \pm standard deviation. For each analysis method, a one-way ANOVA was used to compare the 3 substrates, with a statistically significance at $p \leq 0.05$. It was posited that satellite cells grown on spinach would have comparable average FI and kappa values when compared to satellite cells grown on gelatin coated glass at ($p \geq 0.05$).

3A.3 Results

3A.3.1 DNA Quantification of Decellularized Leaf Scaffolds

Compared to non-decellularized leaf material of the same mass, decellularization removed the majority of plant DNA from the leaf, as measured by DNA quantification of decellularized samples. Decellularized

samples contained an average of 73 ± 8 ng/mg of DNA, whereas non-decellularized leaf samples contained an average of 720 ± 80 ng/mg of DNA.

3A.3.2 Viability Measurement of Satellite Cells

After 7 d incubation in growth medium, the gelatin-cultured control group had an average of 100% viability with no detectable cell death (Figure 6a). This also held true for all groups grown on decellularized leaf scaffolds (Figure 6b). The control group, (Figure 6c), retained an average of 100% viability after 14 d incubation,. Cells cultured on decellularized leaf scaffolds also exhibited evidence of overall cell viability, (Figure 6c). All samples grown on a decellularized spinach scaffold exhibited comparable cell viability compared to the control group, (Figure 6c). Comparing the viability of cells grown on gelatin and decellularized leaf scaffolds using Welch's t-test revealed no statistically significant difference. Additionally, a one-way ANOVA test suggested that there was no significant difference in inter-animal viability among cells from all cows.

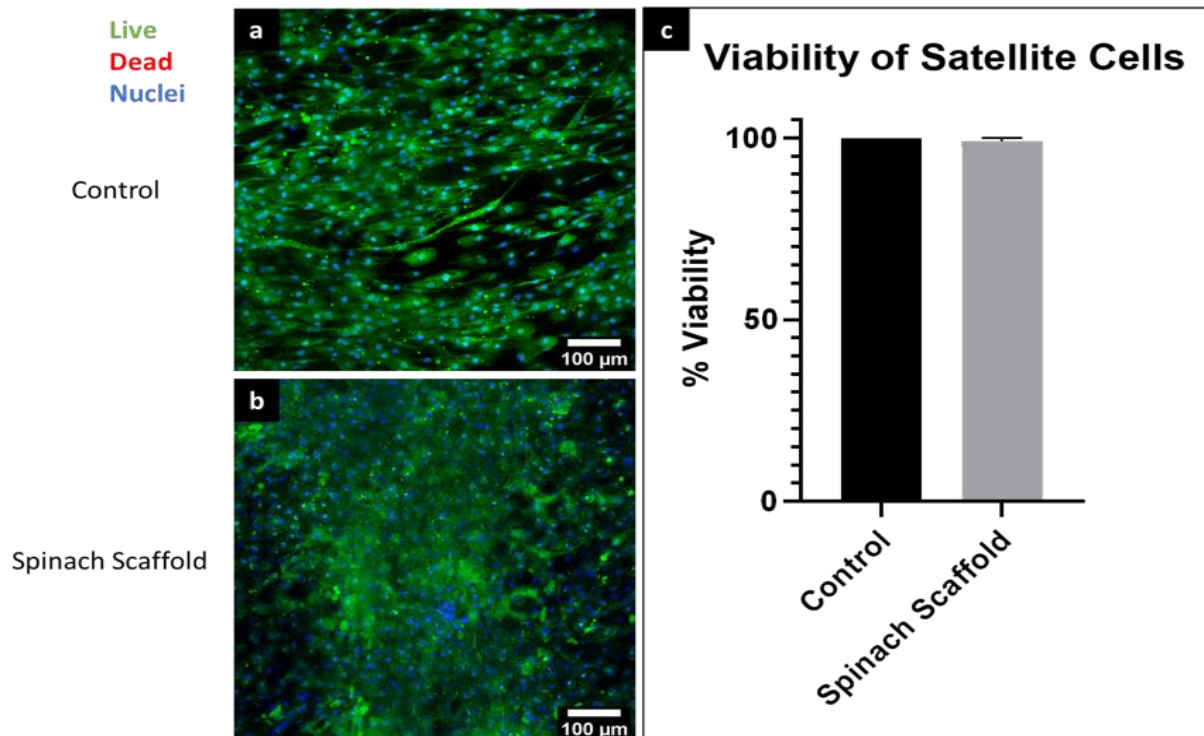


Figure 6] Primary bovine satellite cells (BPSC) remain viable after being cultured on decellularized spinach scaffold for 14 days (n=54). (a) PBSCs on decellularized spinach. (b) PBSCs on gelatin. (c) Comparison of PBSC viability

3A.3.3 Measurement of Differentiation Potential

After 7 d of differentiation, $7.8 \pm 1\%$ of the control population grown on gelatin were positive for MyHC. Cells from cow 1, 2, and 3 grown on decellularized spinach were positive for MyHC at 3.3 ± 1 , 0.48 ± 0.48 , and 0% , respectively, of the population. After 14 d there was no statistical difference between cells grown on gelatin and decellularized leaf scaffolds (Figure 7c). In addition, one-way ANOVA testing suggested that there was no significant difference in differentiation among cells from Cows 1, 2, and 3 at both 7 and 14 d. However, a t-test between 7 and 14 d incubation indicated difference between timepoints and differentiation percentages, suggesting a significant increase in cell differentiation over time.

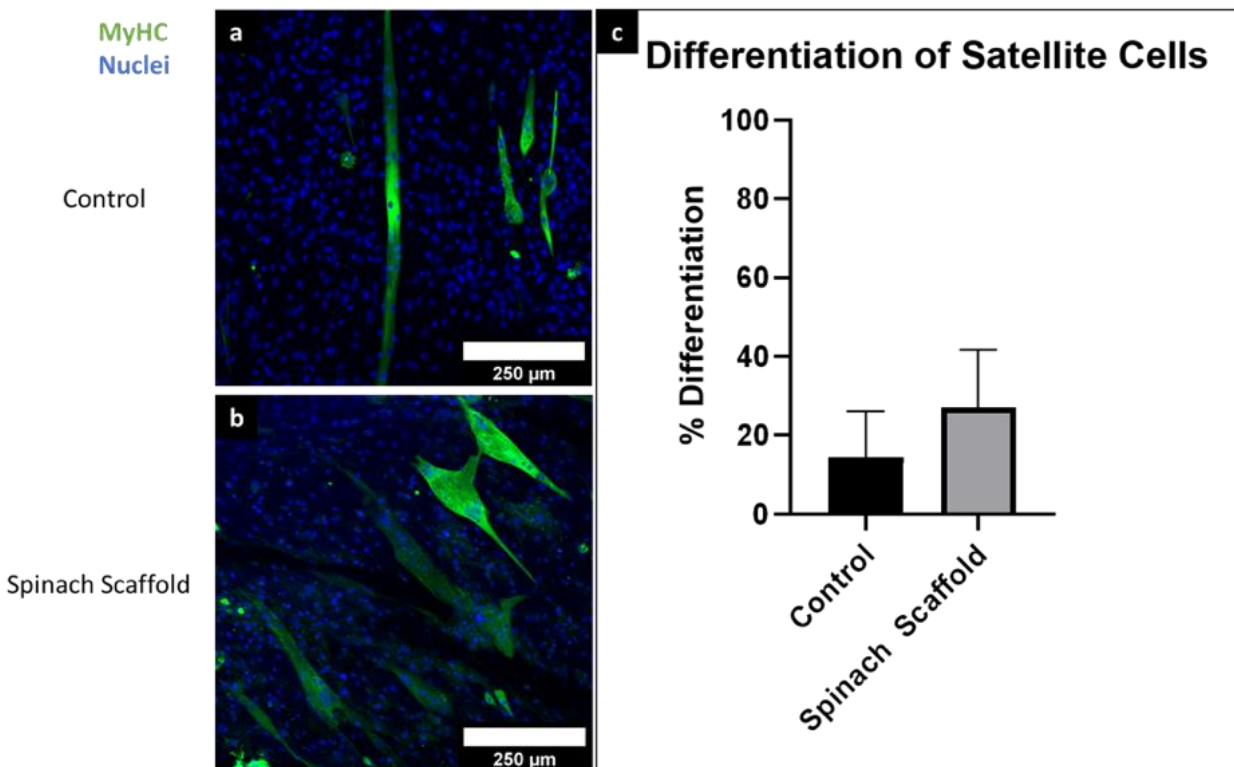


Figure 7 | Satellite cells show comparable differentiation capacity on decellularized spinach scaffolds after 14 days (n=54). (a) PBSC differentiation on gelatin. (b) PBSC differentiation on decellularized spinach. (c) Comparison of PBSC differentiation capacity

3A.3.4 Measurement of Cell Alignment

Cells differentiated on gelatin for 7 d showed signs of alignment within the images, but no indication of alignment throughout the seeding region. The cell population from Cow 1 grown on the decellularized leaf scaffolds showed relative alignment across all technical replicates. However, these results were not shared among the other biological replicates. Cells grown on decellularized leaf scaffolds from Cows 2 and 3 qualitatively showed inconsistent alignment, (Figure 8a). Similar to samples grown for 7 d, control cells differentiated for 14 d showed signs of local alignment within regions of the images, but no definitive alignment across the entire image. Cells from Cow 1 grown for 14 d on decellularized leaf scaffolds showed strong signs of alignment across entire images in all technical replicates. Cow 2 showed similar alignment in some images, but alignment was inconsistent among technical replicates. Cow 3, on the other hand, showed little signs of alignment between technical replicates.

Kappa values were used to quantitatively assess nuclear and cytoskeleton microfilament alignment within images of each sample. Samples differentiated for 7 d on gelatin had a relatively flat distributions with distinct peaks, (Figure 8b). Cells from Cow 1 that were cultured on the decellularized leaf scaffolds showed marginally better cytoskeleton alignment and significantly better nuclear alignment. Cytoskeletal and nuclear alignment for Cow 1 were 0.64 ± 0.05 and 0.37 ± 0.09 , respectively. The average cytoskeleton and nuclear kappa values were 0.13 ± 0.2 and 0.15 ± 0.05 for Cow 2, and 0.17 ± 0.3 and 0.011 ± 0.2 for Cow 3. Cytoskeletal alignment for Cows 2 and 3 on leaf scaffolds were lower than that of their gelatin controls with cytoskeletal and nuclear kappa values of 0.45 ± 0.1 and 0.091 ± 0.1 , respectively. After 14 d of differentiation, cells grown on gelatin showed little change in alignment compared to 7 days. The average kappa values for cytoskeletal and nuclear alignment of the control group were measured as 0.39 ± 0.09 and 0.21 ± 0.13 , respectively (Figure 8c). Similarly, all samples grown on the decellularized leaf scaffolds for 14 days showed comparable alignment to that observed after 7 d.

Cytoskeletal and nuclear alignments for Cow 1 grown for 14 d were 0.71 ± 0.09 and 0.36 ± 0.01 , respectively. The average cytoskeleton and nuclear kappa values were 0.47 ± 0.2 and 0.20 ± 0.03 for Cow 2, and 0.032 ± 0.087 and 0.05 ± 0.04 for Cow 3, respectively. Based on a Welch's t-test, there was no statistically significant difference in local alignment between cells grown on gelatin and on decellularized leaf scaffolds for both cytoskeletal and nuclear alignment. A one-way ANOVA test suggested that there was no statistical significance in relative alignment among cells from Cows 1 and 2 at both time points. However, a comparison of Cows 1 and 3 suggested that there was a significant difference in relative alignment between the groups.

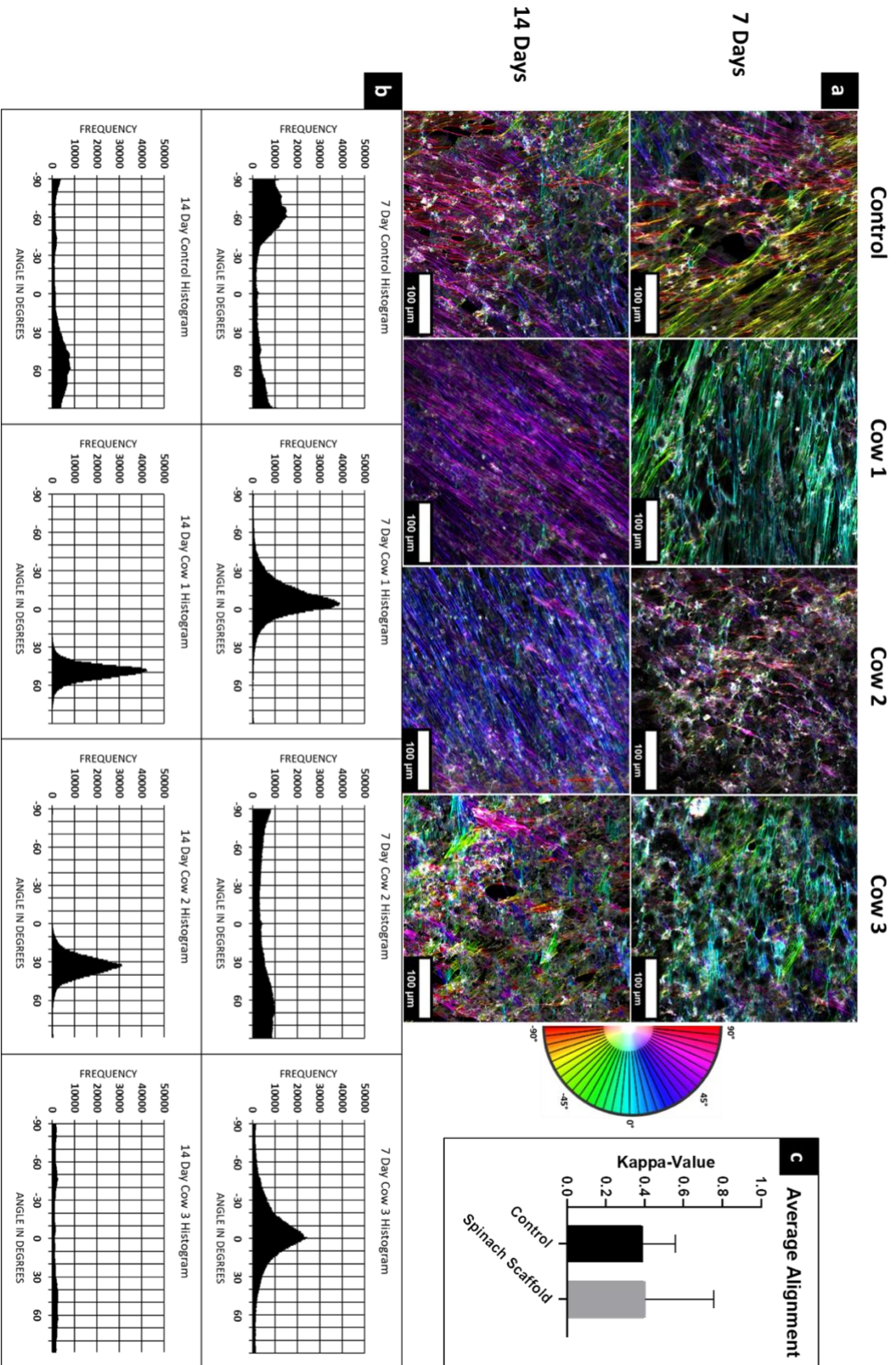


Figure 8 | Decellularized spinach scaffolds do not appear to direct satellite cell alignment (n=54). (a) Color survey of PBSC cytoskeleton. (b) Histogram of PBSC cytoskeleton orientation. (c) Comparison of PBSC alignment

3A.4 Discussion

The animal agriculture industry has long been a primary producer of food for people around the world. However, food production using conventional agriculture accounts for one of the highest contributors to environmental impact and resource usage both domestically and globally ¹⁰⁴. When pondering ways to eliminate the detrimental effects that human activity has on the environment, reforming meat production methods should be considered. Cellular agriculture, the biomanufacturing of animal meat products, presents an alternative to conventional meat production. The use of spinach as a substrate to grow PBSCs was studied. Previous studies showed that various cell types remain viable on decellularized plant scaffolds ^{6,7}

Spinach leaf samples decellularized using the immersion method had an average DNA content of 72 ± 8 ng/mg. Although this value is above of the commonly accepted threshold of ≤ 50 ng/mg for sufficiently decellularized tissue, it is not necessary to meet such a high standard for cultured meat application ¹⁰⁵. The standard accepted DNA threshold was established to minimize adverse host reaction of xenogeneic DNA from implanted decellularized tissues. In this application, decellularized spinach leaves will be used for consumption, not implantation. Spinach is typically consumed whole, and its DNA has no known danger. Any adverse effects stemming from the presence of xenogeneic DNA will likely be observed in the viability assessment of cells seeded on the surface of the scaffold. Although previous studies showed that various cell types can remain viable on decellularized plant scaffolds, it was necessary to confirm that this can be replicated with PBSCs ^{6,7}

Results showed that all cells had an average viability of $\geq 98\%$ after 14 d of culture. This showed that primary bovine satellite cells can remain viable on the surface of decellularized spinach scaffolds for extended periods of time with negligible cytotoxic effect. Should the decellularization process need to be refined for commercial use in food processing, better results may be attained by increasing the concentration of detergents used and the duration of exposure. The decellularization process would need

to be optimized to ensure that all remnants of the detergents have been removed from the tissue. The US Food and Drug Administration (FDA) has established that bleach is safe for use in food products if the final concentration of available Cl is < 200 ppm ¹⁰⁶.

While triton X-100 is not “Generally-Recognized-As-Safe” (GRAS), polysorbate 60, a potential alternative to triton X-100, is approved by the FDA for direct addition to foods ^{106,107}. In addition to being optimized to reduce the concentrations of remaining detergents in the leaf tissue after decellularization, the decellularization process may also need to be characterized and optimized to minimize adverse effects of the integrity of the surface, vascular network, and overall mechanical properties. Preliminary characterization of decellularized plants including decellularized spinach used scanning electron microscopy (SEM) to characterize the surface of decellularized leaves ^{6,7}

Mechanical testing showed that decellularized leaves have some mechanical properties similar to cardiac muscle. Decellularized spinach leaves had a maximum tangent modulus, a measure of elasticity, ranging from 0.2 – 0.5 MPa ⁶

While these results showed that primary bovine satellite cells can differentiate on the surface of decellularized spinach, for commercial use it will be necessary to optimize the differentiation conditions to increase the number of differentiated cells in the tissue. Such refinement may include further purification of the satellite cell population with the use of cell sorting tools such as fluorescence activated cell sorting (FACS) and magnetic activated cell sorting to isolate PAX7+ cells ⁹⁸. Vascular cell adhesion molecules have been shown to be a useful surface marker for achieving pure populations of PAX7+ satellite cells using FACS ¹⁰⁸. Differentiation efficiency may also be improved by modifying the media formulation of satellite cells grown on tissue culture plastic. Such changes may include elimination of growth factors and significant reduction or elimination of animal derived serum. Further studies can be done to assess the maturity and function of differentiated cells by staining for additional markers such as

desmin and sarcomeric α -actinin. In addition to the composition of the tissue, the arrangement of cells within the tissue is important.

To replicate the structure of muscle tissue *in vivo*, cells must be aligned with one another to form muscle fibers. Measurements of cellular alignment suggested that primary satellite cells do not spontaneously align on the surface of the scaffold. However, on many samples there were examples of high alignment across entire regions. It is possible that the local surface topography may have had some influence on how cells arranged themselves. Fontana et al. (2017) showed various surface topography in different plant species, which varied depending on location within the leaf. They also showed that cells aligned to topographical cues, suggesting that these features may be able to direct cell alignment and differentiation. For example, regions of the leaf that coincide with large vascular channels have crevasses directly above them. Cells that are seeded onto the leaf in these regions will settle into these crevasses. It is possible that local alignment is encouraged along the axis of the channel. Whereas regions that do not coincide with a vascular channel may lack these topographical cues. To assess the impact that surface topography may have on alignment, future studies could compare local alignment of cells grown on various regions of the leaf as this may be useful for creating organized muscle structures. Alternatively, plant leaves with grooved topographical features, such as banana leaves and turmeric leaves, could be explored. Another important factor in cell alignment could be the specific animal source used to acquire primary cells. To minimize biological variation, muscle samples were taken from the same region of cows of similar age, same sex, and same breed. However, there is still the possibility that the animals may have been raised in separate herds. This may have contributed to the significant variation observed in alignment. Cells isolated from one cow consistently showed cellular alignment, whereas one cow consistently showed minimal alignment. This variable could be eliminated by repeating the experiment using genetically identical cows. Potential sources of variation should be investigated to optimize cell alignment by sourcing tissues from different cow herds with different environmental factors and genetics.

This study showed the potential use of decellularized spinach leaves for the development of laboratory-grown meat. More work is needed before this technology can be used commercially. One of the challenges is acquiring a sufficiently large and homogeneous satellite cell population ⁴

Aim 1B: Evaluate the significance of decellularization in the long-term culture of satellite cells.

3B.1 Introduction

A healthy diet has long been believed to include copious amounts of leafy greens, such as spinach. These green vegetables naturally contain dietary fiber (indigestible cellulose), but they have also been linked to other nutritional benefits that reduce the risk of chronic disease ^{109–112}. Additionally, leafy vegetables contain substances that enhance their flavor. Similar to antioxidants, these astringent substances may be lost during the decellularization process ^{112–114}

3B.2 Materials and Methods

3B.2.1 Cell Attachment to Decellularized Scaffolds vs. Non-decellularized Scaffolds¹¹⁵

PBSCs were sown onto decellularized and non-decellularized spinach scaffolds to evaluate the significance of decellularization. The cuticle layer was removed from the non-decellularized scaffolds using hexanes, as described previously, but the non-decellularized leaves were stored and prepared for seeding in the same manner as the decellularized samples. As previously described, the decellularized samples were processed and prepared using TX100 as the secondary detergent. 2×10^5 PBSCs were sown onto the decellularized and non-decellularized scaffolds using the previously described seeding procedure. Each group contained 3 biological replicates of cells isolated from cows 1, 2, and 3, and each biological replicate had 3 technical replicates for a total of 9 samples. The samples were then incubated for 7 d at 37 °C and 5% CO₂ in growth media. Every 48 hr, the growth media was replaced. After 7 d of incubation, samples were stained with a LIVE/DEAD[®] staining kit and fixed for 10 min in 4% PFA. As a control, cells were

incubated in 70% ethanol for 30 min at room temperature. Hoechst was also used to confirm the presence of a cell nucleus in the samples.

3B.2.2 Imaging and Analysis

Images of specimens were captured using an Axioimager Z2 microscope (Zeiss, Oberkochen Germany). The center image of a 3 x 3 array of images was positioned near the center of the seeding area of each sample. Using ZEN 3.4 Blue Edition imaging software, the images were pieced together to create a composite, tiled image (Carl Zeiss Microscopy).

3B 2.3 Nuclear Density Analysis

Fiji's trainable WEKA Segmentation Plug-in, the autofluorescence signal was classified independently from fluorescent nuclei to ensure that the autofluorescence of the leaf was not considered during image analysis. This plugin was used to assign a probability to every pixel in an image. This probability was derived from a supervised machine learning algorithm and reflected the likelihood that the pixel corresponded to a positive nucleus signal and a positive dead signal ¹¹⁶

3B.2.4 Statistical Analysis

The prior DNA quantification data were used to determine an appropriate power analysis. G*Power RRID:SCR 013726 was used to calculate the sample size required to achieve a statistical power of 0.80 using the calculated effect size. This yielded the required minimum of 3 samples for decellularization experiments. As a result, a sample size of 6 was used for all leaf decellularization experiments. GraphPad Prism was used for all statistical analysis. All data are presented as mean \pm standard deviation. All comparisons were made using either an ordinary one-way ANOVA or a Welch's t-test with two-tailed distributions, with p-value \leq 0.05 as the statistical significance threshold.

3B.3 Results

3B.3.1 Adhesion of Cells to Decellularized vs. Non-decellularized Scaffolds

The non-decellularized samples exhibited an almost complete absence of visible cells, with an average ND of 1.2 ± 3.9 cells/mm², whereas the decellularized samples displayed an average ND of 69.8 ± 22.8 cells/mm² (Figure 9). Among the decellularized leaf samples, Cow1, 2 and 3 had an average ND of 61.3 ± 21 cells/mm², 81.3 ± 22.8 cells/mm², and 61.0 ± 10.6 cells/mm² respectively. A one-way ANOVA indicated that there were statistically significant differences between cow1 and cow2 ($p = 0.0045$) and cow2 and cow3 ($p = 0.0033$). However, there was no statistically significant difference between cow1 and cow3.

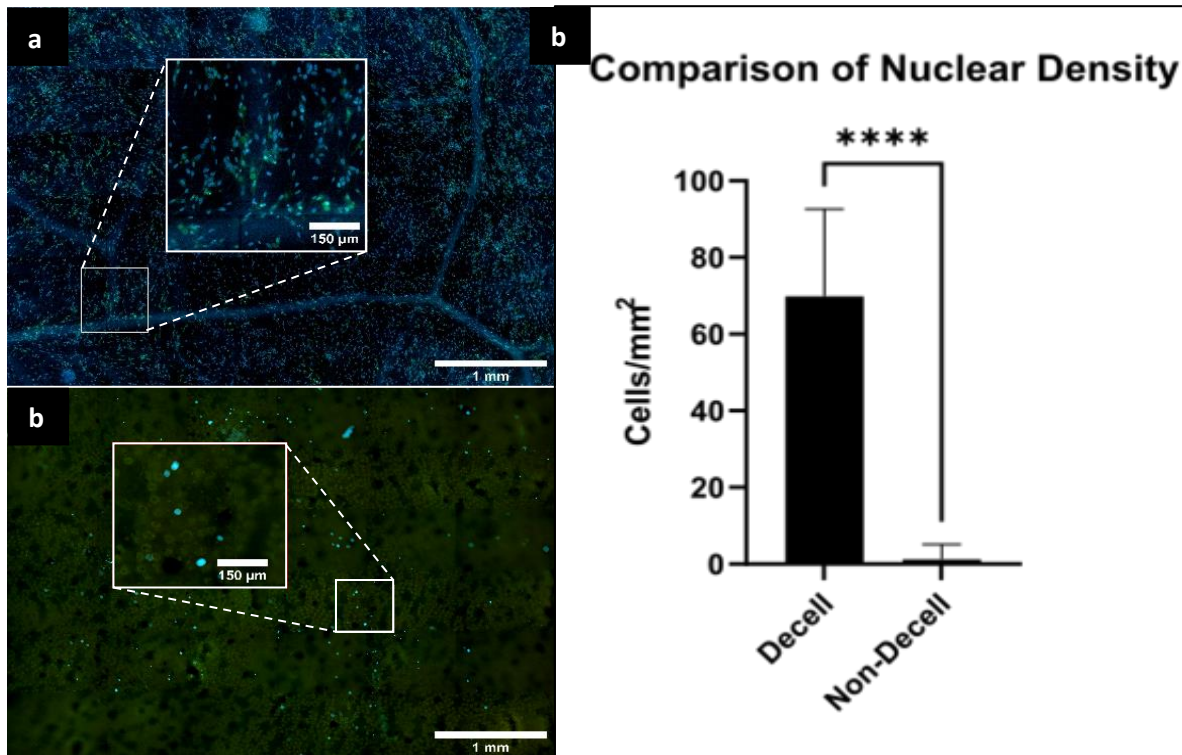


Figure 9| Primary bovine satellite cells have a higher nuclear density when cultured on decellularized spinach compared to non-decellularized spinach after 7 d ($n = 6$). (a) PBSCs on decellularized spinach. (b) PBSCs on non-decellularized spinach. (c) Comparison on nuclear density.

3B.4 Discussion

The decellularization process originated in the tissue engineering field. Proposed as a method to reduce implant rejection, decellularization provided an ECM-based scaffold for cell repopulation. As neither of these capabilities are necessary for the cellular agriculture industry, we explored the importance of decellularization in the development of plant-based scaffolds for use in food. However, our results showed few cells remained viable when grown on non-decellularized leaves. The reason behind the lack of cells on the surface is not readily apparent. It is possible that the cells were successfully seeded onto the surface of the leaves but died over time, but there is no evidence to suggest that the cells successfully adhered to the surface of the non-decellularized leaves. Degradation of the leaf samples in culture can be categorized as necrotic plant cell death ¹¹⁷. One of the hallmarks of this form of necrotic plant cell death is rapid permeabilization of the cell membrane ¹¹⁷. This rapid permeabilization is also experienced by the lysosomes within the plant cells causing the release of proteases such as cathepsin ¹¹⁷. Release of cathepsin into the culture could trigger lysosomal-dependent cell death (LDCD) in the satellite cells that are growing on the surface of the leaf ¹¹⁸. Regardless, these results suggest that spinach leaves that are treated only with hexanes are not suitable for supporting primary bovine satellite cells, and that further decellularization is required.

Chapter 4 – Decellularization as a Food Processing Step

Some of the content in this chapter is contained in the publications:

1. Jones, J. D. *et al.* Decellularization : Leveraging a Tissue Engineering Technique for Food Production. (2023) doi:10.1021/acsbmaterials.2c01421.

Current detergent based decellularization methods use detergents that are not safe for use in food processing. In this aim, the use of alternative detergents that are currently considered safe for use as a food additive were tested to uncover any changes to decellularization efficacy and satellite cell viability. It was hypothesized that the outlined food safe modification will not have a statistically significant effect on cell viability without significantly reducing the quality of decellularization.

Aim 2: Modify the decellularization procedure to be applied as a food processing step.

4.1 Introduction

Lab-grown structured meat products hold great potential to reduce the demand for traditional meat because they can be used in a larger variety of dishes and compete directly with traditional meat products. A vascularized scaffold could potentially support the growth of 3D tissues and pave the way to structured meat products such as steak^{3,5}

Decellularized plant tissue has been shown to have potential to address several tissue engineering challenges^{6,7,119}. Chemical decellularization strategies, using acids and bases, are useful for breaking down cellular materials. The use of hypotonic and hypertonic solutions can successfully breakdown cellular structures but still leave behind cellular residue¹⁰⁵. Enzymes such as trypsin and dispase can also be used to break down cellular material in tissues but are difficult to remove from the ECM^{105,120}. Mechanical

strategies like freezing and thawing, direct force, applied pressure, and electroporation can disrupt cellular structures but can also potentially damage the ECM ^{121,122}.

Supercritical carbon dioxide ScCO₂ has been proposed as a technique for the decellularization of both mammalian and plant tissues ^{123,124}. This process involves utilizing carbon dioxide in a supercritical state, where it exhibits properties of both a liquid and a gas. ScCO₂ acts as a solvent, removing cellular components while preserving the underlying extracellular matrix. This method offers some advantages over traditional decellularization techniques, such as reduced processing time and minimal use of chemicals. However, the relatively high cost associated with the equipment and infrastructure required for this technique is concerning, particularly in comparison to chemical decellularization methods.

Some of the most successful decellularization strategies employ the use of ionic and non-ionic detergents. Ionic detergents such as sodium dodecyl sulfate (SDS) are effective at solubilizing cell and nuclear membranes in addition to denaturing intracellular proteins ^{105,120,125}. Non-ionic detergents such as Triton X-100 (TX100) have a similar mode of action but are less effective than ionic detergents when used in thicker tissues ¹⁰⁵. Using multiple detergents simultaneously may result in ECM damage, therefore subsequent decellularization steps using different detergents may be needed to decellularize thicker tissues. One such strategy is use of an ionic detergent to break down cellular materials in the thick tissue and then follow with a non-ionic detergent to further evacuate the cellular material from the tissue.

Some ionic detergents such as SDS are regulated (REG) by the United States Food and Drug Administration (FDA) for specific uses in food, while many of the non-ionic detergents, including TX100, are not. Polysorbate-20 (PS20) is a non-ionic detergent that is used in various food processing steps as a wetting agent, emulsifier, and flavoring agent and is a REG substance according to the FDA ¹⁰⁶. This study expanded upon the results of previous studies to evaluate the efficacy of a modified decellularization protocol that

eliminates or replaces non-REG solution, further enabling the use of decellularized plant scaffolds for lab-grown meat products.

Another concerning reagent commonly used to aid in the decellularization of plant leaves is hexane, which is used to remove the cuticle layer of the leaf. Like TX100, Hexane is not regulated to be used in food in any way. Ingestion of hexane can cause gastrointestinal issues like nausea, vomiting, and abdominal pain. Neurotoxic symptoms such as peripheral neuropathy, characterized by numbness and pain in extremities, may also be observed ¹²⁶. Additionally, inhalation of hexane vapors can result in respiratory complications, including dizziness, headache, and central nervous system depression. The cuticle layer is a hydrophobic, waxy layer that covers the epidermal cells of many plants. This protective layer primarily serves to control water loss from the plant, acting as a safeguard against desiccation ⁸⁷. Additionally, the cuticle protects the plant from harmful UV radiation and pathogens ⁸⁷. This layer is synthesized by the cells in the plant's epidermis and consists mainly of cutin, a complex polymer, combined with waxes ⁸⁷. These components are secreted onto the external cell surface where they gather to form the cuticle ⁸⁷. Depending on the plant species and environmental conditions, the presence and density of the cuticle can vary. The waxy nature of the cuticle makes the surface of the leaf hydrophobic, potentially preventing cells from adhering to the surface. It is also posited that the hydrophobicity of the waxy cuticle layer that covers the epidermis of the leaf may prevent sufficient decellularization of the leaves, justifying the use of hexane to treat the surface of the leaf prior to decellularization ⁶. Hexane, being nonpolar, has an affinity for other nonpolar compounds. When hexane is applied to the cuticle, it solubilizes the waxes, effectively breaking down and removing the cuticular layer.

After the decellularization process, it's possible that most of the hexane has been washed out from the remaining leaf tissue; however, for adoption of decellularization in food processing, complete removal of hexanes is the ideal choice. Removing hexane not only makes the process safer for food use but also reduces the number of processing steps and associated costs. While it is presumed that the cuticle

removal process is essential for successful decellularization of plant leaves, there isn't empirical data to support it. The cuticle layer might not impede the decellularization process and could even be inherently removed in the process.

4.2 Materials and Methods

4.2.1 Spinach Leaf Decellularization, REG Modification, and Scaffold Preparation

To develop a REG decellularization process, the cuticle removal step and the secondary detergent step need to be altered. REG modifications to the decellularization process include elimination of the hexanes cuticle removal step and substitution of TX100 with PS20 as the secondary detergent. To explore the elimination of the cuticle removal steps, spinach leaves were decellularized using the current decellularization process including the hexanes removal step, acting as a control group. The second group of spinach leaves underwent decellularization without the cuticle removal step. To explore the substitution of TX100 with PS20, spinach leaves were decellularized with the current decellularization protocol using TX100 as the secondary detergent. Additional spinach leaves used PS20 as the secondary detergent. The decellularization protocol that does not involve the hexanes cuticle removal step and used PS20 as the secondary detergent instead of TX100 is referred to from here on as the “REG decellularization protocol” and the scaffolds it produces as “REG scaffolds”.

Decellularized spinach leaves were prepared similarly to the process outlined in Jones et al ⁹⁴. Triple washed packaged baby spinach leaves (Nature’s Promise Organic, Landover, MD, USA) were acquired from a local food store. Spinach cuticles were removed by agitation in hexane (Extreme Environment Orbital Shaker, OHAUS, Corporation, Parsippany, NJ, USA). Twenty-five spinach leaves were placed in a 1 L beaker in 300 mL of 98.5% hexanes for 3 min, immediately followed by agitating for 3 min in 300 mL diH₂O water. This process was repeated 3 times, for a total of 6 washes, to ensure complete cuticle removal. Each individual leaf was placed in a 50 mL conical tube and submerged in 40 mL of 1x (w/v) sodium dodecyl sulfate SDS for 5 d on a rotating platform. The solutions were refreshed every 24 hr. After

5 d, leaves were placed in 0.1% TX100 and 10% concentrated bleach for 48 hr, as the control secondary detergent, or in 1% PS20 (Sigma-Aldrich) and 3% concentrated bleach in deionized water for 48 hr. Additionally, leaves with cuticle intact were placed in 1% PS20 and 3% bleach solution. Each solution was refreshed every 24 hr. Leaves were then incubated in diH₂O for 24 hr. After incubation, the liquid was drained, and the leaves were frozen at -80°C for a maximum of 2 wk. Groups of normal spinach leaves that did and did not undergo cuticle removal and were not decellularized were used as controls for DNA quantification.

Immediately after the decellularization process was completed, the leaves were stored at -20°C overnight. The leaves were lyophilized and stored at room temperature until needed for a maximum of 2 wk.

4.2.2 DNA Analysis of Decellularized Leaf Scaffolds

DNA content was quantified to evaluate completeness of decellularization. Samples were weighed and homogenized in 400 µL 1x PBS using iris surgical scissors. The DNA content of the samples was measured using a CYQUANT® DNA assay kit. To release the DNA present in the sample, the homogenized samples were each combined with 100 µL of the lysis buffer solution made from the CYQUANT® DNA assay kit. The released DNA was fluorescently labeled by adding 100 µL of the CYQUANT® GR dye/lysis buffer solution. Decellularized leaf samples were compared to a standard curve created by serial dilution of the DNA standard solution and non-decellularized leaf samples as controls. Fluorescence intensity was measured using a SpectraMax M3 multi-mode microplate reader (Molecular Devices San Jose, CA, USA) with an excitation wavelength of 480 nm and an emission wavelength of 520 nm. The fluorescence intensity value was converted to DNA content through a linear regression of the standard curve values.

4.2.3 Histological Analysis of the Scaffolds

Fresh spinach leaves and those decellularized with both decellularization methods were fixed in 4% paraformaldehyde for 30 min. Samples were then dehydrated and embedded in paraffin wax with a

Tissue-Tek VIP 6 AI tissue processor (Sakura Finetek USA, Torrance, CA). The processing procedure consisted of 30 min in 70% and 80% ethanol sequentially, followed by 30 min of 95% ethanol and then 3 separate rinses in 100% ethanol. The samples were then submerged in xylene 3 times for 20 min, and then, under vacuum, infiltrated with 4 rinses of paraffin wax. Paraffin blocks were prepared and sectioned at 6µm onto charged microscope slides.

Hematoxylin and eosin stains were performed by first deparaffinizing the sections in xylene and rehydrated by sequentially dipping them in 100%, 95%, and 70% ethanol. Samples were then rinsed in running water for 5 min. Slides were dipped in Harris Hematoxylin for 10 min, rapidly differentiated in acid alcohol via 3 quick dips, and placed in 0.2% ammonium hydroxide in diH₂O for 1 min. Samples were then placed in 1:1 solution of eosin and 70% EtOH for 1 min and then dehydrated in 95% and 100% ethanol. Samples were placed in xylene and coverslipped. All samples were imaged with an Axioimager Z2 microscope. Background gradients were removed using ZEN 3.4 Blue Edition© imaging software.

Sections from all samples were stained with calcofluor white (Sigma-Aldrich). Sections were deparaffinized as described above and exposed to calcofluor white (Sigma-Aldrich) for 1 min. Samples were rinsed by pipetting PBS over the slides until the samples appeared clear. Samples were coverslipped and imaged as previously described in section 3B.2.2.

4.2.4 Primary Satellite Cell Isolation and Culture Conditions

PBSCs were isolated and cultured as described in section 3A.2.4. Primary bovine satellite cells were isolated from fresh gastrocnemius samples collected from the front legs of 3 different cows sourced from a local slaughter facility (Adams Farm, Athol, MA, USA). Cell banks developed from these 3 animals were used as biological replicates for the viability experiments in this study. These biological replicates were referred to as cow 1, cow 2, and cow 3.

The cell isolation process was conducted as described in Jones et al. ⁹⁴. The final filtrate was plated and incubated overnight at 37 °C and 5% CO₂ to allow cell attachment. The cell population that this process produces is inherently heterogeneous. As such, additional purification steps were required to further isolate the satellite cells from the initial population. This was done by plating the cell suspension on non-tissue culture polystyrene Petri dishes and incubating at 37 °C and 5% CO₂ for 30 min. The cells that were not attached to the plate were collected and the adhered cells were discarded.

4.2.5 Seeding Cells on the Decellularized Scaffolds

PDMS coated multiwell plates were used to facilitate the seeding procedure as described in section 3A.2.3. Polystyrene 24-well plates (Thermo Fisher Scientific) were coated with PDMS by mixing the base elastomer and curing agent at a ratio of 10:1. Approximately 0.25 mL of PDMS was deposited at the bottom of each well. The plates were degassed with a Bel-Art benchtop polycarbonate vacuum desiccator for 1 hr to allow the PDMS to spread evenly and remove air bubbles. After degassing, the plates were left overnight on a flat level surface at room temperature to cure.

As described in section 3B.2.5, a 12 mm diameter circular punch was used to create scaffolds of uniform size from the lyophilized leaves. The circular scaffolds were rehydrated in PBS for 15 min on an OHAUS™ Extreme shaker at room temperature. After the rehydration period, the scaffolds were sterilized by 70% EtOH for 30 min on a shaker at room temperature. Ethanol was replaced with sterile PBS for 15 min. Sterile forceps were used to relocate each scaffold into a well of the PDMS coated plate where they were allowed to dry and stick to the PDMS coating for 15 min. One mL of growth media was deposited into each well and the scaffolds were soaked in the media for 1 hr. The PBSCs procedure completed as described in section 3B.2.5. Prior to seeding, cell viability was evaluated using trypan blue staining. The media on the scaffolds was replaced with the cell suspension at 200 x 10³ cells/mL. The scaffolds were incubated overnight for cell attachment at 37 °C and 5% CO₂.after which, cells that did not adhere were removed by gently rinsing the surface of the leaf with sterile PBS.

4.2.6 Imaging and Analysis

The samples were imaged using an Axioimager Z2 microscope (Zeiss, Oberkochen Germany). A 3x3 array of images was captured with the central image centered near the seeding area of each sample. Using ZEN 3.4 Blue Edition imaging software, the images were pieced together to create a composite tiled image (Carl Zeiss Microscopy).

4.2.7 Viability Assessment of the Seeded Satellite Cells

To assess cell viability on REG scaffolds, PBSCs were seeded onto scaffolds decellularized using PS20 as a secondary detergent and scaffolds created using TX100. The two scaffold groups were decellularized as described earlier, with the only differences being the substitution of TX100 for PS20 and the omission of the hexanes cuticle removal step in the REG group. 200×10^3 PBSCs were seeded onto the decellularized and non-decellularized scaffolds. The samples were then incubated in growth media at 37 °C and 5% CO₂ for 7 d. The growth media was replaced every 48 hr. After 7 d, the samples were stained and processed as described **section 3B.2.1**.

4.2.8 Statistical Analysis

DNA quantification data from section 3A.3.1 was used to determine an appropriate power analysis. Using the calculated effect size, G*Power was used to calculate the sample size required to achieve a statistical power of 0.80. This results in the minimum number of 3 samples needed for decellularization experiments. Consequently, a larger sample size of 6 was used for all leaf decellularization experiments. All statistical analysis was done using GraphPad Prism. Unless specified otherwise, all the data is expressed as mean \pm standard deviation. All comparisons were made with either an ordinary one-way ANOVA or a two-tailed Welch's t-test. A p value of < 0.05 was used as the threshold of statistical significance.

4.3 Results

4.3.1 DNA Analysis of the Decellularization Protocols

DNA quantification of decellularized leaves showed that both methods removed the majority of the plant DNA from the leaf compared to non-decellularized leaf control, Figure 10a. Non-decellularized leaf samples had an average DNA content of 14.5 ± 2 ng/mg. Samples decellularized with the conventional method that included the use of TX100 as the secondary detergent had an average DNA content of 1.3 ± 0.07 ng/mg. Samples decellularized with the REG decellularization method that used PS20 as the secondary detergent had an average DNA content of 1.3 ± 0.05 ng/mg. A one-way ANOVA test suggested that there was significant difference between both decellularization methods and the control group, but there was no significant difference between the TX100 and PS20 decellularization methods.

Samples that underwent the cuticle removal process prior to decellularization had an average DNA content of 1.2 ± 0.05 ng/mg whereas samples that did not include this cuticle removal step had an average DNA content of 1.4 ± 0.05 ng/mg, shown in figure 10b. A t-test indicated that there was not a statistically significant difference between the groups.

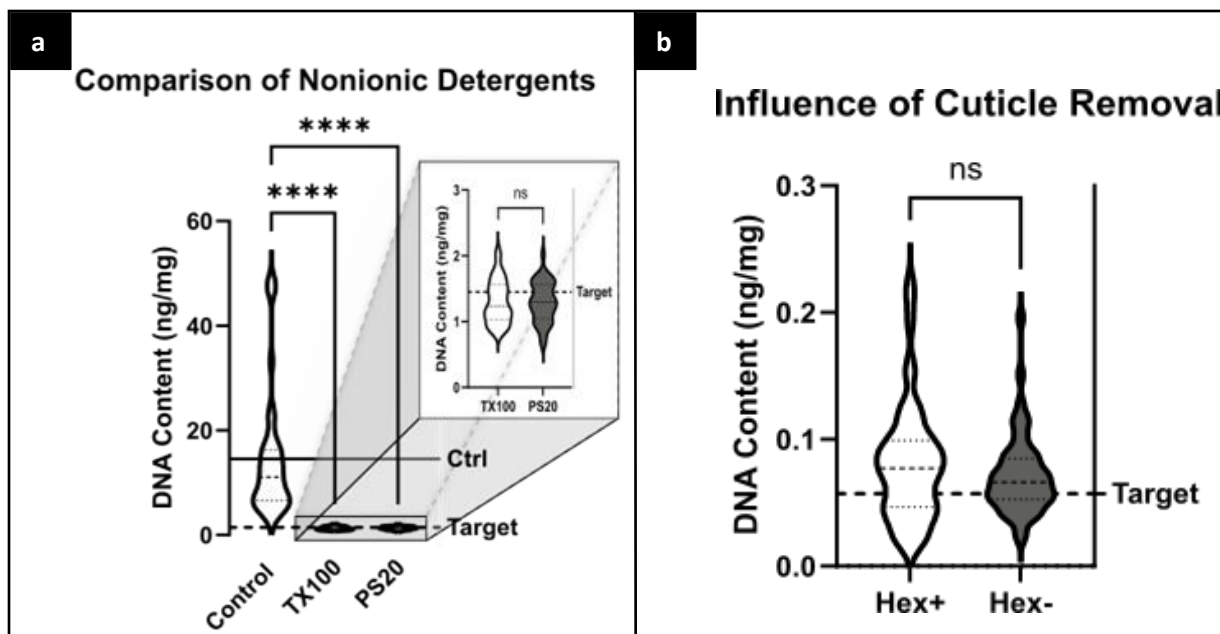


Figure 10| PS20 can be used as an effective secondary non-ionic detergent for the decellularization of spinach leaves. (a) DNA content on decellularized spinach leaves by non-ionic detergent. (n=6) (b) DNA content of decellularized spinach leaves by hexanes inclusion. (n=6)

4.3.2 Histological Analysis

The non-decellularized leaf samples stained with H&E (Figure 11), exhibited dark purple nuclei and a pink color throughout the tissue. Non-decellularized samples stained with calcofluor white exhibit bright blue fluorescent signals marking the cellulose present in the samples. In contrast, leaf samples decellularized with TX100 and PS20 exhibit no coloration from the H&E stain. The leaf tissue that is visible is gray with some regions hardly distinguishable from background. However, both decellularization groups exhibit bright blue fluorescent signals when stained with calcofluor white, similar to the non-decellularized leaves.

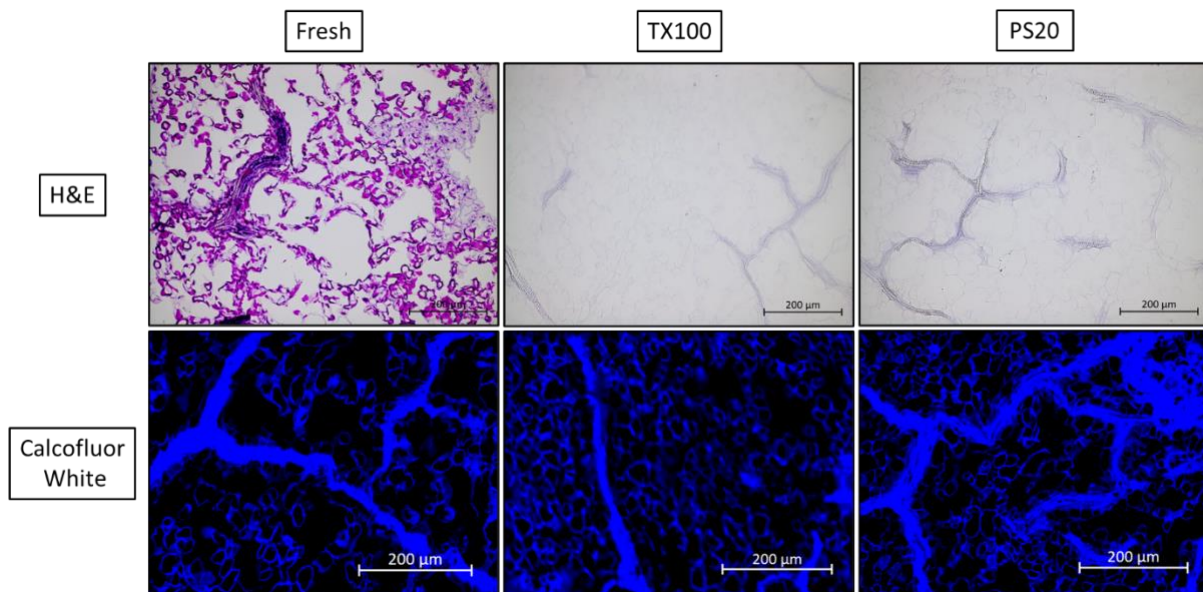


Figure 11 | Histological analysis shows that both TX100 and PS20 result in significant reduction in intracellular context with minimal impact of cellulose structure.

4.3.3 Viability Assessment of the Seeded PBSCs

After 7d incubation, PBSCs grown on the surface of REG scaffolds demonstrated an average viability of $97.4 \pm 0.3 \%$ (Figure 12). Individually, biological replicates Cows 1, 2, and 3 had average viability of $95.5 \pm 0.7 \%$, $98.7 \pm 0.3 \%$, and $98.1 \pm 0.6 \%$, respectively (data not shown). A one-way ANOVA showed there was no significant difference between Cows 2 and 3. However, there was a significant difference between Cow 1 and the other two biological replicates (Cows 2 and 3). Qualitatively, images of the REG samples appeared to have high nuclear density. Image analysis showed that the average VCD of Cows 1, 2, and 3 was 487 ± 45 cells/mm², 535 ± 31 cells/mm², and 254 ± 14 cells/mm², respectively. Cows 1 and 2 were not a significantly different when compared with ANOVA, but both were significantly different from Cow 3.

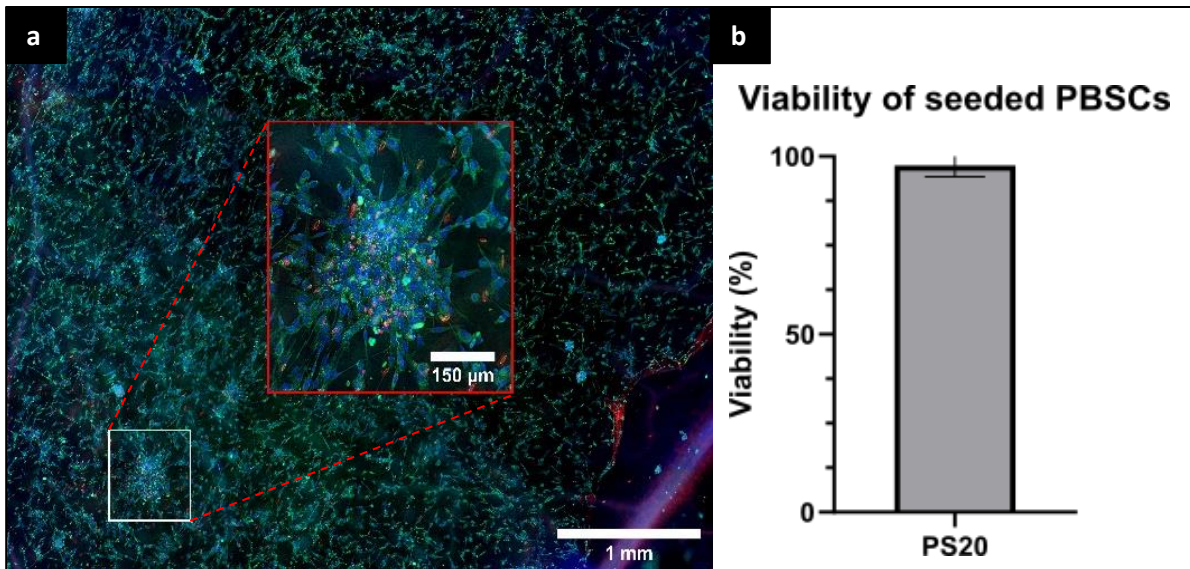


Figure 12| Primary bovine satellite cells viability when cultured on GRAS decellularized spinach after 7 days. (a) PBSCs on REG decellularized spinach. (b) PBSC viability on REG decellularized spinach (n=6)

4.4 Discussion

There are many applications for the decellularization of tissues including the isolation of tissue specific ECM proteins for therapeutics, the development of 2D and 3D scaffolds for tissue regeneration, and the development of allogeneic and xenogeneic organ transplants^{105,120,125,127}. Recently, we demonstrated that decellularization may have use as a food processing step, particularly in the emerging field of lab-grown meat^{94,119,128}. This could potentially bring about the development of new edible scaffold materials from various plants that could mimic the necessary mechanical properties while providing a physical structure conducive to 3D tissue development. To enable decellularization as a food processing method, the process should eliminate the use of potentially harmful processing steps. The use of detergents that are REG by the FDA could potentially reduce the cost of bringing such a process to scale by minimizing processing steps and initiating the exploration of detergent alternatives.

This study explored the importance of decellularization and the modifications of a conventional decellularization protocol to develop a REG protocol that only incorporates REG detergents and is devoid

of potentially harmful substances. More specifically, it explored the importance of cuticle removal and the consequences of eliminating the cuticle removal step. It also investigated the substitution of TX100 with PS20 as the secondary detergent.

In native plants, the cuticle serves to protect the plant against water loss and foreign elements, thus removal of the cuticle prior to decellularization seemed logical. Herein, we explored the necessity of removing the cuticle with hexanes. Histological analysis suggested that there was little degradation of the cellulose structure. Neither hematoxylin nor eosin stain the cell wall of leaves. Therefore, when properly decellularized, the absence of nuclei and cellular proteins should leave the leaf samples gray or colorless. Proper decellularization should leave the cellulose structure intact ¹⁰⁵. Both decellularized and non-decellularized samples demonstrated similar staining, suggesting minimal effects from the decellularization process on the cellulose structure. In addition, omission of the cuticle removal step did not seem to affect DNA content. Omitting the cuticle removal step eliminates hexanes from the process, while also reducing the number of processing steps and material costs.

The substitution of TX100 with PS20 as the secondary detergent in the decellularization process is important for moving towards regulatory approval. Histological and DNA analysis demonstrated that both TX100 and PS20 groups were sufficiently decellularized. The calcofluor white stain suggested no significant damage to the cellulose with no apparent difference between both decellularized groups and the non-decellularized control in regard to blue fluorescent signal. Quantitatively, the DNA content measured from each group suggested that both methods yield scaffolds that are sufficiently decellularized.

The decellularization REG modifications did not appear to affect cell viability. PBSCs grown on the surface of REG scaffolds had an average viability of 97.4 ± 0.3 % viability comparable to the 98 % observed in previous studies by Jones et al. where PBSCs were cultured on scaffolds decellularized with TX100 ⁹⁴.

Another phenomenon that persists from the previous study is that the results vary between biological replicates. This variance is most apparent with respect to the PBSC density on leaves. Cells isolated from

Cows 1 and 2 had similar cell densities, whereas Cow 3 had a PBSC density of about one-half the other cows. Samples from the same leaves were used with the cells from different cows, suggesting a difference in the bovine cells. The same isolation process was used for all samples, hinting at a difference in the cows. However, more research must be done to determine what factors may contribute to the differences in performance between the biological replicates.

Though the data presented in this study are promising, additional experiments are needed to ensure that the protocol yields scaffolds that comply with FDA guidelines regarding the final concentration of each reagent, and how the modified process affects the mechanical properties of the scaffold. According to the FDA, SDS, PS20, and sodium hypochlorite (from bleach) can be present in a food product below 125 ppm, 15 ppm, and 200 ppm, respectively ¹⁰⁶. To ensure compliance, it's imperative to know the final concentration of all the reagents in the process. Should the final concentration of each reagent exceed the specification outlined by the FDA, additional extraction methods may be explored to bring the concentrations within specification. Chemical characterization is a critical consideration for the efficacy of REG scaffolds, but there are other considerations that are less critical yet still important.

It is critical that the mechanical properties of the scaffold material be well characterized. The surface stiffness can influence satellite cell differentiation and myocyte maturation ^{93,129}. Materials with a Young's modulus, or stiffness, comparable to native muscle, approximately 12 Kpa, have been shown to improve satellite cell differentiation ⁹³. However, differentiation begins to decline on materials with stiffnesses higher than 20 Kpa ⁹³. On a larger scale, the global stiffness of the scaffold can play a role in the mechanical properties of the final product. In the case of meat, this could potentially be reflected in the chewiness and tear of the meat ¹³⁰. With these considerations in mind, tools such as atomic force microscopy (AFM) can be used to measure the surface stiffness of the REG scaffolds. Tensile testing can be conducted to shed light on the global mechanical properties of the REG scaffolds.

One of the benefits of using decellularized leaves as a primary mass contributor is that they are inexpensive. This could make them useful for scaling a manufacturing process. Bioreactors may facilitate the decellularization process. More research is necessary to fully comprehend and optimize the decellularization procedure to maximize the amount of spinach that can be decellularized per unit volume.

135–139

More information is needed to definitively confirm that the protocol described herein can be classified as food safe, it offers an effective path toward a food safe decellularization process. From the data in this study, it can be concluded that the cuticle removal is not a critical processing step. Additionally, it can be concluded that the PS20 is a suitable alternative to TX100 as a secondary detergent. Using these conclusions as a foundation, further studies can refine the decellularization protocol through chemical and mechanical characterization.

Chapter 5 – Harnessing Plant Topographies for Engineered Muscle

It is understood that topography of a substrate play a significant role in directing alignment of cells. Topographical cues from natural materials, such as plant leaves, open innovative and sustainable avenues for directing cellular alignment and tissue formation. This aim will explore how the unique topographies of dicot and monocot plants affect the alignment and differentiation of myoblasts on the leaf surfaces of dicot and monocot plants. These data will provide insight into which plant species may be useful for engineering skeletal muscle and other similar tissues.

Aim 3: Examine how the leaf topographies of dicot and monocot plants affect myoblast alignment and differentiation.

5.1 Introduction

Alternative protein sources and plant-based meat substitutes, such as Impossible® and Beyond®, were designed to reduce the demand for traditional meat. These products aim to replicate the flavor and texture of meat without the ethical and environmental concerns associated with conventional livestock production. To reduce reliance on traditional meat products and alter consumer behavior, plant-based substitutes must replicate the inherent organoleptic qualities of traditional structured meat. Despite improvements to the taste and texture of these products, it remains difficult to replicate the structure, texture, and juiciness of traditional structured meats. Despite the rise of vegetarianism and alternative protein sources, the meat industry is likely to remain for the foreseeable future. Therefore, there is a need for more effective means of competing with traditional agriculture. However, even meat products produced *in vitro* may face some of the same hurdles that plague meat analogs.

For example, the texture and fibrous structure of traditional meat, may be challenging to replicate. Myotube alignment has a major effect on the mechanical and functional properties of engineered muscle

tissue. This alignment is necessary to produce force during contraction, which is the direct sum of forces generated by each individual myocyte along the primary axis of the muscle. Consequently, proper alignment is necessary for optimizing muscle force production. Alignment can affect the texture of cultured meat, making it an important variable to consider.

It is well known that topographical factors affect cellular alignment ^{131,132}. Parallel grooved surface topographies that have subcellular widths around 6 – 12 μm enhances myocyte alignment in the direction of the grooves ¹³¹. Two plant species, spinach and corn, have dissimilar surface topographies and offer potential as natural scaffolds for myotube growth. The topography of the leaves of dicotyledonous plants, such as spinach, is not aligned. Nevertheless, their readily accessible vascular network from the stem facilitates an efficient nutrient supply system that is necessary for the development and maturation of cells. Corn is a monocotyledonous plant with linear and aligned topographical features, especially in its leaves and husks which are discarded as waste. This orientation resembles the natural orientation of myofibers in skeletal muscle, making it a potential substrate for the growth and alignment of myotubes. Although their lack of converging vasculature makes it difficult to circulate media throughout, Corn husks offer an experimental model to investigate the potential model of topography on myocyte alignment and, consequently, myotube formation. Despite the distinct advantages and challenges associated with each material, the use of spinach leaves and corn husks in this context represents an innovative approach to studying skeletal muscle tissue engineering.

This aim will explore how the unique topographies of dicot and monocot plants affect the alignment and differentiation of myoblasts on the leaf surfaces of dicot and monocot plants. Myoblasts will be cultured on spinach leaves to represent dicot plants and corn husks to represent monocot plants. This comparison will provide valuable insights into the influence of plant leaf topographies on myotube alignment and differentiation, potentially guiding future strategies for engineering skeletal muscle tissue and providing an innovative, environmentally sustainable use for agricultural waste.

5.2 Materials and Methods

5.2.1 Experiment design

The purpose of this study was to investigate how the distinct topographies of dicot and monocot plants influence the alignment and differentiation of myoblasts on the leaf surfaces. This investigation used fibrosarcoma-derived Quail muscle clone 7 (QM7) cells (ATCC CRL-1962, Manassas, United States) as a model cell type. The QM7 cells were cultured on 2 types of decellularized scaffolds derived from spinach and corn husk, modeling dicot and monocot plants respectively. Using a Matlab script that analyzes the angular orientation of the microfilament visible in fluorescence micrographs, alignment was assessed region by region to determine the relative alignment of cells in a spatial context. This analysis helped uncover correlations between localized alignment and topographical features on the surface of the scaffold. Variance in alignment may also impact differentiation efficiency.

5.2.2 Spinach Leaf Decellularization and Scaffold Preparation

Spinach leaves and corn husks were decellularized according to the REG decellularization protocol described in Aim 2. Baby spinach leaves and fresh corn husk were placed in separate 50 mL conical tubes and submerged for 5 d in 1% SDS in diH₂O, with the solution refreshed every 24 hr. After 5 d, the SDS solution was replaced with 1% PS20 and 10% concentrated bleach in diH₂O for 48 hr, with the solution refreshed every 24 hr. The spinach leaves were then washed for 24 hr in diH₂O. The leaves were drained and stored overnight at 20 °C. Lyophilization was performed at 25 °C and 0.210 Torr for 24 hr. Decellularized spinach scaffolds were stored at RT for up to 2 wk until required. The room's ambient temperature was not monitored. The decellularized plant scaffolds were then prepared as described in section 3A.2.2.

5.2.3 DNA Analysis of Decellularized Leaf Scaffolds

DNA content of the decellularized plant scaffolds was quantified as described in section 3A.2.3

5.2.4 Culture Conditions

QM7 cells were incubated at 37 °C and 5% CO₂ in growth medium (Ham's DMEM/F12, 10% hiFBS, 1% P/S, 4 ng/mL FGF2) during expansion phase¹³³. Once seeded on the scaffold the cells were incubated in growth media for 48 hours. Afterwards, the media was replaced with differentiation media Ham's DMEM/F12, 2% hiFBS, 1% P/S) for 3 d.

5.2.5 Seeding Cells on Decellularized Leaf Scaffolds

QM7 cells were sown onto the surface of the decellularized scaffolds as described in section 3A.2.5.

5.2.6 Imaging and Analysis

The samples were imaged using an Axioimager Z2 microscope. A 5 x 5 array of z-stacks was captured with the central image positioned near the center of the seeding area of each sample. Using ZEN 3.4 Blue Edition imaging software, the images were pieced together to create a composite tiled z-stack series. The ZEN software was also used to generate 3D models of the scaffold surface.

5.2.7 Topographical Analysis

To examine the plant scaffolds' surface Calcofluor white was used to stain all the samples. For 1 minute, the samples were exposed to 50% calcofluor white stock solution in diH₂O. To remove the excess calcofluor white solution, the samples were washed 3 times with PBS. The sample was then coverslipped and imaged as previously described. Zen 3.4 was used to generate a 3D model of each surface, and the Z position of each point on the surface was measured, resulting in elevation heatmaps for each surface. Using the metadata from Zen 3.4, Fiji was used to measure the feature width at any given location on the scaffold's surface. Manual measurements of feature width and depth were collected by picking channels of varied sizes over the surface of the scaffold.

5.2.8 Assessment of Cell Alignment and Visualization “Cellular Alignment Cartography”

After the culture period the samples were fixed and stained with Phalloidin 488 nm (Life Technologies, Carlsbad, CA, USA) and Hoechst 33342 to detect F-actin. This study's alignment software version AlignmentQuant 2 (AQ2) employed a visualization technique known as Cellular Alignment Cartography (CAC). Unlike the software iteration used for Aim 1 AlignmentQuant 1(AQ1), AQ2 enables the program to assess the alignment of up to 1×10^5 discrete regions of interest (ROIs) over a single tiled image, resulting in the creation of a new image that offers spatial context to the alignment data (Figure 13). This is significant because an image may contain areas with high alignment and others with low alignment. The low-alignment regions would diminish the average alignment of the entire image in the first iteration of the software, resulting in the loss of valuable data in the high-alignment areas.

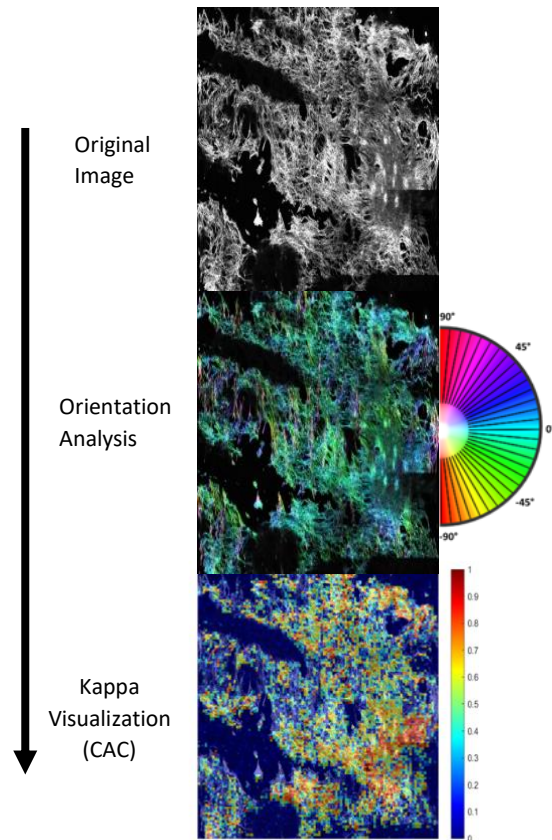


Figure 13| Cellular Alignment Cartography (CAC) workflow diagram. Phalloidin images are recolored based on the orientation of each microfilament using OrientationJ. Kappa values are calculated for 1×10^5 regions throughout the image. A heatmap representing the Kappa values is superimposed over the original image displaying relative alignment at specific location on the scaffold.

AQ2 begins by taking the tiled image created from the 5×5 array and dividing it into 1×10^5 smaller images corresponding to each ROI. As described in Aim 1, OrientationJ was used to generate a color survey of each ROI in order to better visualize the orientation of each microfilament as previously shown in Figure 4. The angle distribution of the cytoskeleton is derived from these data. Each distribution's kurtosis was

compared to another distribution's kurtosis to determine the degree of their relative alignment, captured in the kappa index.

The directional data from each region of interest was imported into MATLAB and analyzed using the CircStat toolbox. The mean vector length, angular standard deviation, and kappa of the distribution was calculated using the Circstat toolbox. The average kappa value for each ROI was used to represent the overall percentage of alignment for that region.

5.2.9 Assessment of differentiation potential

After the culture period the samples were fixed and stained with MyHC primary antibody, alexa fluor 568 and Hoechst 33342 to detect the myosin protein. If the nucleus coincided with the fluorescent signal of the secondary antibody of the MyHC antibody, it was determined that the cell had differentiated. The remainder of the nuclei were identified as non-differentiated cells. The average of these images was used to represent the overall percentage of differentiation for the sample.

5.2.10 Statistical Analysis

GraphPad Prism 9.0.0_121 was used for statistical analysis. In previous studies, the FI and kappa values for satellite cells cultured on gelatin covered glass were previously shown to be 0.14 ± 0.09 and 0.39 ± 0.13 , respectively ⁹⁴Click or tap here to enter text.. When cultured on spinach leaf scaffolds, the differentiation and alignment values were 0.27 ± 0.1 and 0.4 ± 0.3 respectively ³⁶. The calculated potential impact sizes for the data produced by this experiment are 1.06 and 0.036. Using the smaller of the 2 effect sizes would require a total sample size of $n=17,163$, providing the maximum statistical power. This sample size was calculated by entering the previously mentioned parameters into G*Power ¹³⁵. Each experiment produces 1×10^5 data points, for a total of 6×10^5 data points. The values of FI and kappa will be given as mean standard deviation. A one-way ANOVA will be performed to compare the 3 substrates for each analysis method. With $p \leq 0.05$ denoting statistically significant results, meaning that alignment and

differentiation will be greater in regions where linear topography is present on both surfaces. In addition, overall alignment and differentiation was expected to be greater on corn husk than on spinach due to the higher instance of linear topography.

5.3 Results

5.3.1 Scaffold Topographical Analysis

The surfaces of the two plants were notably different. The surface of the decellularized spinach was relatively planar and the surface height was relatively consistent. Aside from the stomata, the decellularized spinach's surface was devoid of prominences. Surface analysis of decellularized spinach revealed many crevices, each corresponding to vascular bundles within the leaf. (Figure 14) The width of the crevasses appeared to vary with the generation of the associated vascular bundles. The primary vascular bundle, for instance, had the widest crevasse width. As the vascular bundles became thinner, each succeeding crevice generation became narrower. The surface features of decellularized spinach had an average feature width of $1200 \pm 480 \mu\text{m}$ and an average feature depth of $102 \pm 25 \mu\text{m}$.

In contrast to the decellularized spinach, the corn husk possessed many trichome hairs across its surface, with a higher density near the crests of each ridge. The decellularized corn husk also exhibited greater variation in both feature width and feature depth. The average feature depth of the corn husk was comparable, but it varied substantially depending on location. on the other hand, the average feature width was significantly greater than that observed in spinach samples. The surface features of decellularized corn husk had an average feature width of $5500 \pm 4500 \mu\text{m}$ and an average feature depth of $106 \pm 99 \mu\text{m}$.

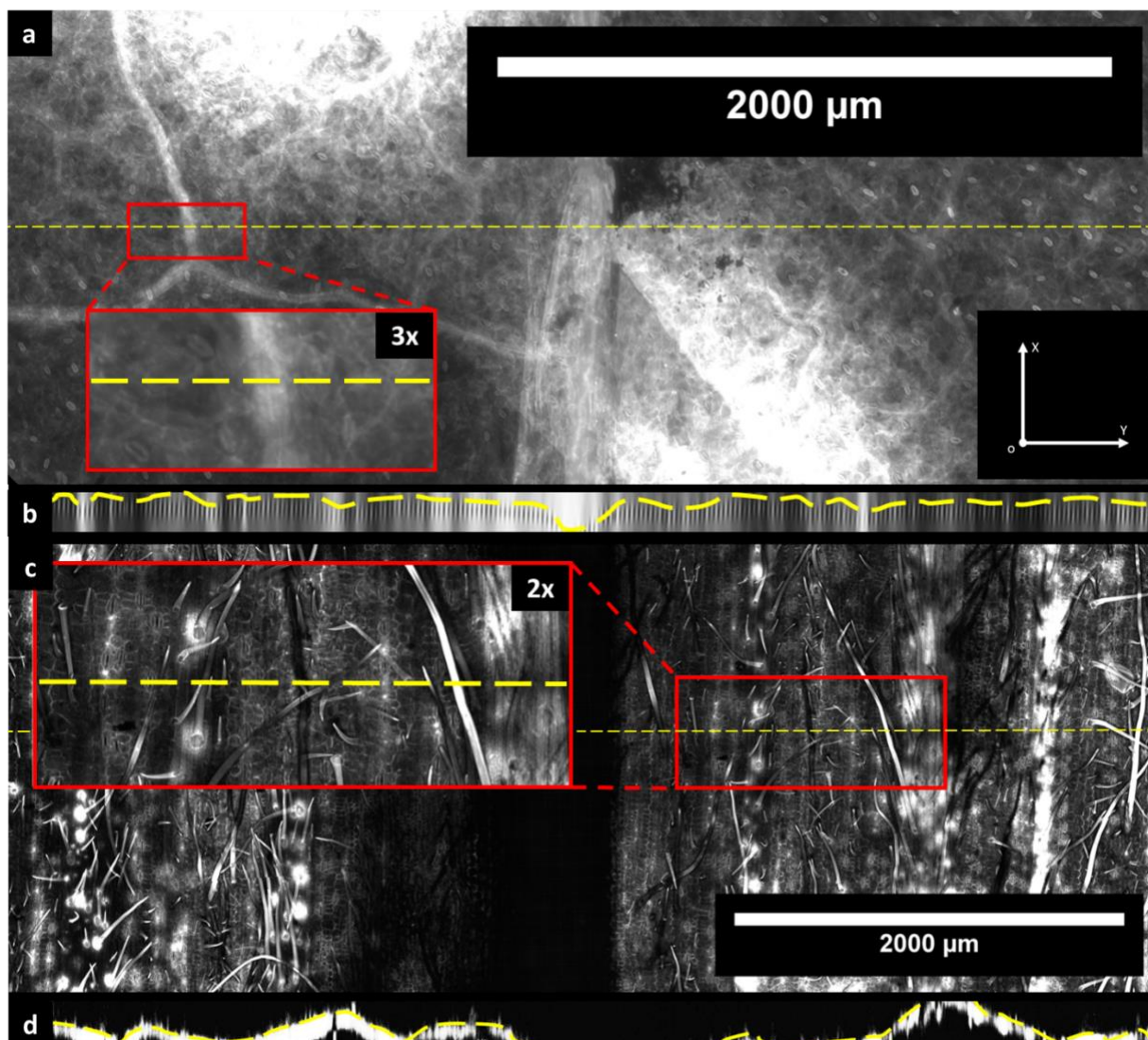


Figure 14 | Surface micrographs of decellularized spinach and decellularized corn husk (a) Calcofluor white stain of decellularized spinach. (b) Cross section of spinach leaf surface. (c) Calcofluor white stain of decellularized corn husk. (d) Cross section of corn husk surface.

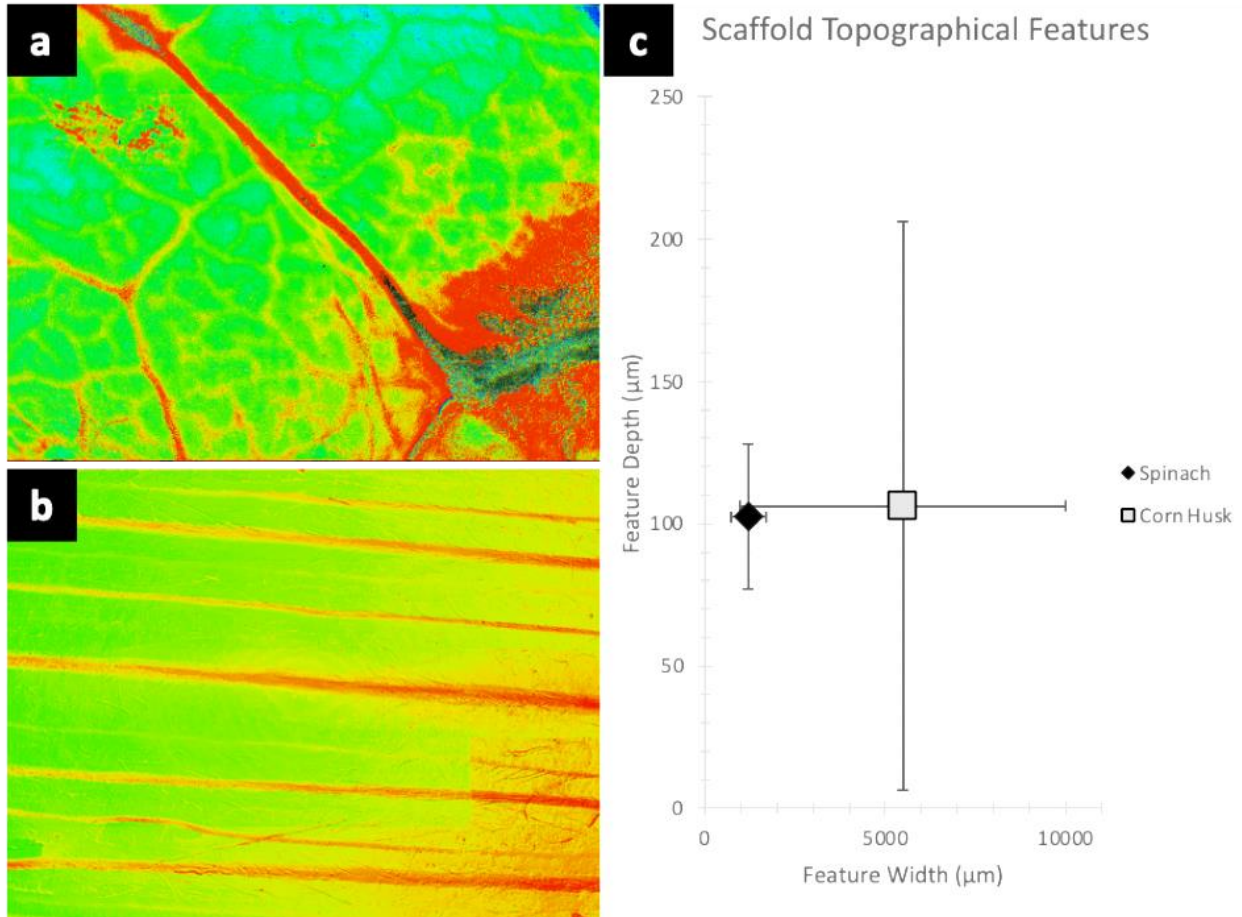


Figure 15| Corn husk possess significantly wider feature widths and higher variability in both width and depth. (a) Depth heatmap of decellularized spinach leaf surface. (b) Depth heatmap of decellularized corn husk surface. (c) Topographical comparison of decellularized scaffolds. (n=6)

5.3.2 Assessment of Cell Alignment and Visualization “Cellular Alignment Cartography”

QM7 cells that differentiated on spinach and corn husk for 7 d exhibited few signs of alignment (Figure 16). This was particularly observed within the large cell aggregates present across the surface of the scaffolds, within which microfilaments can be seen in seemingly all directions. Figure 17 illustrates this apparent randomness within one of the aggregates on samples from each leaf type. The aggregates present on the spinach scaffolds appeared considerably larger than those that formed on the corn husk scaffold. The kappa values were used to quantify the alignment of cytoskeleton microfilaments within each sample’s image. QM7 cells cultured on decellularized spinach scaffolds exhibited an average kappa value of 0.204 ± 0.45 . The corresponding histograms on the cytoskeletal orientation showed a single mode peak. Their counterparts that were cultured on decellularized corn husk had an average kappa value of 0.13 ± 0.1 . The corresponding histograms showed bimodal distributions of cytoskeletal alignment. Further separation of distinct cell populations isolated by cornhusk ridges also displayed bimodal orientation distributions. A t-test revealed that the difference was statistically significant with a p-value of 0.03.

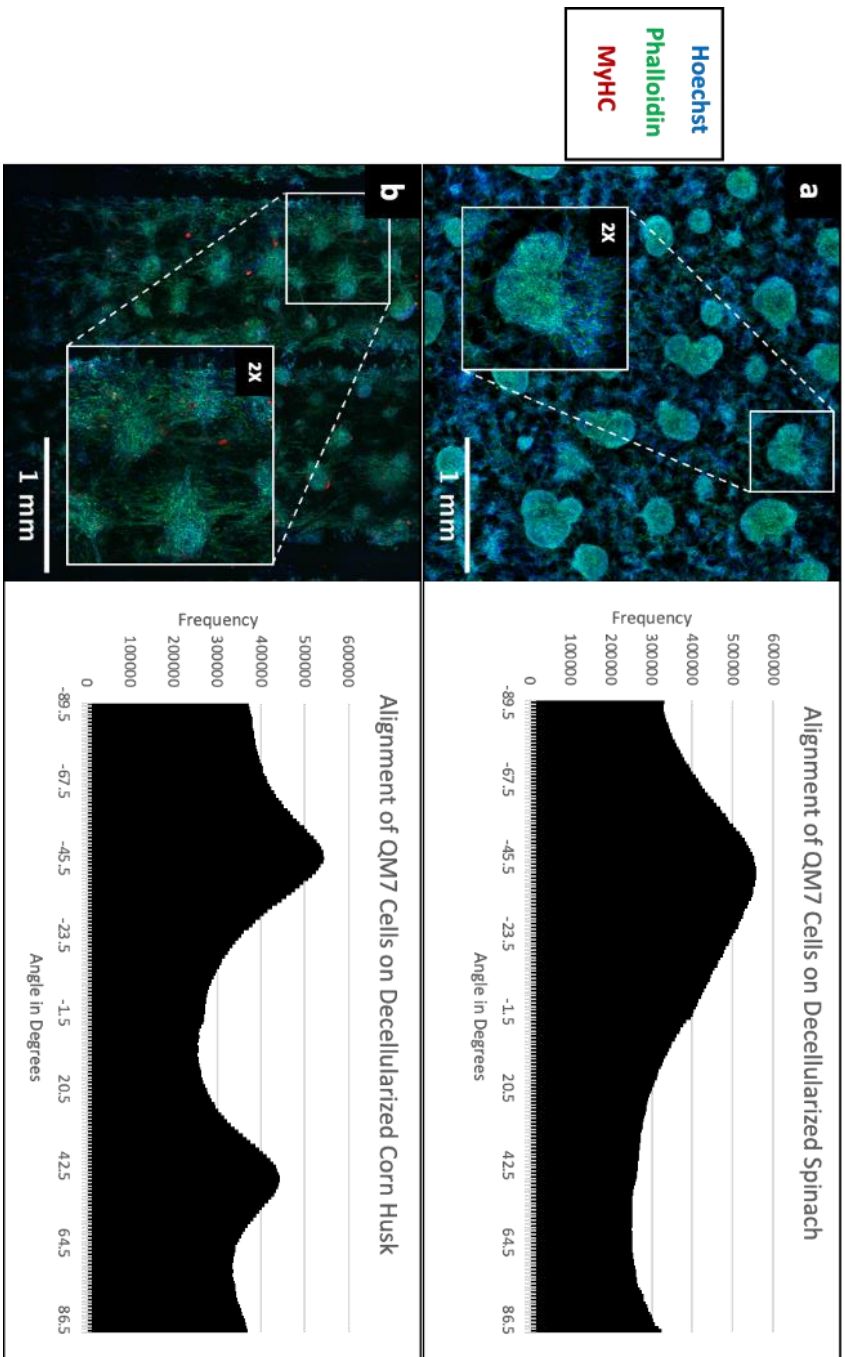


Figure 16| QM7 cells exhibit superior alignment characteristics on decellularized spinach compared to decellularized corn husk. (a) Tiled array of micrographs of QM7 cells on decellularized spinach. (b) Tiled array of micrographs of QM7 cells on decellularized corn husk. (c) Global alignment of QM7 cells on decellularized spinach and corn husk. (n=6)

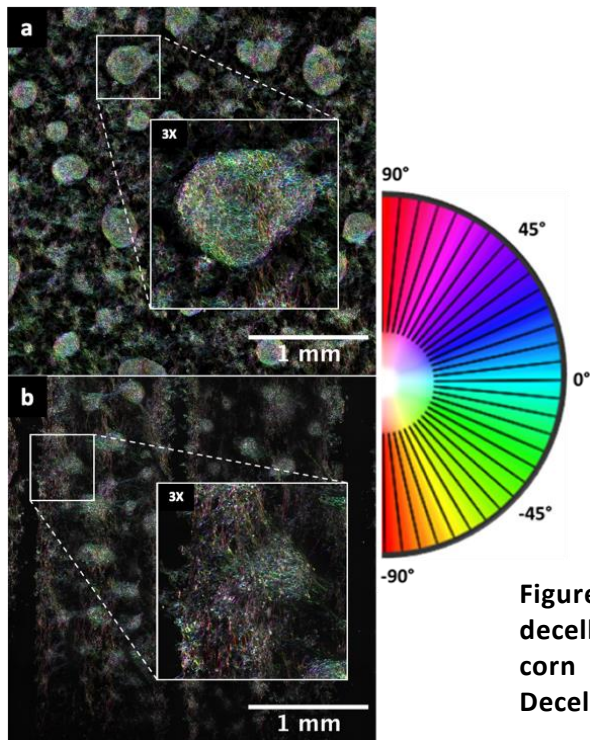


Figure 17 | Color survey of cell aggregates on decellularized spinach and decellularized corn husk. (a) Decellularized spinach. (b) Decellularized corn husk

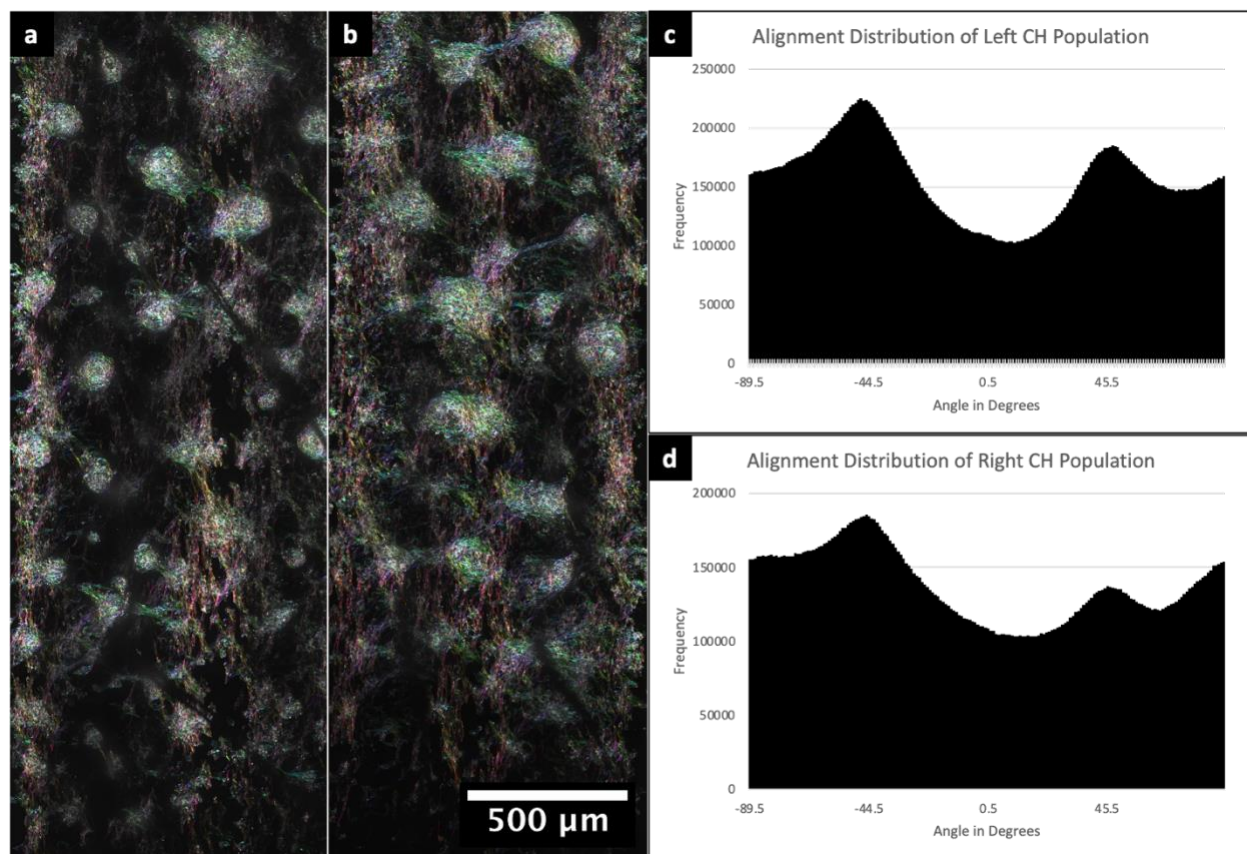


Figure 18 | Bimodal distribution of corn husk persists even after isolation of cell populations. (a) Left QM7 population. (b) Right QM7 population. (c) Orientation distribution of left population. (d) Orientation distribution of right population

CAC was used to generate kappa heatmaps that revealed regions of high alignment on the scaffolds' surface (Figure 19). Low alignment was observed across the surfaces of the decellularized spinach samples, with sparse ROIs that exhibited marginally higher kappa values. Similar results were observed in decellularized corn husk samples, albeit with an even fewer ROIs exhibiting high kappa values than observed in the decellularized spinach samples. Although most ROIs had kappa values near 0, it is possible that some of them had kappa values above the mean. The heatmaps were normalized so that the highest values on the color scale corresponded to the highest kappa values within the image, and vice versa for the lowest kappa values. After normalization, the heatmaps of both groups appeared excessively noisy and lacked distinct areas of high alignment.

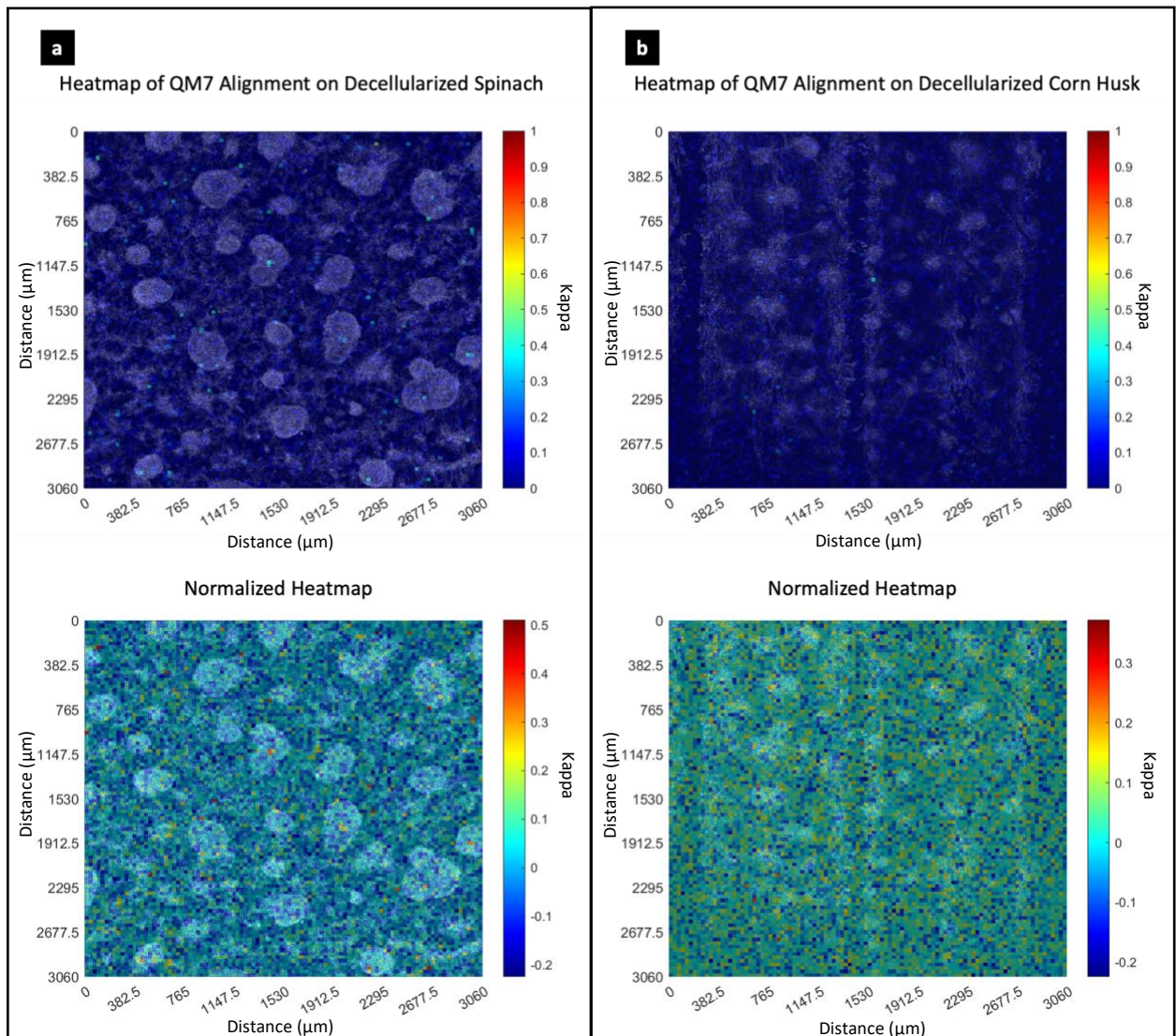


Figure 19|Kappa heatmaps of QM7 cells cultured on decellularized spinach and decellularized corn husk. (a) Kappa heatmap of decellularized spinach samples. (b) Kappa heatmap of decellularized corn husk samples

5.3.3 Assessment of differentiation potential

The fusion index of QM7 cells that were differentiated on the surface of decellularized spinach was not significantly different from that of QM7 cells on the surface of decellularized corn husk (Figure 20). After 7 d of differentiation, $12 \pm 13\%$ of the control population grown on spinach was MyHC-positive. Of the population of cells from all cows grown on decellularized corn husk $3.2 \pm 2.2\%$ were positive for MyHC. A t-test revealed that there was no significant difference in differentiation between cells grown on each substrate.

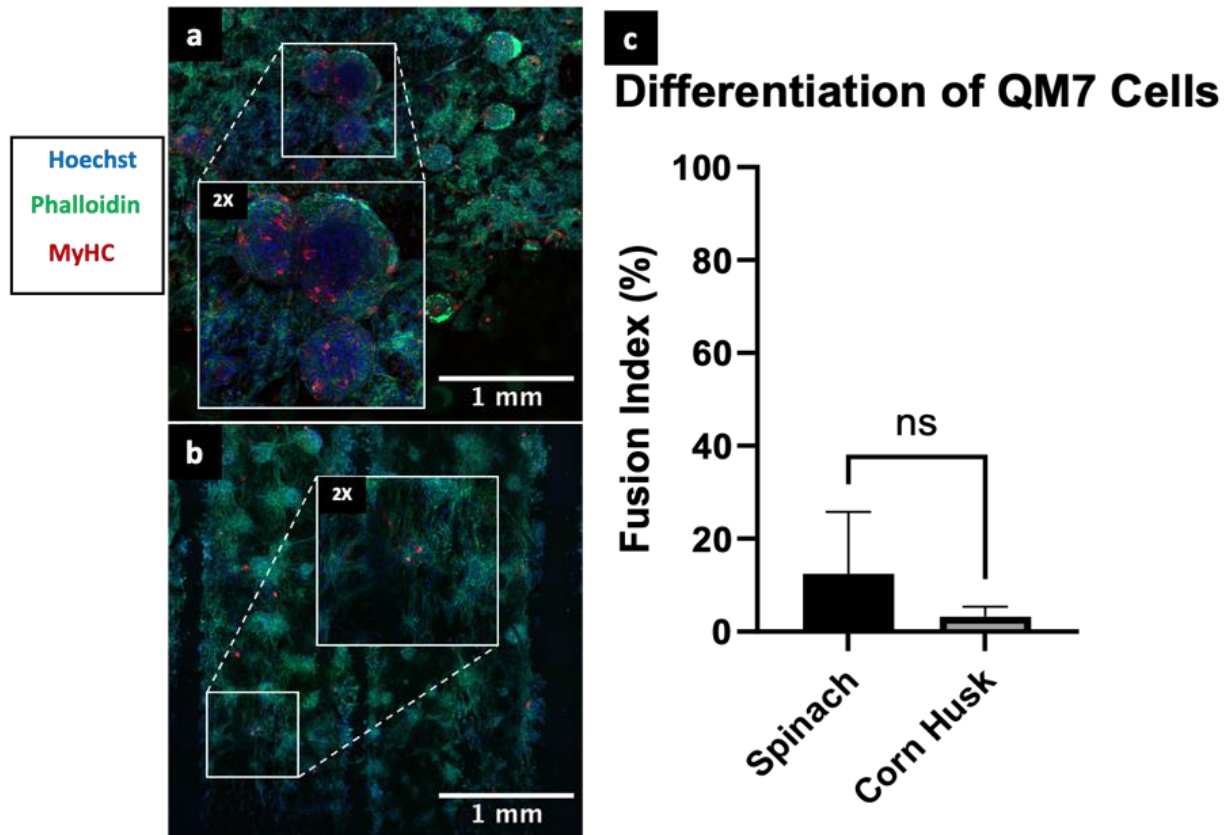


Figure 20| QM7 cells exhibit little differentiation of both scaffolds. Differentiation was slightly higher on decellularized spinach compared to decellularized corn husk. (a) QM7 cells differentiated on decellularized spinach. (b) QM7 cells differentiated on decellularized corn husk. (c) Comparison of QM7 differentiation capacity (n=6).

5.4 Discussion

Due to its low cost, availability, familiarity, and demonstrated biocompatibility, decellularized spinach was initially chosen as a model plant for the development of decellularized plant scaffold. As a dicot plant, spinach has a readily accessible vascular structure, making it ideal for perfusing oxygenated media in advanced cell culture applications. Previous research showed that decellularized spinach can support the growth of numerous cell types, including human mesenchymal stem cells (hMSCs), human umbilical vein endothelial cells (HUVECs), and human pluripotent stem cell derived cardiomyocytes (hPS-CM) ⁶. Similar support for PBSCs has been demonstrated in section 3A.3. However, spinach is not the only plant that may be useful for tissue engineering applications. Due to their linear morphology, leek, asparagus, green onion, and celery may also be beneficial for skeletal muscle cultures. Similarly, corn husk has a linear topography. Although ethnic dishes, such as tamales, use corn husk, it is usually discarded as food waste. In addition to its topographical characteristics, the use of corn husk as a scaffold material for skeletal muscle cultures could contribute to the reduction of food waste, adding further value to corn husk as a scaffold material.

In skeletal muscle culture, a high level of cell alignment on the substrate is crucial. Alignment facilitates not only myoblast fusion but also myotube orientation in the same direction. This detail is important to the efficacy of skeletal muscle tissue. From a biological standpoint, the force generated by muscle tissue equals the sum of the forces generated by each myotube along the axis of contraction. If some myotubes are not colinear with the axis of contraction, only the portion of the force that is colinear with the contraction will be contributed, while the remaining force will be wasted. In terms of food, the orientation of the myotubes may affect the mouthfeel, texture, and fibrous structure of the meat. Like the biological effects of cell alignment, the mechanical and electrical conditioning of muscle tissue may also be affected by cell alignment.

It is widely accepted that topographies with recurring linear features can affect the alignment of cells cultured on these surfaces. Parallel grooved surface topographies with subcellular widths between 6 -12 μm have been shown to improve myocyte alignment in the direction of the grooves ¹³¹. It has also been observed that myoblasts cultured on substrates with feature widths between 5 – 75 μm are subject to topographical influence ¹³⁶. One advantage of using synthetic materials for scaffolds is that they can be manufactured with specific topography to improve cell alignment ⁷³. Identifying natural scaffolds with optimal topographical characteristics is a more challenging task.

This study sought to understand the contribution of the topography of monocot plants such as corn in comparison to dicot plants such as spinach. It was hypothesized that the linear topography of corn husk may provide an advantage in directing the alignment of cells compared to the spinach scaffolds and their fractal patterned topography. The surface features of decellularized spinach had an average feature depth of $102 \pm 25 \mu\text{m}$, whereas decellularized corn husk had an average feature depth of $106 \pm 99 \mu\text{m}$. The two scaffolds have similar average feature depth measurements, but feature depth is much more variable in corn husk than spinach. However, feature depth may be less important for cell alignment than feature width. This is due to the ideal feature width being smaller than the average width of the cells themselves ¹³¹.

The surface features of decellularized spinach had an average feature width of $1,200 \pm 480 \mu\text{m}$, whereas decellularized corn husk had an average feature depth of $5,500 \pm 4,500 \mu\text{m}$. Like the average feature depth, the average feature width observed in the corn husk is much more variable than that observed in the spinach. The average feature depth of the spinach and corn husk are both well beyond the previously mentioned ideal feature width. However, it is still possible that the linear topography of the corn husk may offer a marked improvement over the decellularized spinach scaffolds which have crevasses that are not aligned with one another.

Upon inspecting the micrographs of the QM7 cells on the surface of the decellularized spinach scaffolds, many cell aggregates were found across their surfaces. While it is not readily apparent why these aggregates formed, they may be due to over population of the scaffold. Similar aggregates were found on the surface of the decellularized corn husk samples, although smaller in size. Another potential reason for aggregate formation might be the presence of trichome hairs. These hairs could prevent the cells from establishing proper contact with the leaf surface, leading the cells to bond preferentially to other cells than with the leaf surface. After 7 days in culture, QM7 cells differentiated on spinach and corn husks exhibited low alignment, as shown in figure 16. Microfilaments were observed oriented in what appears to be all directions within the aggregates and may have contributed to the low kappa values. This apparent randomization within the aggregates from both groups is shown in Figure 17. QM7 cells cultured on decellularized spinach scaffolds exhibited an average kappa value of 0.204 ± 0.45 . The corresponding histograms on the cytoskeletal orientation showed a single mode peak. The corn husk group had an average kappa value of 0.13 ± 0.1 . The corresponding histograms showed bimodal distributions of cytoskeletal alignment, which further reinforce the low kappa values. Looking at the micrographs of the cells growing on the surface of the corn husk the QM7 cells were not present at the crest of the corn husk ridge. It is not readily apparent why the cells are absent in this region, but it may be due to the higher density of trichome hairs.

Regardless of the cause, this void of cells resulted in the formation of isolated cell populations in the valleys between the corn husk ridges. A possible explanation for the bimodal distribution is that each population within the image has its own distribution peak because they do not interact. To test this hypothesis, the image was cropped to include only a single population of continuous cells. After analyzing each half of the image separately, the individual populations continued to exhibit bimodal distributions at approximately the same angles. This suggests that the bimodal distribution was caused by the orientation

of the cell cytoskeleton, and not by the presence of 2 distinct cell populations in the original image. A t-test revealed that the differences observed were not statistically significant with a p-value of 0.61.

CAC analysis and cells grown on spinach showed only a few regions of interest (ROIs) exhibited marginally higher kappa values. Similar outcomes were observed in decellularized corn husk samples, albeit with fewer ROIs exhibiting high kappa values. Even though most ROIs had kappa values close to 0, it is possible that a few of them have kappa values above the mean. The heatmaps were normalized so that the highest color values corresponded to the highest kappa values within the image, and vice versa for the lowest kappa values. After normalization, the heatmaps of both groups exhibited excessive noise and lacked distinct regions of high alignment.

In this study, the topography of the corn husk appeared to provide no advantage for cell alignment. In fact, the higher alignment on the decellularized spinach scaffold was statistically significant with a p-value of 0.03 suggesting that the spinach scaffold had a greater effect on directing cell alignment than the corn husk scaffold. Recall that the width of the feature plays a major role in directing cell alignment and that the range of influence for myoblasts is between 5 and 75 μm ¹³⁶. The spinach scaffold's feature width is significantly shorter than that of the corn husk. As feature width increases, it is expected that the influence of the topography will decrease. Due to cell aggregation, it is challenging to distinguish between the alignment of the cells in direct contact with the surface and the cells within the aggregates. However, CAC analysis did not reveal clusters of higher alignment outside of the aggregates, indicating that the lack of alignment may not be solely attributable to the randomness of the aggregates, but may also be attributable to the surface of the scaffolds.

The capacity to differentiate is just as important as the ability to align properly. It was hypothesized that the linear topography of the corn husk would enhance the differentiation capacity by directing alignment. The findings from this study suggest that there was no such influence over the cellular alignment. The same can be said about the topography's influence over fusion index. Figure 20 shows that the fusion

index of QM7 cells differentiated on the surface of decellularized spinach was marginally higher than that of QM7 cells differentiated on the surface of decellularized corn husk. $12 \pm 13\%$ of the control population grown on spinach was MyHC-positive after 7 days of differentiation. $3.2 \pm 2.2\%$ of the cell population from all cells grown on decellularized corn husk contained MyHC. A t-test revealed that there was no significant difference between cell differentiation on each substrate. These findings suggest that the topography had no significant effect on the differentiation capacity of the cells.

The overall findings of this investigation are inconsistent with the hypothesis. In terms of average cell alignment, it appears that the linear topography of the corn husk provided no advantage over the spinach scaffold. However, the kappa heatmaps suggest that the higher alignment observed in the spinach may not have been directly related to the crevices on the scaffold's surface. Considering that both substrates presented low alignment throughout their surfaces, it is just as possible that corn husk has a negative effect on cell alignment due to the numerous trichomes and large feature width rather than spinach offering an advantage due to its narrower feature width ^{93,144}. In fact, it is questionable whether the topography of the corn husk had any influence on the morphology of the cells at all.

There are a few questions that this study leaves unanswered. Measurements of the surface stiffness of each of the scaffolds could have provided further insight into some of the data, most notably the difference in differentiation. Regarding alignment, the inclusion of a surface that was completely flat would make it more evident whether the topography of the spinach had any favorable impact on cell alignment. Previous research suggests that there is no alignment advantage to using decellularized spinach as a scaffold; however, the kappa measurements in that study covered a significantly smaller region than the area that was measured in this investigation ⁹⁴. Another limitation of this research was that it only compared corn husk to spinach. Other monocot plants with a topography comparable to corn husk exist. There could be other plant species with narrower grooves and few or no trichomes. While many plants contain linear grooves on their surfaces, it is unclear whether there are any with grooves

narrow enough to influence myoblast alignment. Incorporating data from a broader range of plant species might aid in answering this question while also possibly uncovering other beneficial traits. Future studies could address these questions by measuring the stiffness of the surfaces using methods such as AFM and exploring a larger variety of plant species. There may be a plant out there with all the traits ideal for skeletal muscle culture, but it may be possible to alter plant attributes by changing the environment in which they grow. For example, to alter the stiffness of plant leaves. Satellite cell development has been demonstrated to be improved by materials with a Young's modulus, or stiffness, comparable to native muscle (12 KPa). However, the effect diminishes when stiffness exceeds (20 KPa)⁹³.

Plants mechanically reinforce themselves by depositing secondary cell walls in the vascular system's xylem tissue^{86,137}. This strengthening is most apparent in the plant's stem, although it also occurs in the leaves. Secondary cell walls are mostly made up of lignin^{86,88,137}. Blue light with wavelengths about 470nm has been demonstrated in studies to stimulate secondary cell wall deposition via stimulation of the cryptochrome1 (cry1) photoreceptor and upregulation of NST-161. Cry1 stimulation promotes the production of transcription factors MYC2 and MYC4, which bind to the NST-1 promoter. Given that secondary cell walls are responsible for mechanical strengthening of the plant's body, an increase in secondary cell wall deposition may influence the surface stiffness of leaves. More research is needed to determine which plant species are best suited for skeletal muscle culture and, specifically, lab-grown meat production. There are still major obstacles ahead on the path of developing an ideal sustainable meat product, but each piece of data brings us closer.

Chapter 6: Conclusions and Future Work

6.1 Conclusions

This body of research set out to study the possible use of plant leaves as a scaffold for *in vitro*-produced structured meat products. Given escalating demand and limited resources, this research is motivated by the urgent need to develop sustainable alternatives to traditional livestock meat products. This chapter summarizes the study by reviewing the key research findings related to the 3 research aims and their contribution to the field, discussing the study's key limitations, and proposing future studies to further advance the field.

6.2 Key Findings and Contribution to the Field

6.2.1 Decellularized Plant Scaffolds for PBSC Cultivation (Aim 1A): The first aim was to investigate the possibility of using plant leaves as a scaffold for the cultivation of PBSCs for human consumption, as previous studies have demonstrated their ability to support the growth of various cell types. The hypothesis was that decellularized plant scaffolds will have no significant impact on the survival or differentiation of PBSCs cultured on their surface. To investigate this hypothesis, Aim 1 had two subaims. In Aim 1A, both the gelatin-cultured control group and the decellularized leaf scaffold groups demonstrated sustained viability, with 100% viability and no cytotoxic effects observed after 7 d. Viability was maintained even after 14 d of incubation. After 14 d of differentiation, there was a significant increase in the number of MyHC-positive cells compared to 7 d of differentiation. The analysis of cell alignment revealed that cells cultured on gelatin for 7 d exhibited signs of alignment within the images, albeit without clear alignment across the seeding region. Cells from Cow 1 grown on decellularized leaf scaffolds demonstrated more consistent relative alignment than Cows 2 and 3 .

Measurement of the cytoskeletal alignment indicated that decellularized leaf scaffolds slightly improved cytoskeleton alignment and significantly improved nuclear alignment in Cow 1 cells. In contrast to their

gelatin controls, however, the alignment of cytoskeletons in cells from Cows 2 and 3 on leaf scaffolds was less pronounced. Both gelatin-grown cells and cells on decellularized leaf scaffolds exhibited minimal alignment change after 14 d of differentiation, compared to 7 d.

Decellularized spinach has been demonstrated to support various cell types including hMSCs, HUVECs, and hPS-CMs. However, prior to this study it was not clear whether satellite cells remain viable and differentiate on decellularized spinach^{6,7}. This study reinforces the potential of decellularized plant leaves, particularly spinach leaves, as a suitable scaffold for PBSC cultivation. The viability and differentiation of PBSCs on these scaffolds matched those of more conventional gelatin-cultured controls. This introduces a sustainable and potentially economical alternative for lab-grown meat production. Previous studies involving decellularized spinach used immortalized cell lines to explore decellularized plant leaves as a scaffold. By using PBSCs, this study provided insights into how satellite cells behave on decellularized spinach scaffolds. The use of primary cells also exposed the prevalence of biological variation observed in alignment characteristics. The data supporting data can be found in section 3A.3.

6.2.2 The Importance of Decellularization (Aim 1B): It was posited that decellularization was necessary to culture cells on the surface of a leaf⁶. Although decellularization provides a scaffold material shown to support PBSCs, it removes many characteristics of the underlying plant. Leafy greens inherently contain dietary fiber, but they are also associated with other nutritional benefits that reduce the risk of chronic disease. Additionally, vegetables contain flavor-enhancing compounds. Like antioxidants, these astringent substances may be lost during the process of decellularization. Eliminating the decellularization process from the theoretical workflow of culture meat development based on this technology would help preserve the health benefits of the underlying vegetable, preserve its flavor profile, and reduce processing steps and associated costs. Retaining these characteristics could enable the production of lab-grown meat that incorporates both the health benefits of the plant and its complex flavor profiles. In Aim 1B, the findings demonstrated the importance of the decellularization procedure and its role in assisting with cell

attachment and growth on the leaf scaffolds. The hypothesis was that decellularization is necessary for the survival of cells in long term cell culture on the surface of leaves. Cell density analysis in Aim 1B revealed there were nearly no cells found on non-decellularized samples after 7 d, despite going through cuticle removal. This revealed a fundamental conflict between preserving the inherent nutritional properties of plant matter and fostering an environment conducive to cell culture. These findings supported the hypothesis that decellularization was essential to support cell culture for sustained periods. The supporting data can be found in section 3B.3.

6.2.3 A Food Safe Decellularization Method (Aim 2): Conventional decellularization methods used reagents that were not compatible with human consumption. The study introduced an improved decellularization method that used REG detergents that better align with FDA recommendations for food additives. This not only improved the safety profile of the process but also eliminated the need for potentially harmful agents like hexanes.

The hypothesis was that the use of REG detergents will not inhibit the decellularization of spinach leaves or the viability of cells sown on REG scaffolds.

DNA analysis revealed that plant DNA was effectively extracted from leaf samples using both the REG and conventional decellularization protocols. Histological staining demonstrated the near-total removal of cellular material by both decellularization methods, which left the cellulose structure intact. After 7 d of culture, the average viability of cells cultured on scaffolds produced by both methods was near 100%. Contrary to prior understanding, the results of this study indicated that hexanes were not required to decellularize plant leaves. Moreover, the results suggested that PS20 is a suitable substitute for TX100 as a secondary detergent. The resultant scaffolds also had no cytotoxic effect on cells. These findings produced a decellularization method that was more in line with FDA recommendations for food additives

and paves the way to making decellularization an accepted food processing step. The supporting data can be found in section 4.3.

6.2.4 The Influence of Plant Leaf Topographies on the Alignment of Myoblasts (Aim 3): The literature suggests that substrates with linear topographies may influence the alignment of cells growing on the surface of the substrate. This study sought to understand the influence of the linear topographies of monocot plants relative to Dicot plants. This work builds on previous studies that focused on the use of food waste items like corn husk ¹³⁸. The hypothesis was that alignment and differentiation will be greater in regions where linear topography is present on both surfaces and therefore greater overall on corn husks than on spinach due to the greater prevalence of linear topography. Surfaces of decellularized spinach and corn husk were characterized in terms of feature width and depth using fluorescence microscopy and depth mapping. CAC analysis was used to determine the average cytoskeletal alignment of cells on scaffold surfaces and to generate alignment heatmaps to offer spatial context for the alignment data. Finally, differentiation was evaluated to investigate the influence of the topography on differentiation capacity.

The surface topography of both scaffolds revealed that crevasses on the surface of the corn husk scaffolds were significantly wider than the spinach scaffolds, with the largest features being nearly 1 cm wide. Similarly, the variability of the feature width of the corn husk was significantly greater than that of the spinach scaffolds. The two scaffolds exhibited comparable average feature depths, but variability in feature depth in the corn husk was substantially greater when compared to spinach. The average feature width of the spinach and corn husk are both well beyond the previously mentioned ideal feature width. Furthermore, the corn husk featured many hairlike trichome projections on its surface. The projections appeared at larger concentrations towards the corn husk crests. These hairs likely impeded cell adhesion, reducing cell seeding efficiency and confounding alignment measurements.

Upon examination of micrographs of QM7 cells on the surface of decellularized spinach scaffolds, numerous cell aggregates were observed. While it is not immediately clear why these aggregates formed, it is possible that they are the result of an overpopulation of the scaffold. On the surface of the decellularized corn husk samples, similar but smaller aggregates were observed. These clusters could complicate the analysis of alignment in both groups. After 7 d in culture, QM7 cells that had differentiated on spinach and corn husk displayed poor alignment. The corresponding cytoskeletal orientation histograms displayed a single mode peak. The corn husk group was also poorly aligned. The corresponding histograms revealed bimodal distributions of cytoskeletal alignment, supporting the low kappa values. CAC analysis of the spinach group revealed that only a few ROIs had marginally higher kappa values. Similar outcomes were observed in samples of decellularized corn husk, with even fewer ROIs with high kappa values. After normalization, the heatmaps of both groups displayed excessive noise and lacked distinctly high alignment zones.

The overall findings of this investigation indicate that the linear topography of the corn husk did not provide any advantage over the spinach scaffold in terms of average cell alignment. However, the lack of alignment on the corn husks can be attributed to the trichomes on the corn husk's surface, which likely confounded the alignment measurements. However, the kappa heatmaps indicate that the higher alignment observed in the spinach may not have been directly related to the topography. Considering that both substrates exhibited low alignment throughout their surfaces, it is just as likely that corn husk's large feature width has a negative influence on cell alignment as spinach's narrower feature width offers an advantage. This study contributed to the field by highlighting the challenges that may arise when culturing cells on different plant species. The QM7 cells may have had difficulty adhering to the surface of the corn husk and spinach, evident by the prominence of large cell aggregates on the surface of both plants. These complications underscore yet another source of cell-based variation to accompany the biological variation first observed in Aim 1. The supporting data can be found in section 5.3.

6.2.5 CAC Analysis (Aim 3): In addition to the presented data, this study used CAC analysis which not only quantifies the relative alignment of cells across a surface but also offers spatial context to the findings. The integration of alignment and spatial measurements yields insights into which surface features most significantly impact alignment and the extent of this influence across a cell population. Though the mechanics of this analysis method may not be novel, its application offers a visualization of the data previously unseen in the literature. The supporting data can be found in section 5.3.

6.3 Key Limitations and Shortcomings

As with any study, there is room for improvement and unanswered concerns. Identifying the factors responsible for the observed biological variation in differentiation and alignment among primary cell isolations is one example of the first objective. To establish stable and consistent cell lines for *in vitro* meat production, it is necessary to investigate and comprehend the underlying causes of these differences, such as cell donor age, genetics, tissue source, and specific environmental conditions.

In addition, the capability of cells to infiltrate the leaf structure is an important issue that must be addressed. Current evidence suggests that cells do not penetrate the leaf, resulting in a substantial amount of cellulose rather than muscle tissue in the proposed meat product. Perfusion of cell-attracting factors can be tested to promote cell migration into the spongy mesophyll of the leaf, allowing to produce meat with a higher protein content that resembles traditionally produced meat more closely. It may be necessary to optimize the decellularization process to preserve essential dietary components, such as vitamins, minerals, antioxidants, and astringent compounds. This development would enable scientists to develop meat products with distinct flavor and nutritional attributes.

It is also necessary to assess the viability of perfusion as a method for delivering oxygenated media and nutrients to cells within the leaf scaffold, especially for the proposed construct consisting of layered muscle tissue. Designing perfusion systems and evaluating their efficacy in delivering nutrients

and removing impurities can yield insightful information. Establishing effective perfusion techniques will ensure adequate oxygen and nutrient supply within the scaffold for cell growth and function.

In Aim 2, the impact of the modifications on the mechanical properties of the scaffold remains unclear, warranting further investigation. Tensile testing, atomic force microscopy (AFM), and micro-indentation can be used to assess the scaffold's global and micro-mechanical properties. Additionally, the influence of the modified decellularization method on cell differentiation can be examined once the mechanical properties have been studied. Evaluating cell behavior and phenotype, including differentiation markers such as MyHC and desmin, will provide insights into the scaffold's effect on cell differentiation. Second, the presence of residual decellularization agents in the finished scaffold must also be assessed to ensure compliance with FDA guidelines. Quantifying residual agents using liquid chromatography – mass spectrometry (LC-MS) can determine if the scaffold meets the required safety thresholds for food usage

139,140

In Aim 3, measurements of the surface stiffness of each scaffold could have provided additional insight into some of the data, most notably the differentiation disparity. Repeating this study with corn husks that have had their trichomes removed, or with another monocot species that doesn't have trichomes, could provide a clearer assessment of how topography influences cell alignment. There exist additional monocots with a similar topography to corn husks. There may be other plant species with channels that are narrower and free of trichomes. While numerous plants have linear grooves on their surfaces, it is unknown whether any of these grooves are narrow enough to affect myoblast alignment. Incorporating data from a broader range of plant species could aid in answering this question, while also possibly revealing other advantageous characteristics.

6.4 Defining Success in lab-grown meat

Broadly speaking, defining the criteria for success in the realm of lab-grown meat products is a multifaceted challenge. There are several dimensions to consider, including technological advancement, economic viability, sustainability, ethical considerations, and social acceptance. Technological success in the lab-grown meat industry necessitates meeting specific criteria that position these products as viable alternatives to traditional meat. This entails satisfying customer expectations in terms of sensory factors like taste, aroma, appearance, and texture. Additionally, it involves more intricate technological advancements, such as the efficient proliferation and differentiation of muscle tissues used in these products. Economic success is contingent upon developing cost-effective production processes that can meet the scale of demand while maintaining an affordable price point for consumers. Achieving this is crucial for the widespread adoption of lab-grown meat.

Sustainability success is a critical dimension and involves quantifiable reductions in the environmental impact of the agriculture industry. This can manifest as decreased energy consumption, reduced ecological degradation, and lower greenhouse gas emissions. Ethical success entails improvements in animal welfare, including minimizing harm to animals involved in the lab-grown meat production process and enhancing their living conditions. However, the path to success in these tangible metrics is accompanied by the formidable challenge of social acceptance.

Meat has played a pivotal role in the development of human societies and has facilitated numerous technological advancements. It is deeply ingrained in our culture and holds a significant place in our collective memories. Due to its association with positive experiences across various cultures, it appears nearly irreplaceable. Shifting societal behaviors away from meat consumption is akin to asking people to distance themselves from their cultural heritage, cherished memories, and, on a societal scale, one of the most reliable sources of nutrition. Replacing traditional meat with a more sustainable alternative presents a daunting challenge that extends beyond the scope of this research. Within the scope of this study,

success can be best assessed by examining technological advancements that have the potential to pave the way for further sustainability improvements in the lab-grown meat industry.

The affordability, widespread availability, and familiarity of decellularized spinach position it as a potentially valuable tool for propelling lab-grown meat toward success. However, before its application on a larger scale can be realized, certain technological advancements must be achieved. There is a need to enhance the efficiency of cell seeding. Previous studies have suggested that cells can be cultured on the surface of decellularized plant leaves without surface functionalization. However, there is still the challenge of cells that may not readily adhere to the surface, resulting in significant losses. Maximizing cell seeding efficiency in a cost-effective way is imperative to harness the full potential of decellularized leaf scaffolds.

Once the cells are seeded onto the scaffold's surface, the cells must show high viability, proliferate, and show high differentiation efficiency. While the data presented in this study suggest that the sown cells can retain their viability and differentiation capacity, it lacks insights into cell proliferation. The data also show a low fusion index and overall differentiation among the sown cells. Several factors could contribute to this outcome, including the choice of cell type, the differentiation protocol used, the mechanical properties of the scaffold, or a combination of these factors. Gaining a comprehensive understanding of these elements is imperative for achieving success. Targeting an average fusion index around 40% would put the scaffolds on par with conventional substrates like Matrigel¹⁴¹. It is also important to consider the alignment of the cells. To replicate the texture characteristic of traditional meat, it is essential for the cells to align correctly with one another. This alignment is necessary for recreating the fibrous structure and the tactile sensation experienced when tearing meat apart. Whether achieved through surface modifications or the selection of a different plant species with advantageous surface properties, ensuring proper cell alignment will be a critical factor in the success of decellularized leaf scaffolds. The target for alignment will depend largely on the alignment of skeletal muscle in vivo. This target will be reached when

there is no statistically significant difference between the average kappa of cells sown on the scaffold and the cells found in vivo.

The use of decellularized leaf scaffolds is predicated on their ability to support thicker tissues and stack to form substantial meat samples. It has not yet been demonstrated that tissues with thicknesses ranging from 100 - 200 μm can be developed and sustained on these leaf scaffolds. Achieving this may require the active perfusion of the leaf scaffold—a feature that is theoretically advantageous but has yet to be empirically proven to be effective. The success of this technology is likely contingent on the successful demonstration of this perfusion feature. Once demonstrated, it should be validated within a multi-scaffold stack, affirming its applicability in real-world conditions.

6.5 The Social Challenge

Lab-grown meat faces significant technical and economic challenges in replacing traditional meat products. However, it's the social challenges that may pose an even greater obstacle. The most apparent challenge is replicating the sensory experience of consuming traditional meat products, but several other factors are equally concerning, including perceptions of safety, issues of trust, and access to information. As lab-grown meat technology advances, understanding public acceptance will become integral to its commercial success.

The foundation of social acceptance is the perception of safety. If consumers believe that lab-grown alternatives are riskier than traditional meat products, public adoption will likely remain low. People tend to be cautious about unfamiliar food products. Understanding consumer behavior and attitudes towards genetically modified foods can provide insights into their potential attitude towards lab-grown meat products. Consumers tend to perceive genetically modified foods as being riskier, despite limited knowledge ¹⁴². This emphasizes the need for education and transparent communication between the science community and the public. To foster understanding, the scientific community must prioritize

informative campaigns, safety assurance, and addressing consumer concerns to ensure a more informed and receptive consumer base. However, this task is further complicated by the prevalence of misinformation and a lack of trust on the internet.

Studies on acceptance of the COVID-19 vaccine, suggest that misinformation can profoundly impact the acceptance of emerging technologies ¹⁴³. Just as false information about the vaccine led to skepticism and decreased vaccination intent, similar misinformation campaigns that include unfounded claims about lab-grown meat's safety, nutritional value, or environmental benefits could foster fear and skepticism impeding the acceptance of lab-grown meat. Countering potential misinformation will be crucial in building trust and promoting informed consumer choices. Proactive efforts to provide accurate information, transparent research, and open dialogues with the public will be essential in overcoming these social challenges.

6.6 Future Work

The research presented in this dissertation reveals multiple promising avenues for future research. For instance, future studies can be designed to explore methods to increase cell infiltration into the interior regions of the scaffold to address the cell to scaffold ratio. By perforating the surface of the scaffolds, cells may have better access to the interior mesophyll of the leaf (Figure 21). Future studies can also explore potential methods to manipulate the thickness of leaves and their nanomechanical properties. The

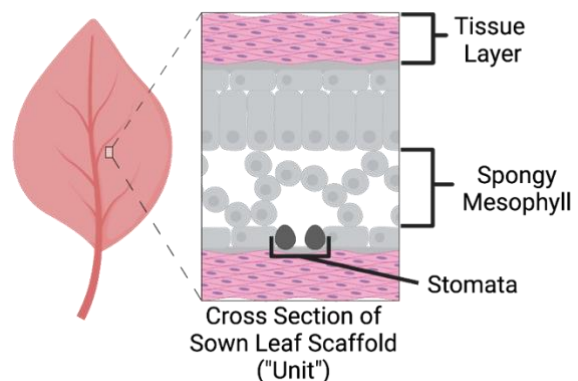


Figure 21 | Meat "unit" diagram. The spongy mesophyll is a porous tissue that tissue that could possibly be inhabited by mammalian cell growing on the surface of the leaf.

proposed method of using leaves as a scaffold develop meat requires that the skeletal muscle laden leaves be stacked to create thicker tissues. With the average leaf thickness ranging from 400 μm – 800 μm , and

the maximum tissue layer thickness of 200 μm , the body of the leaf will be a major portion of the final product^{86,144}. Reducing the thickness of the leaf scaffold would allow for a higher tissue/scaffold ratio. It is well known that nitrogen availability is one of the primary factors that support sustained plant growth^{144–146}. Studies have shown that by manipulating the nitrogen composition of fertilizers, the thickness of the various tissue layers of leaves can be changed in some plants. Regarding the manipulation of the surface stiffness of plant leaves, it is understood that plants mechanically reinforce themselves by depositing secondary cell walls in the xylem tissue of the vascular system^{86,147}. This reinforcement is typically seen in the stem of the plant, but the same mechanism works in leaves as well. Secondary cell walls are composed primarily of lignin^{86,88,147}. Studies have shown the exposure to blue light, with wavelengths around 470nm, can stimulate secondary cell wall deposition via stimulation of the cryptochrome1 (cry1) photoreceptor and upregulation of NST-161. Stimulation of cry1 leads to increased expression of MYC2 and MYC4 transcription factors that bind to the NST-1 promotor. Given that secondary cell walls are responsible for mechanical reinforcement of the body of the plant, it is reasonable to believe that an increase in secondary cell wall deposition may influence the surface stiffness of leaves. This proposed study focuses primarily on the optimization of the scaffold, but there is also a great deal left to understand about the scaffold's interaction with the skeletal muscle tissue. Utilizing a wider variety of cells, such as those from different species and the coculture of adipocytes and myoblasts on decellularized leaf scaffolds is a potential area for further investigation. Such studies would provide insight into the suitability of the scaffold for producing meat-like products with a wider variety of characteristics and architectures, such as fat content and marbling.

Additionally, transitioning to 3D tissue constructs would permit the creation of more complex and functional muscle tissue structures that more closely resemble traditional meat. By building multilayered tissue constructs with the leaf scaffold and incorporating transglutaminase, thicker tissue can be

produced. Adding transglutaminase to meat units composed of a decellularized leaf scaffold and muscle tissue can also improve the structural integrity and texture of *in vitro* produced meat.

Comparative protein analysis of *in vitro*-produced and traditionally sourced meat will be instrumental to understanding the protein profiles and compositions of these two varieties of meat can shed light on their nutritional value and potential differences in protein quality. Analytical techniques such as mass spectrometry and proteomics can be used to compare the abundance and varieties of proteins in the two meat sources.

Another key characteristic of meat is its texture. Conducting sensory evaluations and instrumental texture analysis, such as Warner-Bratzler shear force testing, can assist in evaluating the *in vitro* meat product's textural attributes, such as tenderness, juiciness, and mouthfeel, relative to traditionally produced meat

¹⁴⁸.

The results presented in this study provide a foundation for future research and innovation in this field. As we continue to unravel and navigate the complexities of tissue engineering and agriculture, we are poised to revolutionize the way in which we produce meat and other animal agricultural products by providing sustainable and ethical alternatives that are in line with the evolving needs of our planet. As stated by Albert Einstein, "in the midst of every crisis, lies great opportunity." Decellularized leaf scaffolds are an example of the kind of thinking that is required to build a future in which we may produce satisfying and nutritious meat products without compromising the well-being of animals or the planet. By investing in research, development, and implementation of tissue engineering, we may be able to foster the growth of a thriving agriculture sector that will not only provide alternative and ethical food choices but also generate a multitude of new jobs and economic opportunities. We can embrace this opportunity and shape a more sustainable and compassionate food system for future generations with sustained dedication and collaboration.

References

1. Aiking, H. Future protein supply. *Trends Food Sci Technol* **22**, 112–120 (2011).
2. Sha, L. & Xiong, Y. Plant protein-based alternatives of reconstructed meat: Science, technology, and challenges. *Trends Food Sci Technol* **102**, 51–61 (2020).
3. Datar, I. & Betti, M. Possibilities for an in vitro meat production system. *Innovative Food Science and Emerging Technologies* **11**, 13–22 (2010).
4. Zhang, G. *et al.* Challenges and possibilities for bio-manufacturing cultured meat. *Trends Food Sci Technol* **97**, 443–450 (2020).
5. Novosel, E. C., Kleinhans, C. & Kluger, P. J. Vascularization is the key challenge in tissue engineering. *Adv Drug Deliv Rev* **63**, 300–311 (2011).
6. Gershlak, J. R. *et al.* Crossing kingdoms: Using decellularized plants as perfusable tissue engineering scaffolds. *Biomaterials* **125**, 13–22 (2017).
7. Fontana, G. *et al.* Biofunctionalized plants as diverse biomaterials for human cell culture. *Adv Healthc Mater* **6**, 1–9 (2017).
8. Zeder, M. A. Core questions in domestication research. *Proc Natl Acad Sci U S A* **112**, 3191–3198 (2015).
9. statistic_id542890_beef-consumption-in-the-us-2002-2021.
10. statistic_id194297_total-number-of-cattle-and-calves-in-the-us-2001-2022 (1).
11. United States Department of Agriculture (USDA). National Animal Nutrition Program (NANP) Feed Composition Database. <https://data.nal.usda.gov/dataset/national-animal-nutrition-program-nanp-feed-composition-database>.
12. Brambilla, G. & De Filippis, S. Trends in animal feed composition and the possible consequences on residue tests. *Anal Chim Acta* **529**, 7–13 (2005).
13. Van Kernebeek, H. R. J., Oosting, S. J., Van Ittersum, M. K., Bikker, P. & De Boer, I. J. M. Saving land to feed a growing population: consequences for consumption of crop and livestock products. *International Journal of Life Cycle Assessment* **21**, 677–687 (2016).
14. Finley, J. W. & Seiber, J. N. The nexus of food, energy, and water. *J Agric Food Chem* **62**, 6255–6262 (2014).
15. Reisinger, A. & Clark, H. How much do direct livestock emissions actually contribute to global warming ? **2010**, (2018).
16. Burton, N. M., Vierck, J. L., Krabbenhoft, L., Byrne, K. & Dodson, M. V. Methods for animal satellite cell culture under a variety of conditions. *Methods in Cell Science* **22**, 51–61 (2000).
17. Leahy, E., Lyons, S. & Tol, R. S. J. An Estimate of the Number of Vegetarians in the World An Estimate of the Number of Vegetarians in the World. *ESRI Working Paper* 1–44 (2010).

18. Hargreaves, S. M., Raposo, A., Saraiva, A. & Zandonadi, R. P. Vegetarian diet: An overview through the perspective of quality of life domains. *International Journal of Environmental Research and Public Health* vol. 18 Preprint at <https://doi.org/10.3390/ijerph18084067> (2021).
19. Kyriakopoulou, K., Dekkers, B. & Goot, A. J. Van Der. *Plant-Based Meat Analogues. Sustainable Meat Production and Processing* (Elsevier Inc., 2019). doi:10.1016/B978-0-12-814874-7.00006-7.
20. Globe Newswire. Plant-based Meat Market To Reach USD 30.92 Billion By 2026 | Reports And Data. *Plus Company Updates 2018–2020* (2019).
21. Smetana, S., Sandmann, M., Rohn, S., Pleissner, D. & Heinz, V. Autotrophic and heterotrophic microalgae and cyanobacteria cultivation for food and feed: Life cycle assessment. *Bioresour Technol* **245**, 162–170 (2017).
22. van der Weele, C., Feindt, P., Jan van der Goot, A., van Mierlo, B. & van Boekel, M. Meat alternatives: an integrative comparison. *Trends Food Sci Technol* **88**, 505–512 (2019).
23. Zhang, R., Chen, J. & Zhang, X. Extraction of intracellular protein from *Chlorella pyrenoidosa* using a combination of ethanol soaking, enzyme digest, ultrasonication and homogenization techniques. *Bioresour Technol* **247**, 267–272 (2018).
24. Alexander, P. *et al.* Could consumption of insects, cultured meat or imitation meat reduce global agricultural land use? *Glob Food Sec* **15**, 22–32 (2017).
25. Van Huis, A. *et al.* *Edible Insects: Future prospects for food and the feed security*. (Food and Agriculture Organization of the United Nations, 2013).
26. Sari, Y. W., Mulder, W. J., Sanders, J. P. M. & Bruins, M. E. Towards plant protein refinery: Review on protein extraction using alkali and potential enzymatic assistance. *Biotechnol J* **10**, 1138–1157 (2015).
27. O'brian, M. R. *Heme Synthesis in the Rhizobium-Legume Symbiosis: a Palette for Bacterial and Eukaryotic Pigments*. *JOURNAL OF BACTERIOLOGY* vol. 178 <https://journals.asm.org/journal/jb> (1996).
28. Boatright, W. L. & Lu, G. Hexanal synthesis in isolated soy proteins. *JAOCs, Journal of the American Oil Chemists' Society* **84**, 249–257 (2007).
29. Squire, J. M. Muscle filament structure and muscle contraction. *Annu Rev Biophys Bioeng* **4**, 137–163 (1975).
30. Stehle, R., Krüger, M. & Pfitzer, G. Force kinetics and individual sarcomere dynamics in cardiac myofibrils after rapid Ca²⁺ changes. *Biophys J* **83**, 2152–2161 (2002).
31. Bloch, R. J. & Gonzalez-Serratos, H. Lateral force transmission across costameres in skeletal muscle. *Exerc Sport Sci Rev* **31**, 73–78 (2003).
32. Guan, K., Rohwedel, J. & Wobus, A. M. Embryonic stem cell differentiation models: Cardiogenesis, myogenesis, neurogenesis, epithelial and vascular smooth muscle cell differentiation in vitro. *Cytotechnology* **30**, 211–226 (1999).

33. del Carmen Ortuño-Costela, M., García-López, M., Cerrada, V. & Gallardo, M. E. iPSCs: A powerful tool for skeletal muscle tissue engineering. *Journal of Cellular and Molecular Medicine* vol. 23 3784–3794 Preprint at <https://doi.org/10.1111/jcmm.14292> (2019).
34. Castro-Viñuelas, R. *et al.* Generation and characterization of human induced pluripotent stem cells (iPSCs) from hand osteoarthritis patient-derived fibroblasts. *Sci Rep* **10**, 1–13 (2020).
35. Yablonka-Reuveni, Z. The Skeletal Muscle Satellite Cell: Still Young and Fascinating at 50. *Journal of Histochemistry and Cytochemistry* **59**, 1041–1059 (2011).
36. Pantelic, M. N. & Larkin, L. M. Stem Cells for Skeletal Muscle Tissue Engineering. *Tissue Eng Part B Rev* **24**, 373–391 (2018).
37. Yin, H., Price, F. & Rudnicki, M. A. Satellite cells and the muscle stem cell niche. *Physiol Rev* **93**, 23–67 (2013).
38. Brian C Syverud, Jonah D Lee, Keith W VanDusen, and L. L. Isolation and Purification of Satellite Cells for Muscle Tissue Engineering. *PMC* **3**, (2015).
39. Schultz, E. Satellite cell proliferative compartments in growing skeletal muscles. *Dev Biol* **175**, 84–94 (1996).
40. Greene, E. A. & Allen, R. E. Growth factor regulation of bovine satellite cell growth in vitro. *J Anim Sci* **69**, 146–152 (1991).
41. Cassar-Malek, I., Langlois, N., Picard, B. & Geay, Y. Regulation of bovine satellite cell proliferation and differentiation by insulin and triiodothyronine. *Domest Anim Endocrinol* **17**, 373–388 (1999).
42. In, S. *et al.* Culturing Satellite Cells from Living Single Muscle Fiber Explants Author (s): J . David Rosenblatt , Alison I . Lunt , David J . Parry , Terence A . Partridge Published by : Society for In Vitro Biology Stable URL : <http://www.jstor.org/stable/4294511> . *In Vitro* **31**, 773–779 (2011).
43. Stout, A. J. *et al.* Immortalized bovine satellite cells for cultured meat applications. *bioRxiv* 2022.12.02.518927 (2022).
44. L. Hayflick. The Limited In Vitro Lifetime of Human Diploid Cell Strains. *The Wistar Institute of Anatomy and Biology* **37**, 614–636 (1964).
45. de Bardet, J. C. *et al.* Cell immortalization: In vivo molecular bases and in vitro techniques for obtention. *BioTech* **12**, 14 (2023).
46. Bodiou, V., Moutsatsou, P. & Post, M. J. Microcarriers for Upscaling Cultured Meat Production. *Frontiers in Nutrition* vol. 7 Preprint at <https://doi.org/10.3389/fnut.2020.00010> (2020).
47. Handral, H. K., Wyrobnik, T. A. & Lam, A. T. L. Emerging Trends in Biodegradable Microcarriers for Therapeutic Applications. *Polymers* vol. 15 Preprint at <https://doi.org/10.3390/polym15061487> (2023).
48. Thyden, R. *et al.* An Edible, Decellularized Plant Derived Cell Carrier for Lab Grown Meat. *Applied Sciences (Switzerland)* **12**, (2022).

49. Petry, F. & Salzig, D. Impact of Bioreactor Geometry on Mesenchymal Stem Cell Production in Stirred-Tank Bioreactors. *Chemie-Ingenieur-Technik* vol. 93 1537–1554 Preprint at <https://doi.org/10.1002/cite.202100041> (2021).
50. Humbird, D. Scale-up economics for cultured meat. *Biotechnol Bioeng* **118**, 3239–3250 (2021).
51. Chen, L. *et al.* Large-scale cultured meat production: Trends, challenges and promising biomanufacturing technologies. *Biomaterials* **280**, (2022).
52. Verma, R., Mehan, L., Kumar, R., Kumar, A. & Srivastava, A. Computational fluid dynamic analysis of hydrodynamic shear stress generated by different impeller combinations in stirred bioreactor. *Biochem Eng J* **151**, (2019).
53. Li, X. *et al.* A conceptual air-lift reactor design for large scale animal cell cultivation in the context of in vitro meat production. *Chem Eng Sci* **211**, (2020).
54. Allan, S. J., De Bank, P. A. & Ellis, M. J. Bioprocess Design Considerations for Cultured Meat Production With a Focus on the Expansion Bioreactor. *Frontiers in Sustainable Food Systems* vol. 3 Preprint at <https://doi.org/10.3389/fsufs.2019.00044> (2019).
55. Eghbali, H., Nava, M. M., Mohebbi-Kalhor, D. & Raimondi, M. T. Hollow fiber bioreactor technology for tissue engineering applications. *International Journal of Artificial Organs* vol. 39 1–15 Preprint at <https://doi.org/10.5301/ijao.5000466> (2016).
56. Tuomisto, H. L., Allan, S. J. & Ellis, M. J. Prospective life cycle assessment of a bioprocess design for cultured meat production in hollow fiber bioreactors. *Science of the Total Environment* **851**, (2022).
57. Pennisi, C. P., Olesen, C. G., de Zee, M., Rasmussen, J. & Zachar, V. Uniaxial Cyclic Strain Drives Assembly and Differentiation of Skeletal Myocytes. *Tissue Eng Part A* **17**, 2543–2550 (2011).
58. Miller, K. J., Thaloor, D., Matteson, S. & Pavlath, G. K. Hepatocyte growth factor affects satellite cell activation and differentiation in regenerating skeletal muscle. *Am J Physiol Cell Physiol* **278**, 174–181 (2000).
59. Wang, P. Y., Yu, H. Te & Tsai, W. B. Modulation of alignment and differentiation of skeletal myoblasts by submicron ridges/grooves surface structure. *Biotechnol Bioeng* **106**, 285–294 (2010).
60. Larkin, L. M., Calve, S., Kostrominova, T. Y. & Arruda, E. M. Structure and functional evaluation of tendon-skeletal muscle constructs engineered in vitro. *Tissue Eng* **12**, 3149–3158 (2006).
61. Lisa M. Larkin; Sarah Calve; Tatiana Y. Kostrominova; Ellen M. Arruda. Structure and functional evaluation of tendon-skeletal muscle constructs engineered in vitro. *Tissue Eng* **12**, 3149–3160 (2006).
62. Chandel, N. S. Glycolysis. *Cold Spring Harb Perspect Biol* **13**, (2021).
63. Arora, M. Cell Culture Media: A Review. *Materials and Methods* **3**, (2013).

64. Yao, T. & Asayama, Y. Animal-cell culture media: History, characteristics, and current issues. *Reproductive Medicine and Biology* vol. 16 99–117 Preprint at <https://doi.org/10.1002/rmb2.12024> (2017).
65. Berthois, Y., Katzenellenbogen, J. A. & Katzenellenbogen, B. S. *Phenol red in tissue culture media is a weak estrogen: Implications concerning the study of estrogen-responsive cells in culture (cell proliferation/human breast cancer/antiestrogens/hormone responsiveness/estrogen receptor)*. *Cell Biology* vol. 83 <https://www.pnas.org> (1986).
66. Husmann, I., Soulet, L., Gautron, J., Martelly, I. & Barritault, D. Growth factors in skeletal muscle regeneration. *Cytokine Growth Factor Rev* **7**, 249–258 (1996).
67. Syverud, B. C., VanDusen, K. W. & Larkin, L. M. Growth factors for skeletal muscle tissue engineering. *Cells Tissues Organs* **202**, 169–179 (2016).
68. Kuppusamy, P., Kim, D., Soundharrajan, I., Hwang, I. & Choi, K. C. Adipose and muscle cell co-culture system: A novel in vitro tool to mimic the in vivo cellular environment. *Biology (Basel)* **10**, 1–12 (2021).
69. Khodabukus, A., Prabhu, N., Wang, J. & Bursac, N. In Vitro Tissue-Engineered Skeletal Muscle Models for Studying Muscle Physiology and Disease. *Advanced Healthcare Materials* vol. 7 Preprint at <https://doi.org/10.1002/adhm.201701498> (2018).
70. Stout, A. J. *et al.* Simple and effective serum-free medium for sustained expansion of bovine satellite cells for cell cultured meat. *Commun Biol* **5**, (2022).
71. Ho, Q. T. & Kuo, C. J. Vascular endothelial growth factor: Biology and therapeutic applications. *International Journal of Biochemistry and Cell Biology* **39**, 1349–1357 (2007).
72. Pan, Y. *et al.* Small-diameter hybrid vascular grafts composed of polycaprolactone and polydioxanone fibers. *Sci Rep* **7**, 1–11 (2017).
73. Smoak, M. M. & Mikos, A. G. Advances in biomaterials for skeletal muscle engineering and obstacles still to overcome. *Materials Today Bio* vol. 7 Preprint at <https://doi.org/10.1016/j.mtbio.2020.100069> (2020).
74. Freeman, F. E. & Kelly, D. J. Tuning alginate bioink stiffness and composition for controlled growth factor delivery and to spatially direct MSC Fate within bioprinted tissues. *Sci Rep* **7**, 1–12 (2017).
75. MacQueen, L. A. *et al.* Muscle tissue engineering in fibrous gelatin: implications for meat analogs. *NPJ Sci Food* **3**, 1–12 (2019).
76. Kim, J. H. *et al.* 3D Bioprinted Human Skeletal Muscle Constructs for Muscle Function Restoration. *Sci Rep* **8**, 1–15 (2018).
77. Gungor-Ozkerim, P. S., Inci, I., Zhang, Y. S., Khademhosseini, A. & Dokmeci, M. R. Bioinks for 3D bioprinting: An overview. *Biomaterials Science* vol. 6 915–946 Preprint at <https://doi.org/10.1039/c7bm00765e> (2018).

78. Seyedmahmoud, R. *et al.* Three-dimensional bioprinting of functional skeletal muscle tissue using gelatin methacryloyl-alginate bioinks. *Micromachines (Basel)* **10**, 1–12 (2019).
79. Wang, X., Wang, Q. & Xu, C. Nanocellulose-based inks for 3d bioprinting: Key aspects in research development and challenging perspectives in applications—a mini review. *Bioengineering* **7**, (2020).
80. 3D Bioprinting in Skeletal Muscle Tissue Engineering _ Enhanced Reader.pdf.
81. Orellana, N. *et al.* A new edible film to produce in vitro meat. *Foods* **9**, 1–14 (2020).
82. Bettadapur, A. *et al.* Prolonged Culture of Aligned Skeletal Myotubes on Micromolded Gelatin Hydrogels. *Sci Rep* **6**, 1–14 (2016).
83. Kim, K. *et al.* Control of degradation rate and hydrophilicity in electrospun non-woven poly(D,L-lactide) nanofiber scaffolds for biomedical applications. *Biomaterials* **24**, 4977–4985 (2003).
84. Guyette, J. P. *et al.* Bioengineering human myocardium on native extracellular matrix. *Circ Res* **118**, 56–72 (2016).
85. Khodabukus, A. Tissue-Engineered Skeletal Muscle Models to Study Muscle Function, Plasticity, and Disease. *Frontiers in Physiology* vol. 12 Preprint at <https://doi.org/10.3389/fphys.2021.619710> (2021).
86. Beck, C. B. *An Introduction to Plant Structure and Development*. (Cambridge University Press, 2010).
87. Yeats, T. H. & Rose, J. K. C. The formation and function of plant cuticles. *Plant Physiology* vol. 163 5–20 Preprint at <https://doi.org/10.1104/pp.113.222737> (2013).
88. Edition, S. *The Plant Cell Wall. The Plant Cell Wall* (1962). doi:10.1016/c2013-0-05292-9.
89. Scarpella, E. & Meijer, A. H. *Pattern formation in the vascular system of monocot and dicot plant species*. *New Phytologist* vol. 164 (2004).
90. Monocotyledons vs. Dicotyledons. <http://myriverside.sd43.bc.ca/vivianh-2013/2016/04/17/monocotyledons-vs-dicotyledons/> (2013).
91. Callaghan, P. T., Le Gros, M. A. & Pinder, D. N. The measurement of diffusion using deuterium pulsed field gradient nuclear magnetic resonance. *J Chem Phys* **79**, 6372–6381 (1983).
92. Lundgren, M. R. *et al.* Mesophyll porosity is modulated by the presence of functional stomata. *Nat Commun* **10**, (2019).
93. Engler, A. J. *et al.* Myotubes differentiate optimally on substrates with tissue-like stiffness: Pathological implications for soft or stiff microenvironments. *Journal of Cell Biology* **166**, 877–887 (2004).
94. Jones, J. D., Rebello, A. S. & Gaudette, G. R. Decellularized spinach: An edible scaffold for laboratory-grown meat. *Food Biosci* **41**, (2021).

95. Whitton, C., Bogueva, D., Marinova, D. & Phillips, C. J. C. Are we approaching peak meat consumption? Analysis of meat consumption from 2000 to 2019 in 35 countries and its relationship to gross domestic product. *Animals* **11**, (2021).
96. Hudak, C. S. & Sul, H. S. Pref-1, a gatekeeper of adipogenesis. *Frontiers in Endocrinology* vol. 4 Preprint at <https://doi.org/10.3389/fendo.2013.00079> (2013).
97. Fish, K. D., Rubio, N. R., Stout, A. J., Yuen, J. S. K. & Kaplan, D. L. Prospects and challenges for cell-cultured fat as a novel food ingredient. *Trends in Food Science and Technology* vol. 98 53–67 Preprint at <https://doi.org/10.1016/j.tifs.2020.02.005> (2020).
98. Eberli, D., Soker, S., Atala, A. & Yoo, J. J. Optimization of human skeletal muscle precursor cell culture and myofiber formation in vitro. *Methods* **47**, 98–103 (2009).
99. Kothari, S., Chaudry, Q. & Wang, M. D. Automated cell counting and cluster segmentation using concavity detection and ellipse fitting techniques. in *Proceedings - 2009 IEEE International Symposium on Biomedical Imaging: From Nano to Macro, ISBI 2009* vol. 2 795–798 (IEEE, 2009).
100. Schindelin, J. *et al.* Fiji: An open-source platform for biological-image analysis. *Nat Methods* **9**, 676–682 (2012).
101. Mardia, K. V. Statistics of directional data. *Journal of the Royal Statistical Society* **37**, 349–393 (1975).
102. Dunn, G. A. & Brown, A. F. Alignment of fibroblasts on grooved surfaces described by a simple geometric transformation. *J Cell Sci* **83**, 313–340 (1986).
103. Berens, P. CircStat: A MATLAB toolbox for circular statistics. *J Stat Softw* **31**, (2009).
104. EPA. Sources of greenhouse gas emissions. *Climate Change* 1–2 (2019).
105. Crapo, P. M., Gilbert, T. W. & Badylak, S. F. An overview of tissue and whole organ decellularization processes. *Biomaterials* **32**, 3233–3243 (2011).
106. FDA. *21 CFR Part 172*. vol. 172 1–167 (2022).
107. FDA. Code of Federal Regulations Title 21. 3–6 Preprint at (2021).
108. Riaz, N., Wolden, S. L., Gelblum, D. Y. & Eric, J. Isolation of skeletal muscle stem cells by fluorescence-activated cell sorting. *Nat Protoc* **118**, 6072–6078 (2016).
109. Elaby, S. & Ali, J. The anti-anemic effect of dried beet green in phenylhydrazine treated rats. *Archives of Pharmaceutical Sciences Ain Shams University* **2**, 54–69 (2018).
110. Mzoughi, Z. *et al.* Wild edible Swiss chard leaves (*Beta vulgaris* L. var. *cicla*): Nutritional, phytochemical composition and biological activities. *Food Research International* **119**, 612–621 (2019).
111. Ko, S. H. *et al.* Antioxidant effects of spinach (*Spinacia oleracea* L.) supplementation in hyperlipidemic rats. *Prev Nutr Food Sci* **19**, 19–26 (2014).


112. Bergquist, S. Å., Gertsson, U. E., Knuthsen, P. & Olsson, M. E. Flavonoids in baby spinach (*Spinacia oleracea* L.): Changes during plant growth and storage. *J Agric Food Chem* **53**, 9459–9464 (2005).
113. Turnbull, B. & Matisoo-Smith, E. *Taste sensitivity to 6-n-propylthiouracil predicts acceptance of bitter-tasting spinach in 3-6-y-old children 1,2*. *Am J Clin Nutr* vol. 76 <https://academic.oup.com/ajcn/article/76/5/1101/4689587> (2002).
114. Huang, Z., Wang, B., Eaves, D. H., Shikany, J. M. & Pace, R. D. Phenolic compound profile of selected vegetables frequently consumed by African Americans in the southeast United States. *Food Chem* **103**, 1395–1402 (2007).
115. Jones, J. D. *et al.* Decellularization : Leveraging a Tissue Engineering Technique for Food Production. (2023) doi:10.1021/acsbiomaterials.2c01421.
116. Arganda-Carreras, I. *et al.* Trainable Weka Segmentation: A machine learning tool for microscopy pixel classification. *Bioinformatics* **33**, 2424–2426 (2017).
117. Doorn, W. van *et al.* Morphological classification of plant cell deaths _ Enhanced Reader.pdf. *Cell Death Differ* **18**, 1241–1246 (2011).
118. Wang, F. & Boya, R. G. P. Lysosomal membrane permeabilization and cell death. 918–931 (2018) doi:10.1111/tra.12613.
119. Campuzano, S., Pelling, A. E. & Ellis, M. J. Scaffolds for 3D Cell Culture and Cellular Agriculture Applications Derived From Non-animal Sources. **3**, 1–9 (2019).
120. Gilbert, T. W. Strategies for tissue and organ decellularization. *J Cell Biochem* **113**, 2217–2222 (2012).
121. Phillips, M., Maor, E. & Rubinsky, B. Nonthermal irreversible electroporation for tissue decellularization. *J Biomech Eng* **132**, 1–8 (2010).
122. Roth, S. P. *et al.* Automated freeze-thaw cycles for decellularization of tendon tissue - a pilot study. *BMC Biotechnol* **17**, 1–10 (2017).
123. Topuz, B., Günal, G., Guler, S. & Aydin, H. M. Use of supercritical CO₂ in soft tissue decellularization. in *Methods in Cell Biology* vol. 157 49–79 (Academic Press Inc., 2020).
124. Harris, A. F. *et al.* Supercritical carbon dioxide decellularization of plant material to generate 3D biocompatible scaffolds. *Sci Rep* **11**, (2021).
125. Gilbert, T. W., Sellaro, T. L. & Badylak, S. F. Decellularization of tissues and organs. *Biomaterials* **27**, 3675–3683 (2006).
126. Graham, D. G. *HEXANE NEUROPATHY: A PROPOSAL FOR PATHOGENESIS OF A HAZARD OF OCCUPATIONAL EXPOSURE AND INHALANT ABUSE*. *Chem.-Biol. Interactions* vol. 32 (1980).
127. Guyette, J. P. *et al.* Perfusion decellularization of whole organs. *Nat Protoc* **9**, 1451–1468 (2014).
128. Santiago Campuzno, Nicolette B. Mogilever, and A. E. P. Decellularized Plant-Based Scaffolds for Guided Alignment of Myoblast Cells. (2020).

129. Zhu, Y., Dong, Z., Wejinya, U. C., Jin, S. & Ye, K. Determination of mechanical properties of soft tissue scaffolds by atomic force microscopy nanoindentation. *J Biomech* **44**, 2356–2361 (2011).
130. Adeyemi, K. D. & Sazili, A. Q. Efficacy of carcass electrical stimulation in meat quality enhancement: A review. *Asian-Australas J Anim Sci* **27**, 447–456 (2014).
131. Lam, M. T., Sim, S., Zhu, X. & Takayama, S. The effect of continuous wavy micropatterns on silicone substrates on the alignment of skeletal muscle myoblasts and myotubes. *Biomaterials* **27**, 4340–4347 (2006).
132. Zhao, Y., Zeng, H., Nam, J. & Agarwal, S. Fabrication of skeletal muscle constructs by topographic activation of cell alignment. *Biotechnol Bioeng* **102**, 624–631 (2009).
133. Antin, P. B. & Ordahl, C. P. *Isolation and Characterization of an Avian Myogenic Cell Line*. *DEVELOPMENTAL BIOLOGY* vol. 143 (1991).
134. Jones, J. D., Rebello, A. S. & Gaudette, G. R. Decellularized spinach: An edible scaffold for laboratory-grown meat. *Food Biosci* **41**, 100986 (2021).
135. Erdfelder, E., Faul, F., Buchner, A. & Lang, A. G. Statistical power analyses using G*Power 3.1: Tests for correlation and regression analyses. *Behav Res Methods* **41**, 1149–1160 (2009).
136. Charest, J. L., García, A. J. & King, W. P. Myoblast alignment and differentiation on cell culture substrates with microscale topography and model chemistries. *Biomaterials* **28**, 2202–2210 (2007).
137. Zhang, Q. *et al.* Blue light regulates secondary cell wall thickening via myc2/myc4 activation of the nst1-directed transcriptional network in arabidopsis[open]. *Plant Cell* **30**, 2512–2528 (2018).
138. Perreault, L. R. *et al.* Repurposing agricultural waste as low-cost cultured meat scaffolds. *Frontiers in Food Science and Technology* **3**, (2023).
139. Penfield, K. W. & Rumbelow, S. Challenges in polysorbate characterization by mass spectrometry. *Rapid Communications in Mass Spectrometry* **34**, (2020).
140. Birdsall, R. E. *et al.* *Quantitative Analysis of Polysorbate 20/80 in Protein-Based Biopharmaceuticals Using A One-Pot RPLC-MS Based Platform Method*.
141. Skrivergaard, S., Krøyer Rasmussen, M., Sahebkhari, N., Feveile Young, J. & Therkildsen, M. Satellite cells sourced from bull calves and dairy cows differs in proliferative and myogenic capacity – Implications for cultivated meat. *Food Research International* **173**, (2023).
142. Wunderlich, S. & Gatto, K. A. Consumer perception of genetically modified organisms and sources of information. *Advances in Nutrition* vol. 6 842–851 Preprint at <https://doi.org/10.3945/an.115.008870> (2015).
143. Loomba, S., de Figueiredo, A., Piatek, S. J., de Graaf, K. & Larson, H. J. Measuring the impact of COVID-19 vaccine misinformation on vaccination intent in the UK and USA. *Nat Hum Behav* **5**, 337–348 (2021).

144. Gutiérrez-Rodríguez, E. *et al.* Texture, composition and anatomy of spinach leaves in relation to nitrogen fertilization. *J Sci Food Agric* **93**, 227–237 (2013).
145. Ingstad, T. Nitrogen and Plant Growth: Maximum Efficiency of Nitrogen Fertilizers. *Royal Swedish Academy of Science* **6**, 146–151 (1977).
146. Elia, A., Santamaria, P. & Serio, F. Nitrogen nutrition, yield and quality of spinach. *J Sci Food Agric* **76**, 341–346 (1998).
147. Whitney, S. E. C., Gothard, M. G. E., Mitchell, J. T. & Gidley, M. J. Roles of cellulose and xyloglucan in determining the mechanical properties of primary plant cell walls. *Plant Physiol* **121**, 657–663 (1999).
148. Sañudo, C. *et al.* The effects of slaughter weight, breed type and ageing time on beef meat quality using two different texture devices. *Meat Sci* **66**, 925–932 (2004).

Appendix

ACS Biomaterials Reprint Permission



ACS Publications
Most Trusted Most Cited Most Read

Decellularization: Leveraging a Tissue Engineering Technique for Food Production

Author: Jordan D. Jones, Richard Thyden, Luke R. Perreault, et al
Publication: ACS Biomaterials Science & Engineering
Publisher: American Chemical Society
Date: Apr 1, 2023
Copyright © 2023, American Chemical Society

PERMISSION/LICENSE IS GRANTED FOR YOUR ORDER AT NO CHARGE

This type of permission/license, instead of the standard Terms and Conditions, is sent to you because no fee is being charged for your order. Please note the following:

- Permission is granted for your request in both print and electronic formats, and translations.
- If figures and/or tables were requested, they may be adapted or used in part.
- Please print this page for your records and send a copy of it to your publisher/graduate school.
- Appropriate credit for the requested material should be given as follows: "Reprinted (adapted) with permission from (COMPLETE REFERENCE CITATION). Copyright (YEAR) American Chemical Society." Insert appropriate information in place of the capitalized words.
- One-time permission is granted only for the use specified in your RightsLink request. No additional uses are granted (such as derivative works or other editions). For any uses, please submit a new request.

If credit is given to another source for the material you requested from RightsLink, permission must be obtained from that source.

[BACK](#)

[CLOSE WINDOW](#)

© 2023 Copyright - All Rights Reserved | Copyright Clearance Center, Inc. | Privacy Statement | Data Security and Privacy | For California Readers | Terms and Conditions
Comments: We would like to hear from you. Email us at customerservice@copyright.com

Home ? Live Chat Sign In Create Account

Biorender Publication Rights



49 Spadina Ave. Suite 200
Toronto ON M5V 2J1 Canada
www.biorender.com

Confirmation of Publication and Licensing Rights

June 16th, 2023
Science Suite Inc.

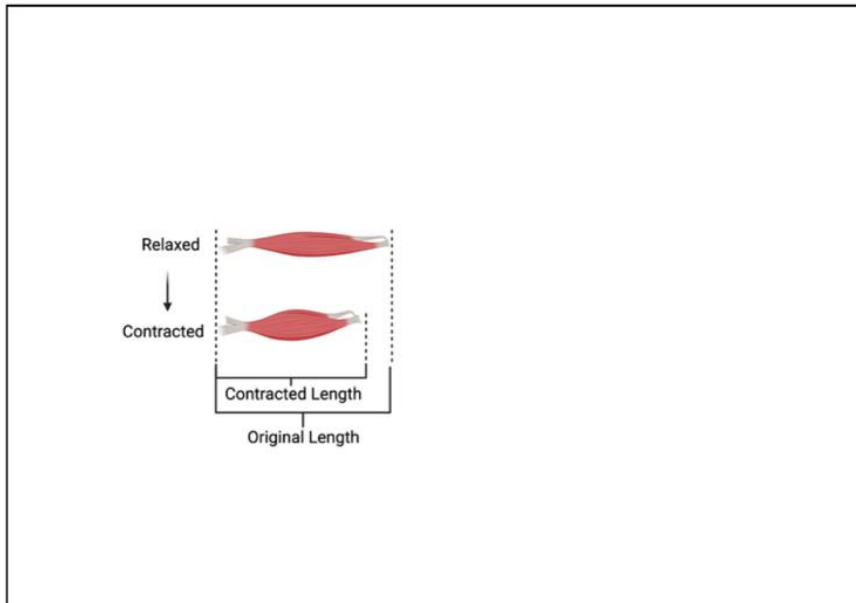
Subscription: Student Plan
Agreement number: AS25HTFF9E
Journal name: WPI

To whom this may concern,

This document is to confirm that Jordan Jones has been granted a license to use the BioRender content, including icons, templates and other original artwork, appearing in the attached completed graphic pursuant to BioRender's [Academic License Terms](#). This license permits BioRender content to be sublicensed for use in journal publications.

All rights and ownership of BioRender content are reserved by BioRender. All completed graphics must be accompanied by the following citation: "Created with BioRender.com".

BioRender content included in the completed graphic is not licensed for any commercial uses beyond publication in a journal. For any commercial use of this figure, users may, if allowed, recreate it in BioRender under an Industry BioRender Plan.



For any questions regarding this document, or other questions about publishing with BioRender refer to our [BioRender Publication Guide](#), or contact BioRender Support at support@biorender.com.

Confirmation of Publication and Licensing Rights

April 26th, 2023
Science Suite Inc.

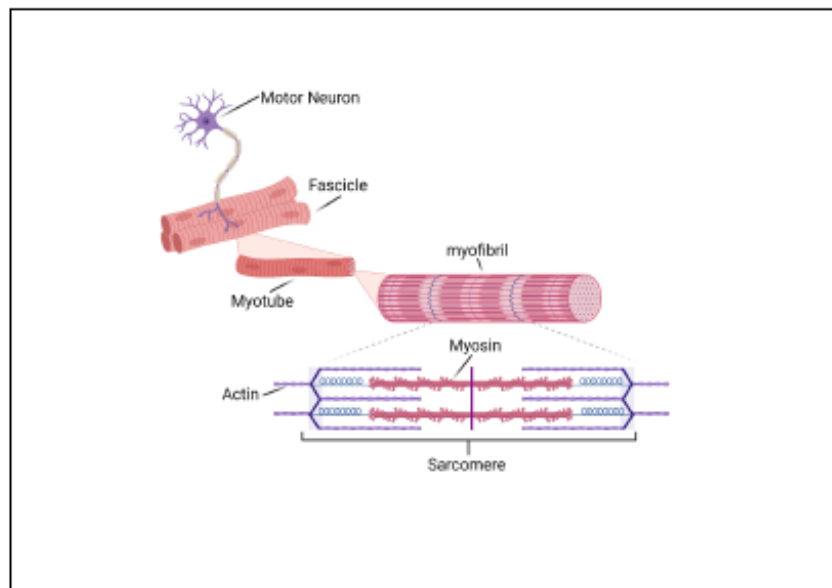
Subscription: Student Plan
Agreement number: WD25AMO3MP
Journal name: Jordan Jones

To whom this may concern,

This document is to confirm that Jordan Jones has been granted a license to use the BioRender content, including icons, templates and other original artwork, appearing in the attached completed graphic pursuant to BioRender's [Academic License Terms](#). This license permits BioRender content to be sublicensed for use in journal publications.

All rights and ownership of BioRender content are reserved by BioRender. All completed graphics must be accompanied by the following citation: "Created with BioRender.com".

BioRender content included in the completed graphic is not licensed for any commercial uses beyond publication in a journal. For any commercial use of this figure, users may, if allowed, recreate it in BioRender under an Industry BioRender Plan.



For any questions regarding this document, or other questions about publishing with BioRender refer to our [BioRender Publication Guide](#), or contact BioRender Support at support@biorender.com.

Confirmation of Publication and Licensing Rights

May 15th, 2023
Science Suite Inc.

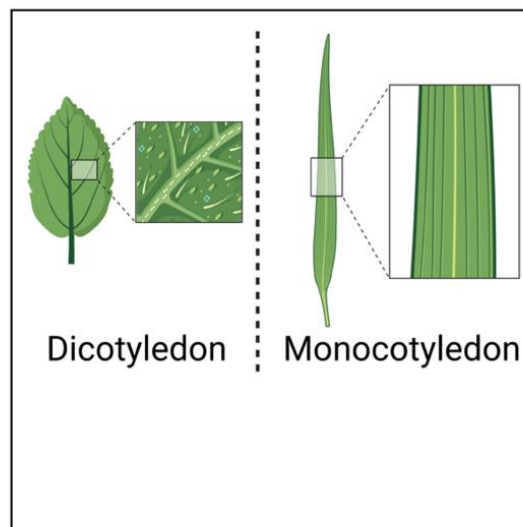
Subscription: Student Plan
Agreement number: MA25DD93S8
Journal name: WPI

To whom this may concern,

This document is to confirm that Jordan Jones has been granted a license to use the BioRender content, including icons, templates and other original artwork, appearing in the attached completed graphic pursuant to BioRender's [Academic License Terms](#). This license permits BioRender content to be sublicensed for use in journal publications.

All rights and ownership of BioRender content are reserved by BioRender. All completed graphics must be accompanied by the following citation: "Created with BioRender.com".

BioRender content included in the completed graphic is not licensed for any commercial uses beyond publication in a journal. For any commercial use of this figure, users may, if allowed, recreate it in BioRender under an Industry BioRender Plan.



For any questions regarding this document, or other questions about publishing with BioRender refer to our [BioRender Publication Guide](#), or contact BioRender Support at support@biorender.com.

Confirmation of Publication and Licensing Rights

May 15th, 2023
 Science Suite Inc.

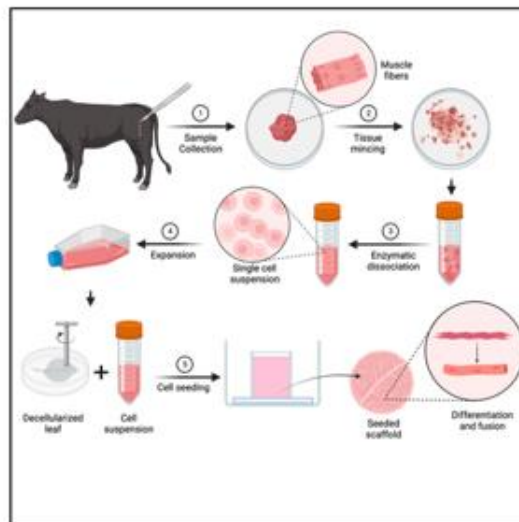
Subscription: Student Plan
Agreement number: SH25DD5AGK
Journal name: WPI

To whom this may concern,

This document is to confirm that Jordan Jones has been granted a license to use the BioRender content, including icons, templates and other original artwork, appearing in the attached completed graphic pursuant to BioRender's [Academic License Terms](#). This license permits BioRender content to be sublicensed for use in journal publications.

All rights and ownership of BioRender content are reserved by BioRender. All completed graphics must be accompanied by the following citation: "Created with BioRender.com".

BioRender content included in the completed graphic is not licensed for any commercial uses beyond publication in a journal. For any commercial use of this figure, users may, if allowed, recreate it in BioRender under an Industry BioRender Plan.



For any questions regarding this document, or other questions about publishing with BioRender refer to our [BioRender Publication Guide](#), or contact BioRender Support at support@biorender.com.

Confirmation of Publication and Licensing Rights

May 23rd, 2023
Science Suite Inc.

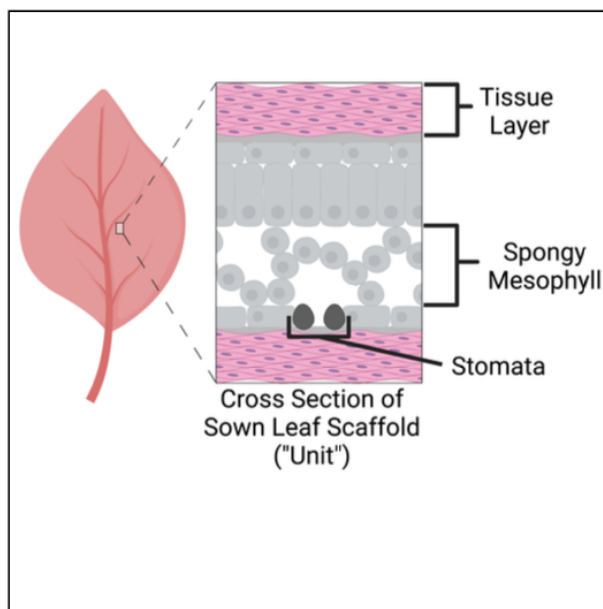
Subscription: Student Plan
Agreement number: BS25EHLNMO
Journal name: WPI

To whom this may concern,

This document is to confirm that Jordan Jones has been granted a license to use the BioRender content, including icons, templates and other original artwork, appearing in the attached completed graphic pursuant to BioRender's [Academic License Terms](#). This license permits BioRender content to be sublicensed for use in journal publications.

All rights and ownership of BioRender content are reserved by BioRender. All completed graphics must be accompanied by the following citation: "Created with BioRender.com".

BioRender content included in the completed graphic is not licensed for any commercial uses beyond publication in a journal. For any commercial use of this figure, users may, if allowed, recreate it in BioRender under an Industry BioRender Plan.



For any questions regarding this document, or other questions about publishing with BioRender refer to our [BioRender Publication Guide](#), or contact BioRender Support at support@biorender.com.

Protocols

Plant Decellularization

Used for spinach (and other) leaves, parsley stems

Materials:

- 27 G Needles
- 0.38 ID 1.09 OD LDPE Medical tubing
- Hexanes
- PBS 1x
- diH₂O
- 1X SDS solution in diH₂O

o For 2 L of solution mix 200 mL of 10x SDS with 1800 mL of diH₂O o 2L of 10x SDS Solution

§ Mix 200 g of SDS powder in 2 L diH₂O until there are no more visible SDS pellets

§ Can be stored at room temperature until needed • 0.1% Triton-X with 10% bleach (or Cl tablets) in DI H₂O

o 48 mL of concentrated Clorox bleach and 20 mL of TritonX-100 Solution are added to 2L of DiH₂O and mixed until in solution

• Tris buffer solution

o 10 mM Tris Buffer (605.7 mg in 500 mL of diH₂O) o Buffered to pH 9.0

• Same protocol applies if using Gaudette (describe the apparatus or provide image) Lab decellularization apparatus or custom set-up.

o Gaudette decellularization apparatus requires ~2-4L of each solution to function efficiently.

Custom decellularization apparatus should use an appropriate amount of solution depending on size.

Decellularization:

1. Cannulate leaves and parsley stems via the stem, affixing cannulas with suture.
2. Once leaves are cannulated, (Repeat 3X times) Submerge in hexanes and wash vigorously for 2 minutes. Remove and rinse in 1x PBS for 2 minutes.
3. Affix plant materials to decellularization set up.
4. Attach 4 L of 1x SDS solution to the set up and begin flow. Monitor plant materials to ensure proper flow through the leaf vasculature, modifying flow rate to ensure a slow, steady drip. Rapid flow rate will deplete SDS too quickly, whereas too little flow runs the risk of dehydrating the plant material and damaging the plant structure.
5. Maintain in SDS for 1 day in order to decellularize plant material, until leaves and stems become more transparent in appearance. Green coloration at this step is normal and not indicative of an unsuccessful decellularization.

6. Remove 1x SDS and add 4L of Triton-X/Bleach solution to set up.
7. Maintain set up in Triton-X/Bleach for 24 hours, can go longer if needed. Watch until leaves and stems have become clear/transparent. This solution should purge any remaining coloration from the plant matter.
8. Remove Triton-X/Bleach solution and attach DI H₂O to set up. Perfuse leaves/stems in DI H₂O for 24 hours.
9. Wash decellularized leaves on rotator in Tris buffer solution overnight.
 1. Replace the solution at least twice (usually after the first hour and then secondly in the morning)
 2. Tris buffer removes residual SDS that maybe left entrapped in the leaf
 3. Make sure the rotator moves the leaf gently
 4. Watch the stem as they become very fragile
10. *****IF FUNCTIONALIZING LEAF WITH RGD DOPA PLEASE SEE RGD DOPA FUNCTIONALIZATION PROTOCOL BEFORE MOVING TO STEP 11*****
11. Remove leaves and stems from solutions, freeze overnight in -20 °C freezer
12. Lyophilize leaf/stem for 24 hours
13. Store at lyophilized leaf scaffold at room temperature until needed
 - a. If functionalized with RGDDOPA, store lyophilized leaves in refrigerator
14. Please see the rehydration protocol for next steps

Leaf Scaffold Sterilization:

1. Decellularize and rehydrate leaf
2. Rehydrate with PBS
3. Sterilization

- o In 10 cm dish containing decelled leaf, add the following: 70% EtOH
- o Agitate gently on shaker table for 30 minutes
- o Transfer leaf to Laminar Flow hood
- o Aspirate EtOH
- o Rinse 3x with sterile PBS

Satellite cell Isolation

Materials:

- Biosafety cabinet
- Tissue sample
- Sterile fine forceps
- Sterile scalpel, blade
- Sterile iris scissors
- 5, 10, 25mL serological pipettes and pipette gun
- 150mm petri dishes
- 15mL and 50mL conical tubes
- 100µm and 70µm cell strainers
- T-75 tissue culture flasks
- Collagenase type 1 (1800 units/mL solution in HBSS)
- Tissue Digestion Medium (DMEM/F12 (Ham's), 1% Pen Strep, 10% collagenase)
- Tissue Rinse Medium (DMEM/F12 (Ham's), 1% Pen Strep, 10% Fetal Bovine Serum)
- Cell Culture Growth Medium (DMEM/F12 (Ham's), 1% Pen Strep, 10% heat-inactivated Fetal Bovine Serum, 4ng/mL FGF2, 10ng/mL EGF, 2.5ng/mL, HGF, 5ng/mL IGF1)

Procedure:

1. Sterilize all instruments in autoclave prior to tissue dissection and bring into biosafety cabinet
2. Take muscle biopsy from interior muscle sample in biosafety cabinet
3. Put tissue samples in 150mm dish with DMEM/F12 (Ham's) with 1% Pen Strep (~30mL medium)
 - a. Soak in medium and rotate to cover tissue samples for 5-10 minutes
4. Make Tissue Digestion Medium and put into a 150mm dish
5. Transfer tissue sample to dish with digestion medium
6. Dissect tissue into 1mm³ pieces with scalpel in dish
7. Move dish into 5% CO₂ incubator and incubate for 1 hour at 37C
 - a. Swirl plate every 15 minutes
8. Bring dish into biosafety cabinet and transfer contents into 50mL conical tube
9. Let larger pieces settle, then transfer small tissue pieces and medium ("supernatant") through 100um cell strainer into a new 50mL conical tube
10. Centrifuge for 5 minutes at 0.3rcf
11. Aspirate supernatant, resuspend cell pellet with Tissue Rinse Medium with 25mL serological pipette and rinse/titrate
12. Pass suspension through 40um cell strainer in new conical tube
13. Repeat spin/rinse/strain 2 more times
14. After the 3rd centrifugation, resuspend pellet in Cell Culture Growth Medium
15. Transfer cell suspension into T75 flasks (10-12mL per flask) and put in incubator
16. Observe cells after one hour. If no cells are adherent, continue incubation overnight (if cells adherent, continue to step 17)
17. After incubation, remove medium and non-adherent cells from flasks and plate into new T75 flasks
18. Replenish Cell Culture Growth Medium in flasks and maintain in incubator
19. Change medium every 2-3 days

Passaging Primary Bovine Satellite cells

1. Place media, trypsin in water bath at 37C.
2. Remove T-75 flask and verify cell viability and confluence with scope. Place in bio-safety cabinet.
3. Remove cap and transfer media off cells with sterile Pasteur pipettes to a 50ml conical tube.
4. Add 5ml of trypsin to flask.
5. Put flask back in incubator and let sit for 5 min.
6. Remove flask and confirm cell detachment with scope. (Detached cells will float freely and appear round)
7. Add 5ml of 10% FBS in DMEM f-12 to T-75 flask. (This deactivates the trypsin)
8. Pipette contents of tube in 25ml pipette and place in the same 50ml conical tube.
9. Centrifuge the 50ml conical tube for 5min @ 1000rpm making sure to balance the centrifuge.
10. Being sure to spray down the 50ml conical tube, reintroduce it into the sterile field and aspirate off the supernatant being sure not to disturb the cell pellet. Resuspend the pellet
11. Resuspend the pellet in 15ml of media.
12. transfer cell suspension to a sterile large non-TCP petri-dish.
13. carefully move cell to 37C incubator and incubate for 30min.
14. Pipette contents of petri-dish in 25ml pipette and place in the same 50ml conical tube.
15. Centrifuge the 50ml conical tube for 5min @ 1000rpm making sure to balance the centrifuge.
16. Being sure to spray down the 50ml conical tube, reintroduce it into the sterile field and aspirate off the supernatant being sure not to disturb the cell pellet.
17. Resuspend the pellet in desired amount of media. (Varies between 0.5ml to 1ml based on pellet size)
18. Triturate the solution with a 1000ul pipette to ensure the solution is homogenous.
19. Remove 30ul of cell suspension and add it to the 30ul of trypan blue stain.
20. Load 10ul of the cell+trypan blue mixture in each side of the hemocytometer.
21. Count enough boxes to achieve a count of 100 cells of greater. Once you begin counting a box you must count the whole box.
22. Use this formula to determine the cell density.

$$\frac{\# \text{ of cells counted}}{\# \text{ of boxes counted}} * 2 * 10,000 * \# \text{ of ml} = \frac{\text{cell count}}{1 \text{ ml}}$$

23. Either seed 500,000 cells per T-75 flask, with 10-12ml of media, or use cells for other intended purpose. Recommended seeding density of ≈ 7000 cells per cm^2

Gelatin coating

- 1) Weigh out 0.1 g gelatin and place into a 500 ml glass bottle.
- 2) Add distilled water to the 500 ml mark, and autoclave. This gelatin will go into solution while being autoclaved. The concentration of the gelatin is 0.02%.
- 3) Fibronectin (1 mg/ml) is received in a tube as a liquid. Dilute 1 ml fibronectin in 199 ml of 0.02% gelatin. Mix gently, and immediately aliquot 6 ml into each labeled 15 ml centrifuge tube. Freeze aliquots at -20°C.
- 4) Before culturing cells, coat tissue culture flasks with gelatin/fibronectin (1 ml/T25 or 3 ml/T75 flask). Cap the flasks and incubate at 37°C for at least an hour (12-24 hrs is okay, if you make the plates the day/night before).
- 5) Remove the gelatin/fibronectin by aspiration just before adding cells/media to the flasks.

Cell Seeding

1. Decellularize and rehydrate leaf
2. Rehydrate with 1X PBS
3. Sterilize leaf
4. Plating:
 - Coat well with PDMS
 - Mix PDMS solution A & B at a 1:10 ratio
 - Add enough to cover well (i.e. 0.25mL in 12 well plate)
 - Incubate at room temperature for overnight
 - ETO sterilize coated plates for 12 hours
 - Plate leaf
 - Lay leaf section flat on coated well
 - Incubate at 37°C for 30 minutes to allow for adherence to plate
 - Let dry in hood if any excess liquid remains
 - Coat leaf with preferred attachment protein according to protein specific protocols
 - Add media gently to side of well
 - Add cells and gently rock

Cyquant DNA Analysis

Materials

- 1x PBS (Dulbecco's Phosphate buffered saline)
- Sterile fine scissors and fine forceps
- 10, 200, and 1000 μ L micropipettes
- Tips for 10, 200, and 1000 μ L micropipettes
- 1.5mL microcentrifuge tubes
- Liquid Nitrogen
- Microcentrifuge tube rack
- Pipette Aid
- Serological Pipettes 10ml
- 50mL conical tube
- 96 well plate
- Cyquant Cell Proliferation Assay Kit (Invitrogen)
 - Cell-lysis buffer (Component B)
 - Dilute 1 mL Lysis buffer to 19mL DPBS (1x Lysis buffer)
 - CyQUANT® GR dye (Component A) (light sensitive)
 - add 50 μ L GR (fluorescent) to 20 mL 1x Lysis buffer
 - λ DNA standard
 - Dilute to 1.0 μ g/mL by mixing 10 μ L of the stock solution with 990 μ L of CyQUANT® GR/cell-lysis buffer

Sample preparation: (A few hours or day before**)**

1. Cut up each leaf sample with sterile fine scissors in very small pieces
2. Place each sample into one 1.5mL microcentrifuge tube and add 500 μ L PBS to each
3. Flash freeze samples by dipping tube into liquid nitrogen
4. Repeat as many times as necessary until you can shatter leaf with fine forceps in tube
5. Spin down leaves by centrifuging at 2,000 rpm for 5 min
6. Remove 400 μ L of PBS
7. Freeze at -80°C for at least 1 hour.

1 hour before assay:

1. Remove samples in microcentrifuge tubes from -80C freezer.
2. Using a micropipette, add 500 μ L of DPBS.
3. Centrifuge microcentrifuge tube at 2,000 rpm for 5 minutes.
4. Using a micropipette, remove 400 μ L of DPBS.
5. Place microcentrifuge tube in microcentrifuge tube rack.
6. Place rack in -80°C freezer for at least 1 hour

Plate standard curve preparation: START AT TIME OF ASSAY

1. Make up standard dilution solutions in dark (see materials)
2. In a 96 well plate, place 100 μ L of CyQUANT dye/lysis buffer into each well in Columns 1-4, Rows B-H.
3. Add additional 100 μ L of CyQUANT buffer to each well of H1-H4.

4. Using a micropipette, take up the DNA Standard solution (1.0ug/mg DNA standard + GR/lysis buffer) and dispense 200 μ L into each of the wells A1-A4.
5. Using a 1000 μ L micropipette, take up 100 μ L of CyQUANT buffer from the topmost well in a Column and dispense it into the well directly beneath it. Mix the solution in each well 6 times. Repeat this step through Row G.
 - a. Each row will have $\frac{1}{2}$ the concentration of the row before
 - b. **Note:** Row H wells have NO standard curve (this is blank).
6. Using a micropipette, add 100 μ L of CyQUANT buffer to each well from A1 to G4.
 - a. **Note:** This will return the full amount to 200 μ L.
 - b. **Note:** Samples will saturate after 5 minutes of light exposure; work fast. Should be 200 μ L in all wells of standard curve, if not add CyQUANT buffer until 200 μ L is reached.

Sample analysis:

7. Remove rack from freezer.

Note: Allow microcentrifuge tube and contents to reach room temperature. Do NOT place in water bath.
8. Using a micropipette, add 400 μ L of CyQUANT lysis buffer.
9. Vortex lightly using the Vortex Genie 2[®].
10. Using a micropipette, remove leaf material from sample.
11. Using a micropipette, take up of solution with cells and dispense 100 μ L solutions into each of 4 wells.
12. Once all intended wells are complete, de-gass plate in vacuum to remove bubbles.
13. Place 96 well plate on plate reader.
14. Run plate reader. (480nm excitation, 520nm absorption)

Calculations

1. Place 96 well plate on plate reader. *See protocol for Plate reader.* Read operation related sections.
2. Copy obtained data into an empty Excel document. Calculate average, correlation coefficient, slope, and x-intercept of standard curve.

Note: To calculate the correlation coefficient type in desired cell (the cell locations should correspond to cells for calculation)

Ex: =CORREL(A3:A10,F3:F10)

To calculate the average type in desired cell (the cell locations should correspond to cells for calculation)

Ex: =AVERAGE(B3:BE3)

To calculate the intercept type in the desired cell (the cell locations should correspond to cells for calculation)

Ex: =INETERCEPT(F3:F10,A3,A10)

To calculate the slope type in the desired cell (the cell locations should correspond to cells for calculation)

Ex: =SLOPE(F3:F10,A3,A10)

3. Using average, multiple the average by 5 for 500 μ L.

4. Cell value for sample = (Average – y-intercept)/slope.

Live/Dead Stain

Solution 1:

- 1.0 mL Serum Free DMEM
- 2.0 μ L Ethidium Homodimer-1
- 0.5 μ L Calcein AM

Solution 2:

- 1.0 mL Serum Free DMEM
- 2.0 μ L Ethidium Homodimer-1
- 0.5 μ L Calcein AM
- 0.5 μ L Hoechst Dye

Concentrations:

- 200 μ L/96 Well plate
- 1 mL/12 Well plate

Process:

1. Incubate dead controls in 70% Ethanol for 30 minutes prior to experiment
2. Mix solution 1 within 1 hour of use
3. Incubate cells with solution 1 for 15 minutes
4. Mix solution 2 within 1 hour of use
5. Incubate cells in solution 2 for 15 minutes
6. Wash cells with 1x PBS 3 times
7. Fix cells in 4% Phosphate buffered formaldehyde for 10 minutes
8. Mount and coverslip cells on an uncharged microscope slide

Phalloidin and Hoechst Stain

Reagents:

- Phosphate Buffered Saline
- 4% Paraformaldehyde (Only needed for tissues/cells that have not been fixed);
- 0.25% Triton-X
 - 0.25% V/V Triton-X in PBS
 - 10 μ L Triton-X in 3990 μ L PBS
- 1% BSA
 - 1% V (W)/V BSA in PBS
 - 40 μ L in 3960 μ L PBS
- Phalloidin (AF 488 Phalloidin A12379 or FITC Phalloidin, Invitrogen)
 - 2.5% V/V Phalloidin in PBS
 - 50 μ L in 1950 μ L
- Hoechst
 - 0.0167% Hoechst dye in PBS
 - 0.5 μ L in 3000 μ L PBS

For unfixed sections/cells:

1. Rinse in PBS x2
2. Fix in 4% Paraformaldehyde for 10 minutes
3. Follow directions for fixed sections

For fixed sections/cells:

1. Rinse with PBS x2
2. Triton-X solution for 10 minutes
3. Rinse with PBS x2
4. Block with BSA solution for 30 minutes
5. Phalloidin solution for 30 minutes
6. Rinse with PBS x2
7. Hoechst solution for 3-5 minutes (typically 3)
8. Rinse with PBS x2
9. Cytoseal and coverslip
10. Store frozen at -20 degrees C.

Results:

- F-actin is stained green if you used 488, red if you used FITC
- Nucleus is stained Blue

Myosin Heavy-chain stain

Reagents:

- Phosphate Buffered Saline
- 4% Paraformaldehyde (Only needed for tissues/cells that have not been fixed);
- 0.25% Triton-X
 - 0.25% V/V Triton-X in PBS
 - 10 μ L Triton-X in 3990 μ L PBS
- 5% normal goat serum
- In 5% goat serums
 - Primary antibody – 1:30 (MF20 - hybridoma Bank)
- In 5% goat serums
 - Secondary antibody – 1:400
- Hoechst
 - 0.0167% Hoechst dye in PBS
 - 0.5 μ L in 3000 μ L PBS

For unfixed sections/cells:

1. Rinse in PBS x2
2. Fix in 4% Paraformaldehyde for 10 minutes
3. Follow directions for fixed sections

For fixed sections/cells:

1. Rinse with PBS x2
2. Triton-X solution for 10 minutes
3. Rinse with PBS x2
4. Block with 5% normal goat serum solution for 45 minutes
5. Leave goat serum on negative controls but aspirate the positive samples
6. Primary antibody solution for 1 hour at room temperature
7. Rinse with PBS x2
8. Secondary antibody solution for 1 hour at room temperature in the dark
9. Rinse with PBS x2
10. Hoechst solution for 3-5 minutes (typically 3)
11. Rinse with PBS x2
12. Cytoseal and coverslip
13. Store frozen at -20 degrees C.

Calcofluor White Stain

Reagents:

- Phosphate Buffered Saline
- 4% Paraformaldehyde (Only needed for tissues/cells that have not been fixed);
- Calcofluor white solution

For unfixed samples:

1. Rinse in PBS x2
2. Fix in 4% Paraformaldehyde for 10 minutes

For fixed sections/cells:

15. Rinse with PBS x2
1. Calcofluor white solution for 1 minute at room temperature in the dark
2. Rinse with PBS x2
3. Cytoseal and coverslip
4. Store frozen at -20 degrees C.

Hematoxylin and Eosin Stain

1. Hydrate Slides in running water for 5 minutes
2. Stain slides in Harris Hematoxylin for 10 minutes
3. Rinse slides in running water for 2 minutes
4. Differentiate in acid alcohol for 2 -3 minutes
5. Rinse in water for 5 dips
6. Dip in ammonia water for 15 – 30 seconds
7. Wash in running water for 10 minutes
8. Place in 95% alcohol for 2 minutes
9. Stain in eosin for 2 minutes
10. Dehydrate in 95% alcohol for 1 minutes
11. Dehydrate in 95% alcohol for 1 minutes
12. Dehydrate in 100% alcohol for 1 minutes
13. Dehydrate in 100% alcohol for 2 minutes
14. Dehydrate in 100% alcohol for 5 minutes
15. Clear in xylene 4 for 2 minutes
16. Clear in xylene 5 for 5 minutes

Time:45 minutes

Results:

Nuclei – Blue

Cytoplasm – Pink

Blood – Red